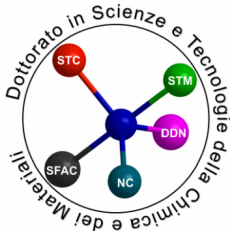

UNIVERSITA' DEGLI STUDI DI GENOVA

Doctorate School in Sciences and Technologies of Chemistry and Materials

Doctorate Course in Medicinal, Food and Cosmetic Sciences

XXXI cycle

Ph.D. Thesis

Studies on Proteolysis Targeting Chimeras: platform technology for targeted protein degradation in drug discovery

Vittoria Zoppi

Supervisor: Professor Andrea Spallarossa

Co-tutor: Professor Alessio Ciulli

Table of Contents

List of Abbreviations

ADME	absorption, distribution, metabolism and excretion
AML	acute myeloid leukemia
ASOs	antisense oligonucleotides
BET	bromodomain and extra-terminal
BRD2/3/4/7/9	bromodomain-containing protein 2/3/4/7/9
CRBN	Cereblon
CRL	Cullin-RING ligase
DDB1	damage-specific DDB1
DIPEA	N,N-Diisopropylethylamine
DLBCL	Diffuse Large B Cell Lymphoma
DUBs	deubiquitinase protease enzymes
HATU	1-[Bis(dimethylamino)methylene]-1H-1,2,3-triazolo[4,5-b]pyridinium 3-oxid hexafluorophosphate
HOAt	1-Hydroxy-7-azabenzotriazole solution
HIF-1α	hypoxia-inducible factor 1α
IMiDs	immunomodulatory drugs
LHS	Left hand side
NaHDMS	Sodium bis(trimethylsilyl)amide
PPIs	protein-protein interactions
POMA	pomalidomide
PROTACs	Proteolysis Targeting Chimeras
RHS	right hand side
RNAi	RNA interference
TEMPO	2,2,6,6-Tetramethyl-1-piperidinyloxy
UPS	ubiquitin-proteasome system
VCB	VHL-ElonginC-ElonginB complex
VHL	von Hippel-Lindau

Abstract

Proteolysis Targeting Chimeras (PROTACs) represent an innovative approach to chemical intervention into biology, with attractive therapeutic potential. In contrast to protein inhibition, PROTACs trigger targeted protein degradation inside cells via hijacking the ubiquitin-proteasome machinery. PROTACs are bifunctional compounds composed by two small molecules connected by a linker; one molecule binds to a protein of interest and the other one binds to an E3 ubiquitin ligase. The ligases most commonly recruited are the von Hippel-Lindau (VHL) protein complex $CRL2^{VHL}$ and the cereblon (CRBN) complex $CRL4^{CRBN}$. To date, different classes of target proteins have been successfully degraded, including epigenetic targets such as bromodomain-containing proteins BRD2, BRD3, and BRD4, BRD9, TRIM24, SIRT2, PCAF/GNC5, protein kinases, nuclear receptors and E3 ubiquitin ligases to self-degrade.

The work described in this thesis is divided into two parts: the first part is about the research activity carried out at the University of Dundee, under the supervision of Professor Alessio Ciulli, while a second part involves the work done at the Department of Chemical Core Technologies, within Nerviano Medical Sciences (Milan), under the supervision of Doctor Eduard Felder.

The aim of the project carried out in Ciulli Lab was to investigate PROTAC-mediated degradation of BRD7 and BRD9 proteins, subunits of the human SWI/SNF chromatin remodelling complexes. These subunits have gained interest as therapeutic target especially in hematopoietic cancers, for example supporting growth of acute myeloid leukemia (AML) cells. Despite inhibitors able to disrupt the interaction of the BRD7/9 bromodomains are known, their cellular activity has remained limited as other non-bromodomain functions of the target remain

unaffected. PROTAC molecules able to induce BRD9 degradation would more profoundly impact on BRD7 and BRD9 function and therefore could be used as chemical tools to better understand its role in BAF complex and in oncogenesis.

Following analysis of the available co-crystal structures of the individual target and ligase proteins with their respective ligands, a library of degraders has been designed and synthesised, involving convergent synthetic strategies to conjugate a diverse range of scaffolds and linkers. All compounds were tested *in vitro* against different cancer cell lines and immunoblotting was carried out to assess the target degradation profile. **VZ185** was found as a highly selective, potent and rapid dual BRD7/BRD9 degrader, with slight preference for BRD9 over BRD7. Degradation was demonstrated to be dependent upon proteasomal activity, cullin neddylation and VHL binding.

The second section of the thesis reports the design, synthesis and biological characterization of PROTACs targeting protein kinases, carried out at NMS for one-year stage. With the future prospect of extending the development of PROTAC to other targets, it was planned to study a literature example, in order to confirm the proof of concept. Amongst those available, we chose **DAS-6-2-2-6-CRBN**, based on a potent tyrosine kinase inhibitor and a CRBN ligand that induce degradation of c-ABL and BCR-ABL. Furthermore, we decided to extend the development of degraders focusing on how target ligand and linker composition affect efficacy and selectivity. The biological evaluation of the synthetized compounds was performed by the Department of Biology of NMS throughout *in vitro* treatments of cancer cell lines and immunoblotting.

1. Introduction

Modulating protein activity as a mean to control, alleviate and in some cases even cure diseases faces a number of challenges in the field of drug discovery. Many of these challenges concern with target validation (i.e. the association of a given target to a given disease progression and morbidity) and target tractability with synthetic agents i.e. drugs. In the early stage of pharmaceutical research, drug hunters typically focus on understanding the function of a protein of interest, its link with the diseases states, as well as the prediction of an efficacious and safe response in patients.[1] Target validation approaches typically involve genetic knockdown and knockout using techniques such as antisense oligonucleotides (ASOs), RNA interference (RNAi) and CRISPR-Cas9 technologies which affect expression of protein levels.[2,3] In spite of the great utility of nucleic acid-based strategies in research, their application as drug candidates presents many challenges due to their physiochemical properties such as narrow bioavailability and poor metabolic stability.[4,5] On the other hand, the identification of small-molecule inhibitors that phenocopy the outcome from knockdown experiments is challenging. Inadequate pharmacokinetic/pharmacodynamics (PK/PD) profiles, off-target effects as well as undesired toxicity profiles often emerge as a result of the high-concentrations required to achieve and maintain maximal drug efficacy for the duration of a function response. On this basis, targeted protein degradation with small molecules has been recently proposed and developed as an alternative approach to successfully target protein-causing diseases.[6–8] This emerging strategy aims to take advantage of the cellular deconstruction machinery to control protein homeostasis. Degraders are revolutionary molecules able to chemically knockdown the protein of interest at post-translational level through the modulation of the ubiquitin-proteasome system (UPS). Degraders combine the advantages of genetic knockdown techniques and the ADME (absorption, distribution, metabolism and excretion) properties of

small molecules.[9,10] This thesis focuses on the development and application of bivalent degrader molecules, also known as Proteolysis Targeting Chimeras (PROTACs), as a new modality of developing chemical tools for a target protein. PROTACs recruit a target protein to an E3 ubiquitin ligase enzyme, as a way to trigger E3-ligase mediated ubiquitination and subsequent proteasomal degradation of the target protein.[9,10] This today represents one of the most exciting and impactful modality of pharmacological intervention into biology and diseases.[6,7] There are other approaches to induce protein degradation that have been described in literature, for examples approaches were based on the inhibition of chaperone heat-shock protein 90 (HSP90), as well as cases of serendipitous compound-induced target degradation, for example the selective estrogen and androgen receptor down-regulators (SERDs and SARDs, respectively) and hydrophobic tagging (HyT).[6] However, the mechanisms of these approaches are not entirely understood or do not function necessarily *via* the UPS, and therefore are outside the scope of this thesis.

1.1 Ubiquitin-Proteasome System (UPS): an overview

The ubiquitin-proteasome system (UPS) is a primary selective cellular machinery responsible for protein degradation that plays a fundamental role in cellular homeostasis.[11,12]

The ubiquitin pathway regulates protein turnover, as initially discovered by Aaron Ciechanover, Avram Hershko and Irwin Rose, for which they were awarded the Nobel Prize in Chemistry in 2004. The key factor to determine the protein's fate is protein ubiquitination.[11,13] This post-translation modification is a multi-step process involving the covalent tagging of a protein substrate with ubiquitin, leading to subsequent recognition and degradation by the 26S proteasome. Ubiquitin (Ub) is a highly conserved 76 amino acid protein which undergoes a covalent isopeptide bond between the C-terminal glycine of ubiquitin and the amino group of a lysine residue on the substrate protein. The ubiquitination process is the result of consecutive

activity of three enzymes: Ub-activating E1 enzyme, Ub-conjugating E2 enzyme and Ub-ligating E3 enzyme (Figure 1). The human genome encodes two Ub-activating E1 enzymes, 37 Ub-conjugating E2 enzymes and over 600 Ub-ligating E3 enzymes. The mechanism of the ubiquitin-proteasome pathway (Figure 1) starts with the ATP-dependent activation of the ubiquitin carboxy-terminal glycine residue following by formation of a reactive thioester bond with a cysteine residue on the active site of the E1 enzyme. Then, the activated ubiquitin is transferred to an E2 enzyme to form a new thioester bond via a *trans*-thiolation reaction. Finally, the E3 ligase facilitates the formation of the isopeptide bond between the ε-amino group of a lysine residue of a target protein and the carboxylic functionality of the terminal glycine residue of ubiquitin. Ubiquitination is a reversible process through the action of deubiquitinase protease enzymes (DUBs) which cleave the isopeptide bond between the protein substrate and ubiquitin.[14]

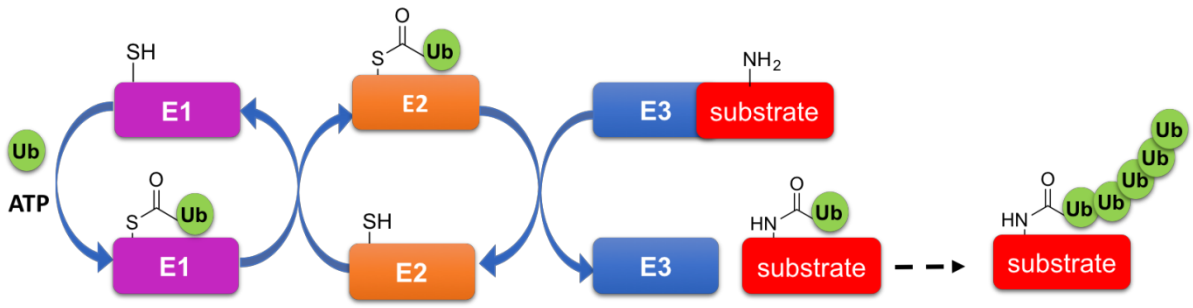

Figure 1. Schematic mechanism of the ubiquitin-proteasome pathway.

Ubiquitin itself can act as acceptor of further ubiquitin molecules because it contains seven lysine residues, leading to ubiquitin polymer chain and, thus, increasing the system complexity.[15] Depending on i) the number of ubiquitin residues, ii) the position of conjugation and iii) the layouts of polyubiquitinated chains, different ubiquitination patterns regulates protein fate (i.e. subcellular localization, protein activation, proteasome inhibition and

lysosomal degradation). Degrading ubiquitin signalling by proteasome mainly occurs for proteins tagged with Lys^{48}-linked ubiquitin chains.[15]

Owing to the effect of ubiquitination on several biological processes and its deregulation in human diseases, targeting the UPS with small molecules has gained significant interest for pharmaceutical research.[16,17] Initially, the UPS was targeted at the proteasome level, leading to the development of several proteasome inhibitors (Figure 2). One of the most studied compound is MG132 (or Z-LLL, Myogenics), a potent proteasome inhibitor that belongs to the class of peptide aldehydes.[18] In recent years, the US Food and Drug Administration (FDA) approved the boronic acid borteozomib (Velcade®, Millennium Pharmaceuticals) and epoxyketone carfilzomib (Kyprolis®, Onyx Pharmaceuticals) as proteasome inhibitors for the treatment of relapsed and/or refractory multiple myeloma.[19,20] Despite the commercial success, patients rapidly developed resistance to proteasome inhibitors and those that do respond suffer from many toxic side effects associated to the pleiotropic effects of proteasome inhibitors. Indeed, the suppression of the entire proteasomal activity in cell prevents degradation of many proteins, leading to dangerous effects. An alternative approach would be targeting upstream enzymes in the UPS cascade. One way to achieve this is to target enzymes that function on a more limited set of substrate proteins, for example the E3 ubiquitin ligases. Small molecule inhibitors of E3 ligases could have value in their own right and can provide suitable handles for PROTACs. For the purpose of this project, we will describe small molecule ligands of $CRL2^{VHL}$, $CRL4^{CRBN}$ and $CRL4^{DCAF15}$ E3 ubiquitin ligases (section 1.1.3 and 1.1.4).

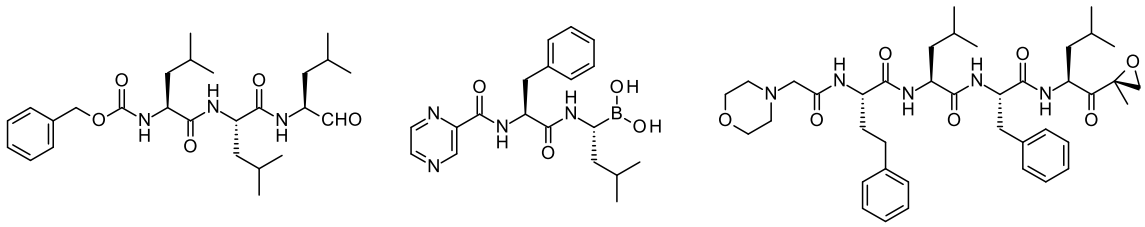

Figure 2. Chemical structures of proteasome inhibitors.

1.1.1 E3 ubiquitin ligases

E3 ubiquitin ligases represent the major class of enzymes in the ubiquitin-proteasome system in terms of diversity and members.[15] In the last decade, E3 ligases have become attractive targets in drug development for their important role in biological process and human disease states.[21,22] Based on their structural domain and their mode of action, E3 enzymes are divided into three subclasses: the homologous to E6-associated protein carboxyl terminus (HECT), RING-between-RING (RBR) and RING families (Figure 3).[23]

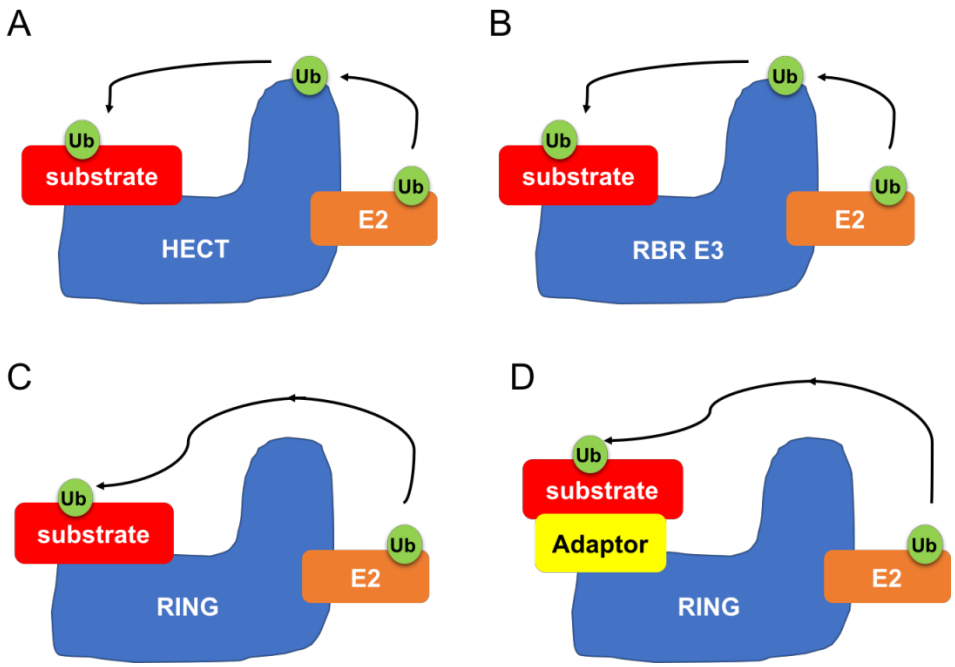

Figure 3. Types and molecular mechanism of E3 ubiquitin ligases. A) HECT E3 ligase; B) RING-between-RING (RBR) E3 ligase; C) and D) RING E3 ligases.

The HECT family receives ubiquitin from an E2 enzyme before transferring it to the substrate, leading to a two-step reaction (Figure 3A). HECT E3s have a L-shaped structure, with a flexible hinge loop connecting the N-terminus and C-terminus lobes. The N-terminus region binds the E2-Ub activated enzyme, then a conserved cysteine residue in the C-terminus lobe forms an intermediate thioester bond with the ubiquitin before catalysing substrate ubiquitylation in region outside the HECT domain. HECT E3 molecules can be divided into three groups based on domain architecture: the Nedd4 family (9 members), the HERC family (6 members) and other HECTs (13 members).[24]

A similar two-step reaction is conducted by the RBR E3 family, which combines characteristics of both HECT and RING E3s (Figure 3B). RBR E3s comprise two RING domains (RING1 and RING2) separated by an in-between-RING (IBR) domain. While E2 binds to RING1, the reactive cysteine catalysing substrate ubiquitination is located in RING2.[25]

The RING E3 ligases are the most abundant type of ubiquitin ligases (Figure 3C, D).[26] They comprise a RING or RING-like domain, responsible for E2 enzyme binding. Upon binding

between E2 and E3 enzymes, ubiquitin is directly transferred to the substrate. There are three RING E3 subfamilies: monomers, dimers and multi-subunits. The cullin-RING ligase (CRL) is the largest family of multi-subunits E3s and comprises a central cullin subunit which binds to E2 binding RING domain (RING-box protein- Rbx1 or Rbx2) at the C-terminus and to a substrate recognition domain and/or adaptor subunit(s) at the N-terminus.[21]

1.1.2 Cullin-RING ligase (CRL)

CRL is the highly diverse class of E3 ligases with over 200 members that mediates up to 20% of proteasome-dependent protein degradation.[27,28] This class comprises multi-subunit organization by using adaptors, receptors, cullin scaffolds and RING-box domains. All these subunits are interchangeable and enable to increase variability and complexity to the E3s. Seven Cullin proteins (Cul1, 2, 3, 4A, 4B, 5 and 7) with similar structural architecture are expressed in human cells.[21] Classification of CRLs is based on the type of Cullin protein in the complex, i.e. CRL2 refers to CRL E3s containing Cul2.

The N-terminal domain (NTD) and the C-terminal domain (CTD) of cullin represent important structural elements of CRLs. The NTD forms tight interaction with substrate receptors directly or via adaptor subunits.[21,29] Examples of adaptors are Skp1, Elongin B and Elongin C (EloBC) binary complex and damage-specific DDB1 (DDB1), amongst others. The CTD interacts with RING-box proteins Rbx1 and Rbx2 which in turn recruit ubiquitin-charged E2 enzyme and promote ubiquitin transfer on the substrate. In the $CRL2^{VHL}$ complex, adaptor EloBC, substrate receptor VHL, scaffold Cul2 and RING protein Rbx1 are assembled together to form the complex.[30] The EloBC adaptor establishes hydrophobic interactions with a conserved helical region called VHL-box domain of the substrate receptor VHL. Larger in size compared to EloBC and made up of three WD40 β-propeller domains (BPA, BPB and BPC), DDB1 adaptor

connect Cul4 to cereblon (CRBN) or DCAF15 in $CRL4^{CRBN}$ and $CRL4^{DCAF15}$ complexes, respectively.[21]

Recent work suggests that CRL complexes exist in "on and off" states, due to a significant conformational changes induced by neddylation of cullin.[31] Neddylation is the covalent attachment of the ubiquitin-like protein NEDD8 to a lysine residue in the cullin CTD, necessary for CRL activity, catalysed by NEDD8-activating enzyme (NAE). Thereby, NEDD8 pathway modulates the ubiquitination kinetics, providing a suitable drug target. Compound MLN4924 is a potent and selective inhibitor of NAE, currently in clinical trials for the treatment of solid tumours and haematological cancer.[27] MLN4924 creates a stable complex with NEDD8 which blocks the NAE active site, thus suppressing neddylation of cullin and consequently overall CRL activity in cell.[27]

1.1.3 $CRL2^{VHL}$ inhibitors

$CRL2^{VHL}$ targets the hypoxia-inducible factor 1α (HIF-1α) for polyubiquitination and proteasomal degradation.[32,33] HIF-1α transcription factor plays an essential role in oxygen homeostasis and tumor angiogenesis.[34,35] HIF-1α binds to VHL substrate recognition receptor (pVHL) throughout protein-protein interactions (PPIs), which is exquisitely dictated by hydroxylation of proline residues in HIF-1α. Under normoxia conditions, HIF-1α is hydroxylated on two proline residues (namely, Pro402 and Pro564) by the prolyl hydroxylase domain (PHD) enzymes in an iron- and oxygen-dependent manner.[36] Then, hydroxyproline residues (Hyp402 and Hyp564) of HIF-1α are recognized by VHL and targeted for degradation. In contrast, under low oxygen levels, PHD catalytic activity is suppressed. HIF-1α remains unhydroxylated and translocates into the nucleus where it dimerizes with HIF-1β. The heterodimer binds to hypoxia response elements (HREs) of HIF-target genes. As result, expression of genes linked to oxygen sensing and hypoxic response is induced.[37]

Inhibition of HIF-1α pathway would be expected to mimic the physiological response to low oxygen levels providing therapeutic benefit for many pathological states, as anemia associated to cancer chemotherapy and chronic kidney diseases, ischemia, inflammation and neurodegeneration.[34,38] Several small-molecule PHD inhibitors of clinical relevance have been developed, but their poor selectivity could promote off-target effects.[39–42] To avoid the unwanted side effects of PHD inhibitors, potent inhibitors of the VHL: HIF-1α PPI leading to HIF-1α stabilization were developed.[43] Ciulli and co-workers in collaboration with Crews laboratory at Yale University identified a first series of VHL:HIF-1α PPI inhibitors (Figure 4).[44–47] VHL inhibitors were designed starting from a hydroxyproline fragment, crucial for interaction with VHL. A structure-guided and fragment-based medicinal chemistry campaign led to the discovery of VH032, bearing optimized binding groups at the left-hand (LHS) and right-hand (RHS) sides of the key Hyp core fragment in the molecule (Figure 4). VH032 is a potent inhibitor (K_d = 185 nM, measured by ITC) able to disrupt VHL:HIF-1α PPI and to stabilize hydroxylated HIF-1α.[43,48] Analysis of the crystal structure of VH032 bound to VHL protein suggested significant scope to further optimize the inhibitor by modifying the LHS of the molecules. Indeed, the acetamide group partially filled the pocket where it is accommodated, providing a space to optimize the compound. Medicinal chemistry campaign within the Ciulli group at Dundee led to the discovery of VH101 and VH298, bearing a fluoro- and a cyano-cyclopropyl moiety, respectively (Figure 4).[49] VH298 [K_d (ITC) = 90 nM] and VH101 [K_d (ITC) = 44 nM] inhibitors showed high binding affinity, good cell permeability and high activity in cells.[43,49] However, cellular studies revealed a degree of cytotoxicity for VH101 when used at high (~100 μM) concentrations.[43] Following thorough biophysical and *in vitro* characterization in cell lines, VH298 was shown to be highly active as VHL inhibitor at concentrations greater than 10 μM without significant off-target effects or cytotoxicity, driving on-target stabilization of HIF-1α and induction of HIF dependent activity and responses in cells.[43] Based on this

extensive data, VH298 has been elected as novel chemical probe of hypoxic signalling pathway (available on the Chemical Probes portal and commercial vendors e.g. Tocris and Sigma Aldrich).

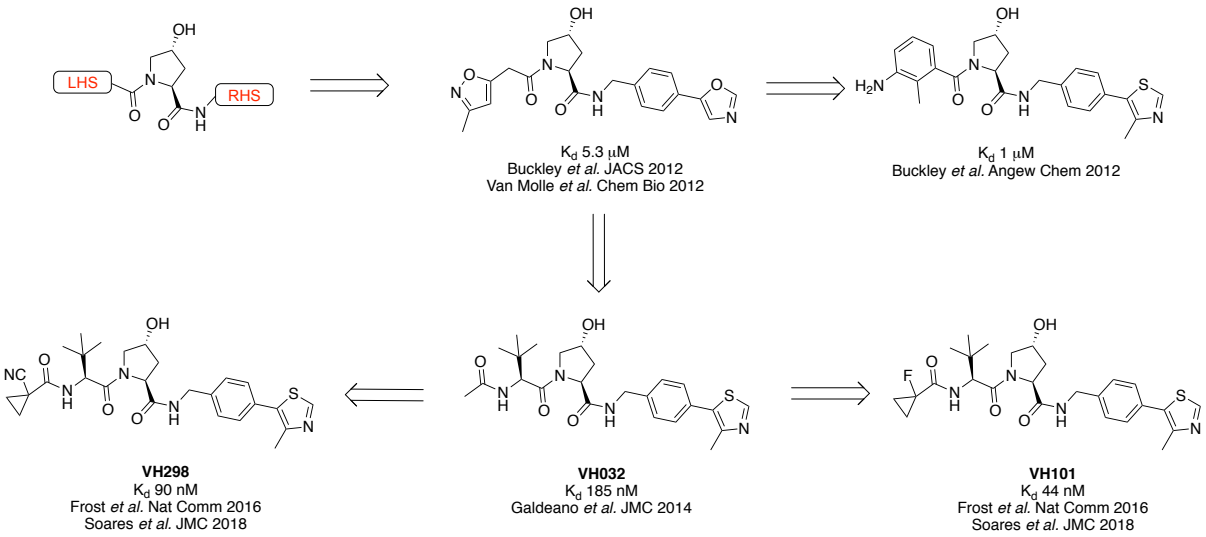

Figure 4. VHL ligands optimization throughout medicinal chemistry campaign

1.1.4 CRL4^{CRBN} and CRL4^{DCAF15} inhibitors

Thalidomide is infamously known for its teratogenicity that emerged following prescriptions in the 1950s as sedative for the treatment of morning sickness in pregnant women. Nowadays, the immunomodulatory drugs (IMiDs) thalidomide and its derivatives lenalidomide and pomalidomide are widely used for the treatment of multiple myeloma (Figure 5). In particular, lenalidomide (marketed as Revlimid® by Celgene) is extensively used as front-line drug for the treatment of multiple myeloma and was the top selling cancer drug in 2016.[50] Indeed, IMiDs were recently found to bind to CRBN, the substrate recognition component of the CRL4^{CRBN} E3 ubiquitin ligase complex, and to prevent binding with endogenous substrate as MEIS2.[51] However beyond their potential inhibitory role, upon binding to CRBN, IMiDs induce degradation of several so-called neo-substrate proteins, as a result of the formation of *de novo*

induced protein-protein interactions (PPIs) with the CRBN-IMiDs complex.[51–53] These neo-substrate proteins include members of the IKAROS family transcription factors IKZF1 and IKZF3 (also known as Ikaros and Aiolos). Degradation of IKZF1 and IKZF3 forms the basis of their anticancer effect in multiple myeloma (MM) and T cells.[51,52] Interestingly, only lenalidomide, amongst IMiDs, induces ubiquitination of Casein kinase 1α (CKIα), resulting in CKIα degradation. Indeed, lenalidomide induces the formation of two β-strands composed of CRBN residues 346-363.[52] In turn, it might contribute to significant changes in the surface of CRBN near the IMiD binding site and thus it may determine differences in decreasing CK1α protein levels. [53]

Therefore, immunomodulatory drugs are a class of mono-functional molecules termed "molecular glues" which enhance PPIs between E3 ligases and neo-substrates for targeted degradation. Similar activity belongs also to the plant hormone auxin which binds to $CRL1^{TIR1}$ to induce depletion of Aux/IAA transcriptional repressor proteins.[54]

More recently, the anticancer sulphonamides indisulam, E7820 and chloroquinoxaline sulphonamide (CQS) (namely SPlicing inhibitor suLphonAMides- SPLAMs) were also described as "molecular glues" (Figure 5).[55,56] Indeed, these compounds were found to mediate interaction between DCAF15 and the pre-mRNA splicing factor RBM39 (or CAPERα), resulting in RBM39 ubiquitination and subsequently proteasomal degradation. However, X-ray crystal structure of DCAF15-RBM39 complex will be necessary to prove the molecular mechanism of SPLAMs and to identify possible additional molecules that mediate this PPI.

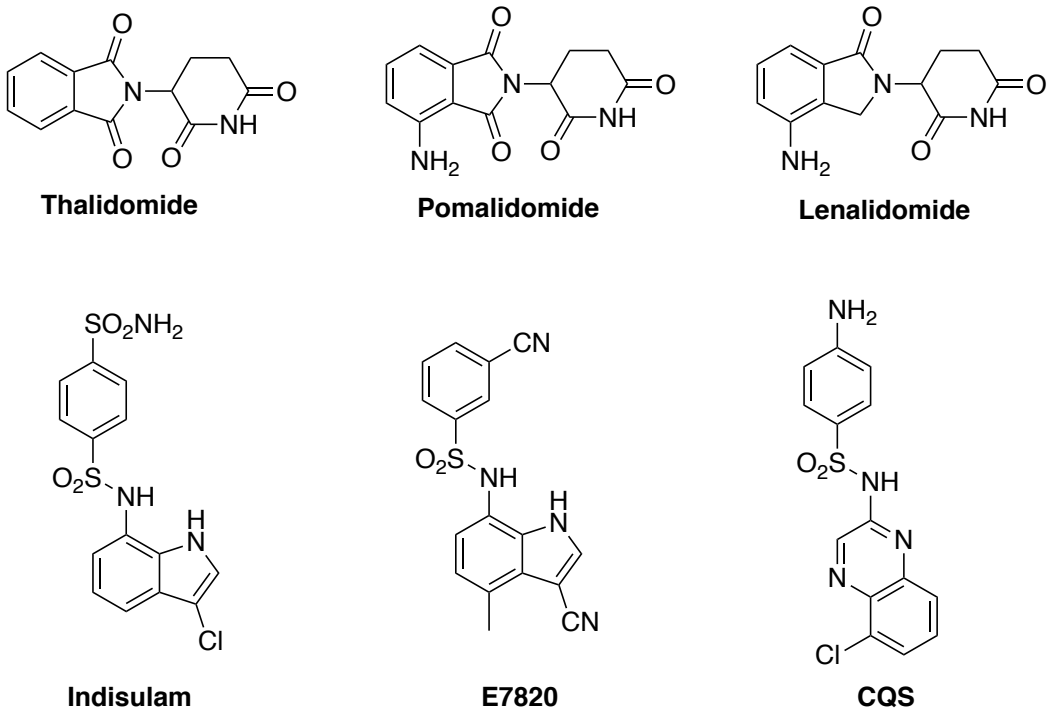

Figure 5. Chemical structure of "molecular glues" targeting CRL4^{CRBN} and CRL4^{DCAF15}

1.2 Proteolysis Targeting Chimeras (PROTACs)

PROTACs are bifunctional molecules characterized by a linker connecting a ligand for a protein of interest (POI) and a second molecule able to recruit an E3 ligase (Figure 6). PROTACs, being able to bind simultaneously both proteins, lead to the formation of a ternary complex POI:PROTACs:E3 ligase. As result, the protein of interest is ubiquitinated and degraded by the proteasome (Figure 6).

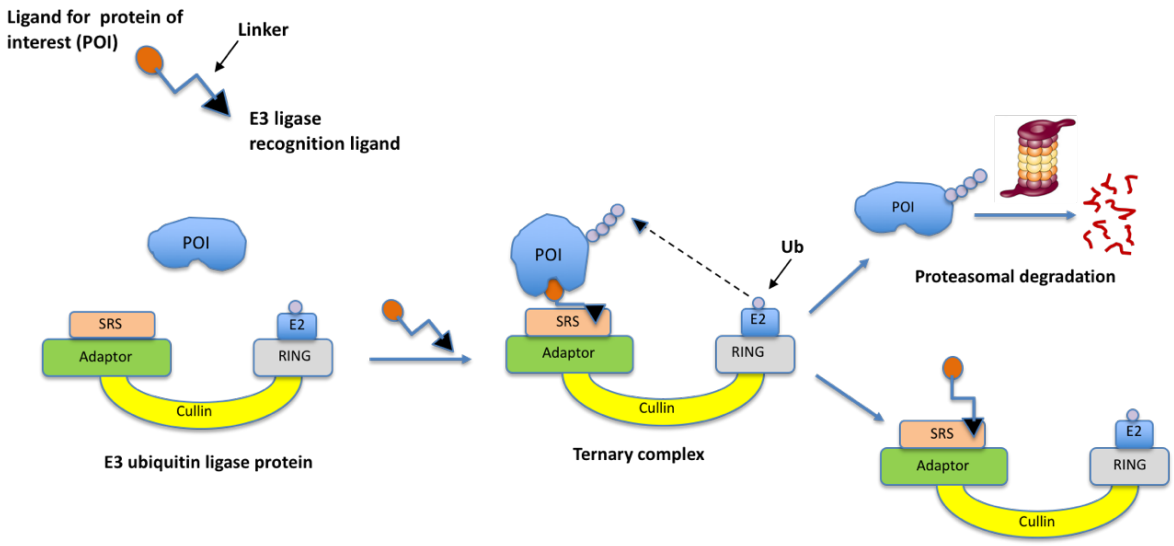

Figure 6. Scheme of PROTAC approach (SRS: substrate recognition subunit)

1.2.1 Peptide-based PROTACs

The first PROTAC described in the literature, reported by Sakamoto *et al.*,[9] aimed to induce degradation of methionine aminopeptidase-2 (MetAP-2). The heterobifunctional molecule consisted of the small molecule ovalicin, which binds to MetAP-2, attached *via* an aminohexanoic acid linker to a phosphor-decapeptide derived from IκBα inhibitor to recruit the E3 ubiquitin ligase $SCF^{\beta\text{-}TRCP}$. Ubiquitylation and degradation of MetAP-2 was demonstrated by adding the compound to *Xenopus* egg extracts using recombinant $SCF^{\beta\text{-}TRCP}$ and substrate proteins. Shortly after, two parallel studies demonstrated the ability of PROTACs to promote degradation of target proteins in the cellular context.[57] Estradiol-SCF and dihydrotestosterone (DHT)-SCF PROTACs were microinjected into Hek293 cells. These two PROTACs demonstrated the ability to target the estrogen receptor (ER) and androgen receptor (AR), deregulated in breast and prostate cancer, respectively.[57]

The first cell-permeable PROTAC was developed by switching the IκBα-phosphopeptide component with a seven-amino-acid sequence (ALA-Hyp-YIP).[58] The ALA-Hyp-YIP is a

HIF1α-derived motif recognized by VHL E3 ligase. Noteworthy, an eight-poly-D-arginine tag was added at the C-terminus of ALA-Hyp-YIP to improve cellular uptake. These compounds were used to induce degradation of FKBP12 protein, estrogen receptor, and the aryl hydrocarbon receptor upon the inclusion in the chemical structure of a cell-penetrating peptidic sequence.[58]

Another interesting example is the discovery of PROTAC targeting the X-protein of the hepatitis B virus (HBV) consisting of the oxygen-dependent degradation domain of HIF1α fused to the X-protein oligomerization domain.[59] Moreover, phospho-dependent proteolysis-targeting chimeras (phosphoPROTACs) were developed to induce chemical knockdown of FRS2α and PI3K. PhosphoPROTACs comprised VHL binding peptide fragment, a receptor tyrosine kinase (RTK) phosphorylation sequence and a poly-D-Arg to enhance cell permeability. Upon RTK activation, the RTK sequence of PROTAC is phosphorylated and recruit downstream targets with phospho tyrosine-binding (PTB) and Src homology 2 (SH2) domains. Meanwhile, the VHL-binding sequence hijacks VHL E3 ligase to induce degradation of proteins of interest. Although their antitumor activity in mouse xenograft models, phosphoPROTACs were characterized by poor drug-like properties.[60]

At this stage, PROTAC technology represented a mere proof-of-concept with potential as a chemical biology tool only. The highly peptidic- and phospho- nature of these early PROTAC compounds presented significant challenges and limitations associated with their metabolic instability, poor cell permeability and high molecular weight. For these reasons, the prospect of real applications in drug discovery remained far-fetched and the pharmaceutical industry did not take notice for many years.

1.2.2 Small molecule-based PROTACs

The much needed improvements of stability, bio-distribution and permeability of PROTACs in cellular and potentially in vivo context motivated the development of more drug-like compounds. Transition from peptide-based PROTACs to small-molecule PROTACs was ushered by breakthrough development of small-molecule drug-like binders of E3 ligases (i.e. MDM2, cIAP1, CRBN and VHL).[48,51] An early study in this direction involved the design of PROTACs targeting the androgen receptor (AR) by hijacking the p53-degrading Mouse Double Minute 2 (MDM2) E3 ubiquitin ligase. A non-steroidal androgen receptor ligand (SARM) was conjugated with the MDM2-TP53 inhibitor nutlin *via* a polyethylene glycol. A SARM-nutlin degrader was able to decrease AR protein level in cells, albeit only at high micromolar concentration (≥10 μM).[61] In parallel, in another small molecule PROTAC approach, also termed SNIPER (Specific and Non-genetic IAPs-dependent Protein ERaser, IAPs = inhibitor of apoptosis proteins), Naito, Hashimoto and colleagues described degrader molecules that targeted the E3 ligase cIAP1 via the aminopeptidase inhibitor methyl ester bestatin.[62] These early SNIPERs demonstrated depletion of cellular retinoic acid-binding protein (CRABP) I and II with all-*trans* retinoic acid ligands at micromolar concentration. Unfortunately, the bestatin methyl ester has off-target effects through inhibition of arginyl amino-peptidases and leukotriene A4 hydrolase, and, crucially, promoted concomitant cIAP1 autoubiquitination and degradation – leading to loss of SNIPER-induced target degradation due to reduced cIAP1 activity. Nevertheless, subsequent SNIPERs were developed and shown to induce knockdown of other target proteins, including the retinoic acid receptor, the ER, the AR and acidic coiled-coil-3-containing protein.[62–64]

Given the micromolar potency of these first small molecule PROTACs comparable to peptide-based PROTACs and the lack in selectivity, a strong incentive to design more potent and higher quality small-molecule PROTACs emerged.

VHL-based PROTACs

The availability of high quality VHL ligands prompted the development of VHL-based degraders.[65–72] VHL ligand VH032 (Figure 4) has been incorporated into PROTACs reported to target the estrogen-related receptor (ERRα) and the serine/threonine kinase RIPK2. A thiazolidinedione-based ERRα ligand was linked to VH032 to yield a selective degrader enable to decrease ERRα protein levels in cells with a DC_{50} of 100 nM. Notably, in vivo experiments in mice demonstrates significant target knockdown in heart, kidney and xenografted tumors. For targeting RIPK2, VH032 was coupled to a RIPK2 inhibitor via a 12-atom linker (Figure 7). PROTAC_RIPK2 shows DC_{50} of 1.4 nM and maximal degradation (D_{max}) of 95% at concentration of 10 nM after 4 h treatment, a very fast effect given the protein's half-life of approximately 60 h.[66]

BRD4 targeted degradation was successfully achieved with VHL-recruiting PROTACs based on VH032 as VHL hijacking moiety.[65,67] Bromodomain-containing protein 4 (BRD4) is an epigenetic protein, member of the bromodomain and external domain (BET) family, which plays a key role in the proliferation of cancer cells by regulating oncogene expression.[73] Ciulli lab reported the first BRD4 degrader MZ1 in which the pan-BET inhibitor JQ1 is linked to VH032 by 3-unit polyethylene glycol linker (Figure 7). MZ1 demonstrated complete degradation of BRD4 after 3 h treatment and sustained up to 24 h. Interestingly, MZ1 and its analogues MZ2 and MZ3 showed preferential depletion of BRD4 over its homologs BRD2 and BRD3. Since MZ1 has comparable binding affinity between all BET homologs, this selective degradation beyond target engagement was an unexpected yet fascinating observation. This evidence suggests the potential of PROTACs to add a new layer of specificity to a promiscuous or non-completely selective binding ligand.[65] A subsequent study reported a second series of

VHL-based BET degraders based on a more potent BET inhibitor I-BET726, which was derivatized via a distinct vector compared to JQ1.[74]

The X-ray crystal structure of MZ1 bound with either VHL and BRD4 provided the first crystal structure of PROTACs reported in literature.[68] This crystal structure shows that the MZ1 linker folds itself making possible novel and distinct PPIs between VHL and $BRD4^{BD2}$ resulting in high stability and high cooperativity of the ternary complex. Based on these observations, rational design led to the discovery of AT1, a highly selective PROTAC active against BRD4 (Figure 7).[68]

ARV-771 represents another BRD4 degrader which links together JQ1 and VH032 (Figure 7). ARV-771 and MZ1 share the same target and E3 ligase, but they bear different linkers and a methyl modification on VHL ligand. This heterobifunctional compound induces depletion of all BET family proteins at concentration of 5-10 nM. Downstream effect was also observed at mRNA and protein level at concentration lower than 10 nM. Moreover, despite possessing K_d values similar to those of the JQ1-inhibitor, the PROTAC's catalytic mechanism of ARV-771 demonstrates a higher efficacy in reducing c-myc levels. Finally, ARV-771 activity in inducing tumor regression was confirmed in in vivo models of castration-resistant prostate cancer.[67]

The bromodomain-containing co-regulator of transcription TRIM24 is another epigenetic target that has been successfully degraded by a PROTAC (Figure 7). dTRIM24 degrader induces rapid and sustained proteasomal degradation of TRIM24. In addition, dTRIM24 shows enhanced anti-proliferative effect compared to the inhibitor alone. Moreover, researchers have demonstrated, using dTRIM24 as chemical probe, the dependency of human acute leukemia cell on TRIM24 function.[69]

Another example of a VHL-based PROTAC is compound 3i (Figure 7) designed to target a serine/threonine kinase, namely TANK-binding kinase 1 (TBK1), implicated in oncogenesis. Different linker lengths and compositions were explored. Compound 3i showed excellent

efficacy and selectivity, inducing a maximal degradation (D_{max}) of 96% and showing a DC_{50} value of 12 nM.[70]

VHL-recruiting PROTACs were also developed as chemical dimerizers, to induce self-ubiquitination and subsequent self-destruction of an E3 ligase, in an approach called Homo-PROTACs. The most active homo-PROTAC compound CM11 (Figure 7) induced rapid, profound and selective degradation of VHL at 10 nM already after 4 h treatment. Moreover, VHL self-degradation with CM11 was found to be preferential for the long isoform of VHL, without significantly depleting the short VHL isoform. As a result, CM11 did not induce a HIF-dependent hypoxic response in cells. This work provided proof-of-concept that homo-bifunctional molecules can be developed as a strategy to dimerize an E3 ubiquitin ligase and target it for degradation, allowing to probe its biology and relevance as therapeutic targets in ways not possible with E3 ligase inhibitors alone.[71] Subsequently, homo-PROTACs for the E3 ligase CRBN were also reported.[75]

VHL-based PROTACs were also designed to target depletion of HaloTag fusion proteins, for example a green fluorescent protein (GFP)-HaloTag fusion.[72] HaloTag is a modified bacterial dehalogenase that covalently binds to hexylchloride for functional protein analysis.[76] HaloPROTACs induced VHL- and proteasome-dependent degradation of GFP-HaloTag. The most potent HaloPROTAC induced more than 90% GFP-Halotag7 reduction and had a DC_{50} value of 19 nM by 6 h. An exploration of linker length highlighted the key role of the linker in PROTAC-mediated protein degradation.[72]

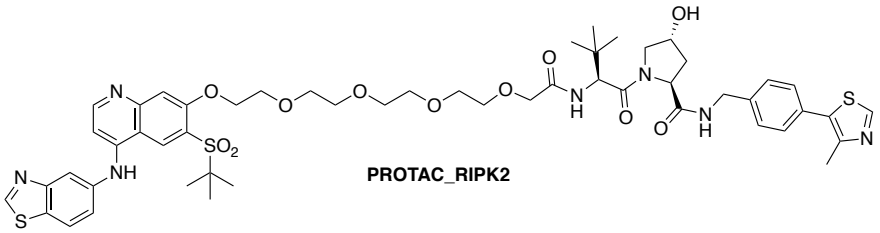

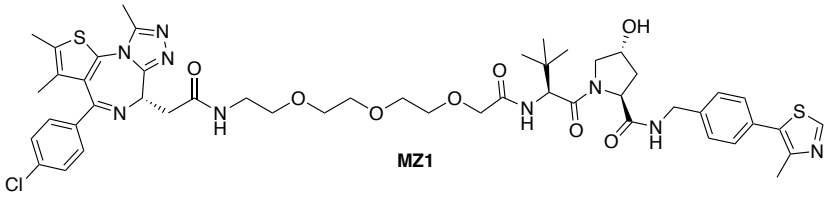

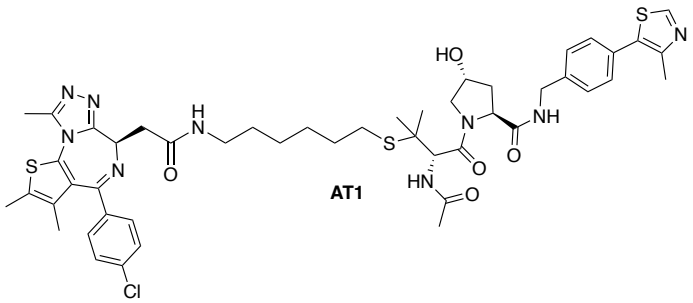

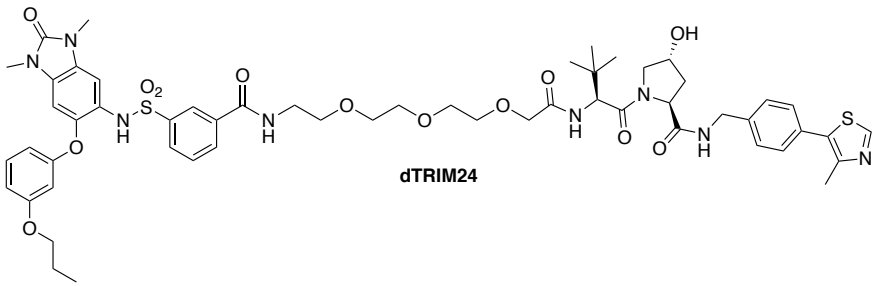

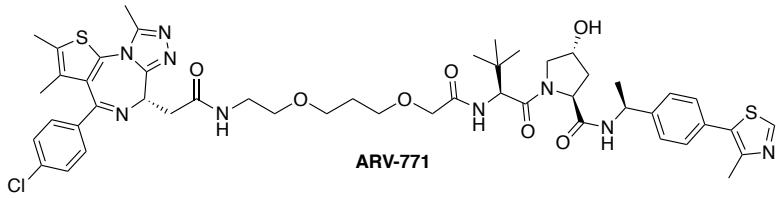

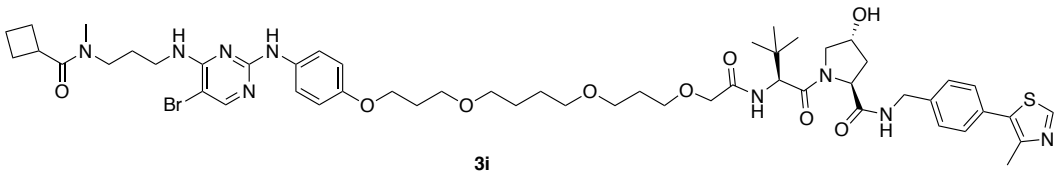

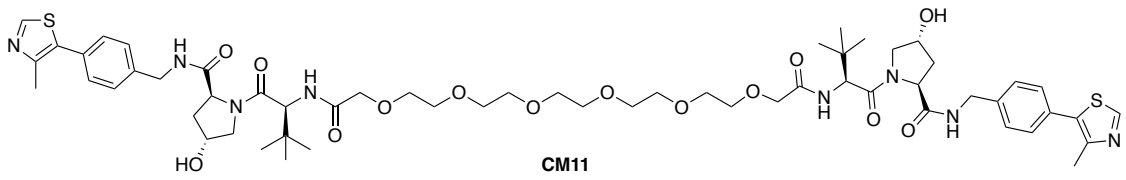

Figure 7. Chemical structures of VHL-recruiting PROTACs

CRBN-based PROTACs

In the recent years, IMIDs have been identified as promising ligands for the development of PROTACs able to recruit CRBN E3 ligase.[51] Two interesting studies were conducted to target degradation of BET proteins.[77,78] In one study, compound ARV-825 was designed by coupling pan-BET inhibitor OTX015 to pomalidomide *via* a four-unit polyethylene glycol linker (Figure 8). This PROTAC showed potent and rapid degradation of all BET homologs (BRD2, BRD3 and BRD4) in Burkitt's lymphoma cell lines. Moreover, ARV-825 exhibited sustained activity up to 24 h and downstream suppression of c-Myc levels, resulting in superior antiproliferative and apoptotic effects in comparison to BRD4 inhibitors JQ1 and OTX015.[77] In a second study, BRD4 inhibitor JQ1 was coupled to a thalidomide derivative *via* a short alkyl linker, resulting in the dBET1 PROTAC (Figure 8). Consistent with the presence of the pan-BET inhibitor JQ1, quantitative proteomics analysis demonstrates chemical knockdown of all BET family and of c-Myc levels in acute myeloid lymphoma (AML) cells. Furthermore, dBET1 activity has been investigated in xenograft mouse model of AML cells, showing tumor regression in a 14-day treatment.[78]

Lai and co-workers described degraders to mediate elimination of the protein kinase c-ABL and its oncogenic fusion protein BCR-ABL. To target c-ABL and BRC-ABL, three tyrosine kinase inhibitors (TKIs, namely imatinib, bosutinib and dasatinib) were employed. Recruitment of CRBN and VHL E3 ligases was directly compared for the same kinase ligands and distinct linker variations. In K562 leukemia cell line, imatinib-based degraders did not induce degradation of the proteins of interest. c-ABL and BCR-ABL proteins were degraded using PROTAC bearing bosutinib linked to pomalidomide, but no activity was detected for VHL ligand-containing compounds. The activity of dasatinib-CRBN degrader (DAS-6-2-2-6-CRBN, Figure 8) was similar to that of the bosutinib-pomalidomide pair, while the corresponding VHL-based PROTAC degraded only c-Abl. Of note, all PROTACs were shown

to bind and inhibit BCR-ABL and c-ABL in cells, irrespective of their degradation activity.[79] This work, together with the study on BRD4 degraders, confirmed that degradation involved more than just target binding, underlining the important influence of the target warheads, the recruited E3 ligase and the linkers on PROTAC functionality.[65,68,77–79]

CRBN-based PROTAC degraders were developed to knockdown the bromodomain-containing protein 9 (BRD9), emerged as an attractive therapeutic target in cancer. Compound dBRD9 (Figure 8), induces rapid, potent and selective degradation of BRD9 and is endowed with anti-proliferative effect against human acute myeloid leukemia cell lines.[80]

Others examples of CRBN-recruits PROTACs aim to target SIRT2,[81] CDK9,[82] PCAF/GNC5[83] and CRBN itself.[75]

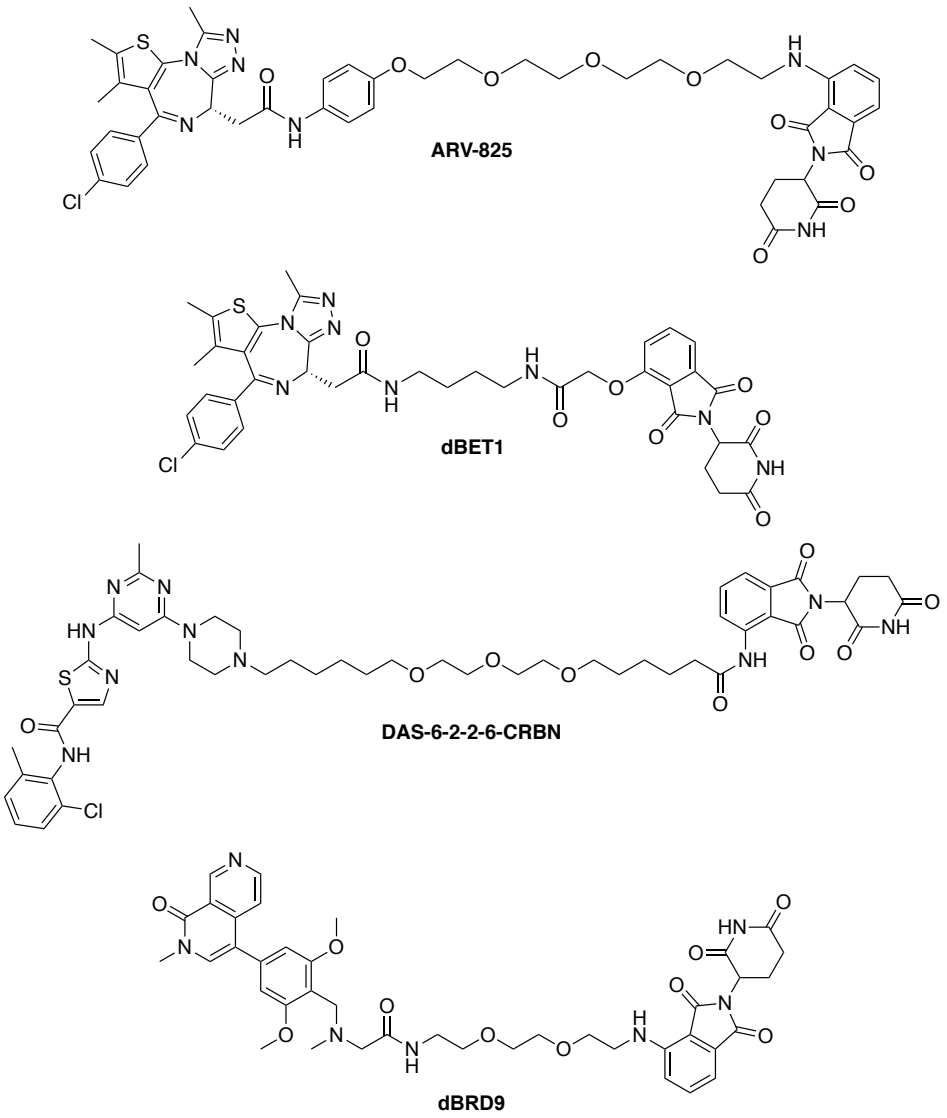

Figure 8. Chemical structures of CRBN-recruiting PROTACs

1.3 Advantages of PROTAC system over inhibition

PROTACs offer a range of unique advantages relative to traditional small-molecule inhibitors. Conventional small-molecule inhibition is based on occupancy of the binding site of target protein. Thus, occupancy-driven strategy requires high concentration of high-affinity drug to achieve and maintain a high level (typically over 90%) of target engagement. In turns, the high dose could limit the duration of a functional response, with the risk of severe off-target or unwanted side effects, leading to toxicity in therapeutic settings. Instead, PROTACs mediate a transient interaction between target protein and an E3 ligase through an event-driven strategy.[66]

Indeed, PROTACs act as agonists to catalytically initiate a degradation cascade: after a first round of target ubiquitination and degradation, the degrading machinery and the compound will be available to start a new catalytic cycle. A consequence of the catalytic mode of action is that degraders can function at sub-stoichiometric receptor occupancies. It means that desired protein degradation can be observed at concentrations much lower than degrader binding dissociation constants (K_d) from the target, reducing the requirement for full target engagement.[84,85] The required PROTAC concentrations are also lower than those needed to achieve E3 ligase inhibition.[85] For example, PROTAC_RIPK2[66] binds to VHL E3 ligase with K_d of 0.5 μM, while induced degradation of RIPK2 results in half-degrading concentration (DC_{50}) of 1 nM. Moreover, to achieve sufficient VHL inhibition, the required PROTAC_RIPK2 concentrations are less than 10 μM leading to a significant window between desired degradation-induced pharmacology and unwanted inhibition-induced effects. A further consequence of the catalytic mechanism is an often time-dependent degradation with greater protein depletion seen over time.[85]

Targeted protein degradation with PROTACs offers a strategy to modulate the functional selectivity of a ligand, thus providing highly selective degraders with reduced side effects. High selective degradation is often achieved incorporating a highly selective ligand into a degrader. However, appropriate designed PROTACs could add a layer of target selectivity compared to the intrinsic binding selectivity of the ligand.[65,68,74,86] Selective stabilization of the ternary complex and subsequent selective degradation could be achieved by rational PROTAC design thanks to the availability of crystal structures.[68,87]

The mounting interest in degraders is also motivated by the possibility to target proteins that lack of suitable binding site, including transcription factors, scaffolding proteins, non-enzymatic proteins, deemed “undruggable” via conventional occupancy-based strategy.[16] In contrast to degraders that act independently from the functional site, inhibitors need to interact

with well-defined pockets to affect protein function which might be insufficient to block protein activity and it could lead to feedback response. Thereby, post-translational protein degradation determines removal of entire protein. This effect is different than simply blocking a binding site and it closely phenocopies genetic knockdown/knockout strategies, leading to significantly improved pharmacology (i.e. more sustained cellular effect and extended duration of action).[85] Once the protein of interest has been degraded, PROTACs are available to deplete the smaller pool of *de novo* re-synthesized protein. Since the slow turnover rate of many proteins, efficient protein knockdown might be maintained with the still available modest concentration of degraders or even after clearance for a significant period of time. This characteristic, together with the catalytic mode of action, allow for low drug exposures (C_{max} and AUC), low dose and long dosing interval, resulting in suitable subcutaneous or intramuscular administration routes in addition to intravenous administration.[85]

Finally, PROTACs can be broadly applicable in light of the conservation and essentiality of the UPS and the fact that E3 ubiquitin ligases such as CRBN and VHL are widely expressed across different cells.

1.4 Challenges of PROTAC development

The PROTAC strategy has been continuously and significantly improved in the last 15 years, yet many questions remain to be addressed that could greatly inform and drive future therapeutic applications.

A general methodology for an efficient PROTAC design would be desirable. Important parameters to keep in consideration during their design are chemical stability, solubility and permeability. Key points of the design are also the choice of the E3 ligase, the selection of target ligands and their conjugation pattern. The properties of the linkers, such as length,

composition and site of attachment are known to be important and to impact on activity varying in a context- and target-dependent manner.[70,71,74,88,89]

Another challenge is the development of ligands binding the target proteins and the E3 ligase; despite the large number of E3 proteins (> 600), only few good-quality ligands have been discovered and successfully used for PROTACs, and CRBN and VHL are to date the only ligases most widely used for PROTACs.[21]

The first barrier to face in PROTAC development is their cellular uptake: the designed degrader must access the appropriate intracellular compartment to bring target protein and UPS in close proximity. The larger size compared to small molecule inhibitors may result in a slower rate of membrane crossing. However, despite their molecular weight (typically in the 700-1100 Da range) and polar surface area values, the examples reported in literature so far have shown that the concentration of degraders achieved inside the cell is clearly adequate to drive highly potent effect.

Once inside the cells, the molecule should enable the formation of the ternary complex bringing target protein and E3 ligase in close proximity. Thermodynamic and kinetic properties of the ternary complex should be considered during PROTAC development.[68,87] In contrast to the binary system, thermodynamics of the ternary complex has been described by bell-shaped dose responses so-called "hook-effect".[90] This effect leads to less efficient ternary complex formation at high concentrations, favouring the saturation of the two proteins with the degrader.

The interaction between degrader and one protein might favour ternary complex formation leading to positive cooperativity (that is a thermodynamic parameter that can be used to describe favourable or repulsive interactions between two proteins) or disfavour it by steric clashes (negative cooperativity).

Appropriate conformation of the ternary complex is also necessary to allow ubiquitination of target protein.[91] Another limiting step might be the activity of deubiquitinase enzymes (DUBs)

which catalyse the removal of ubiquitin from proteins. Indeed, ubiquitination of target proteins should proceed at correct rate to overcome any competing ubiquitin removal by DUBs.[92] Also the ubiquitination patter should facilitate efficient proteasomal recognition and avoid other cellular responses due to different polyubiquitin linkages and chain length.[15]

PROTAC-induced protein degradation has yielded impressive preliminary efficacy in a limited number of cellular and *in vivo* systems, leading to numerous high quality chemical probes and lead compounds with significant therapeutic potential. The first PROTAC compounds are expected to enter clinical trials in early 2019, and these first clinical studies will be important to assess the real potential of PROTACs as new medicines.

1.5 Aims and objectives

The broad research theme of this PhD program is the design, synthesis and evaluation of the biological activity of PROteolysis TArgeting Chimeras (PROTACs), a fascinating novel approach for drug discovery to induce the degradation of a target protein using small molecules.

The aim of my PhD project is to design PROTACs against different target proteins to further contribute to pharmaceutical research in the field of targeted protein degradation. My PhD work has been divided into two parts. One part of my research activity was carried out at the University of Dundee, under the supervision of Professor Alessio Ciulli. This part of my thesis involved the design, synthesis and biological evaluation of PROTACs targeting the bromodomain-containing protein 7 and 9 (BRD7 and BRD9).

The second part of my work was carried out at the Department of Chemical Core Technologies, within Nerviano Medical Sciences (Milan), supervised by Doctor Eduard Felder. With the future prospect of extending the development of PROTACs to other targets, it was planned to study a literature example, in order to confirm the proof of concept. Among the available

molecules, it was chosen a degrader targeting the tyrosine kinase c-ABL and its oncogenic fusion protein BCR-ABL. Then, the development of PROTACs was extended to other protein kinases, focusing on how target ligand and linker composition affect efficacy and selectivity.

Section I

2. BRD7 and BRD9 targeting PROTACs

2.1 Introduction

2.1.1 Bromodomains

In eukaryotic cells, post-translational modification (PTMs) are stable chemical modifications of histone proteins around which DNA is wrapped.[93] PTMs are essential to regulate gene expression because they influence the access of transcription machinery to the chromatin compact organisation of the genetic material. N-acetylation of lysine residues on histones and other proteins is the most abundant and studied PTM process associated with chromatin architecture and transcriptional activation.[94–96] In order to recruit the transcription machinery, the degree of compactness of the chromatin is regulated by acetyltransferases (HATs) and histone deacetylases (HDACs), "writers" and "erasers" of acetyl marks, respectively.

Another class of epigenetic proteins is represented by bromodomain-containing proteins (BRDs), "readers" of acetyl-lysine (KAc) residues.[94] The human genome encodes for 61 bromodomains which are present in 46 diverse nuclear and cytoplasmic proteins divided in 8 subfamilies, based on structure and sequence similarity.[96,97] Despite the large sequence variations, bromodomains are structurally conserved modules that comprise four α-helices (known as αZ, αA, αB and αC), linked by two flexible loop regions (known as ZA and BC loops), to form the KAc binding site.[97] Structural data have showed two hydrogen bonds responsible for acetyl-lysine residue recognition: one between the carbonyl moiety of KAc and the N-terminus of an asparagine residue, and another interaction with the hydroxy group of a Tyr residue *via* a conserved water molecule present in the binding site.[98]

The hydrophobicity of cavity makes the bromodomain attractive target for inhibition of protein-protein interaction.[96] Indeed, BRDs such as transcriptor co-regulators (BET protein

BRD4 and ATAD2), E3 ubiquitin ligases (TRIM24), transcriptional repressors (BAZ2A) and chromatin-remodeling factors (CECR2) represent valuable pharmacological targets for the treatment of different diseases.

In particular, the Bromo- and Extra-terminal (BET) subfamily comprises four members in humans (namely, BRD2, BRD3, BRD4 and BRDT) bearing two related bromodomains (namely, BD1 and BD2) which recognize different KAc residues in H3 and H4 histone tails.[99] Potent chemical probes for BET subfamily registered in clinical trials (i.e. RVX-208,[100] I-BET762,[101] OTX015[102] and (+)-JQ1[103] among others) have shown profound anticancer and anti-inflammatory properties.

More recently, there has been also intense interest in non-BET bromodomains proteins to unravel their biological function and to explore their role in cancer and other human diseases.[80,104–108] Prominent examples are bromodomains of bromodomain-containing protein 9 (BRD9) and its analogue bromodomain-containing protein 7 (BRD7), components of the SWI/SNF chromatin remodelling complexes.[109,110]

2.1.2 BRD7 and BRD9 proteins

BRD7 and BRD9 belong to the forth subfamily of bromodomains sharing 85% of sequence identity between them.[104] These homolog domains have been identified as subunits of BAF (BRG-/BRM-associated factor) and PBAF (Polybromo-associated BAF) complexes, respectively.[109,110] BAF and PBAF represent two variants of the SWI/SNF complex, one of the four mammalian ATP-dependent chromatin remodelling complexes, which plays a key role in gene regulation, DNA replication and DNA repair.[111] SWI/SNF complex modulates access to promoters and coding regions of DNA through modification of the degree of compactness of chromatin. This activity is crucial to the productive recruitment of transcription machineries and therefore controls and regulates gene expression.[112,113] The first relationship between

SWI/SNF complexes and cancer emerged in the 1990s, as several genes coding for SWI/SNF subunits were identified as tumour suppressors.[114,115] For example, loss of the SMARCB1 subunit was identified in malignant rhabdoid tumour (MRT), while loss of BRG1 (brahma-related gene 1) and BRM (brahma), encoded by the *SMARCA4* and *SMARCA2* genes, respectively, was linked to breast cancer.[116,117] However, only recently, deep genome-sequencing has revealed that mutations of BAF/PBAF constitutive subunits are found in 20% of human cancers.[109]

Emerging evidence indicates that BRD7 and BRD9 have key roles in tumorigenesis and, consequently, these proteins are potential drug targets. BRD9 is mainly overexpressed in several malignancies, such as cervical cancer and in non-small cell lung cancer (NSCLC).[118,119] Instead, BRD7 has been proposed as candidate tumour suppressor gene, being frequently down-regulated in malignancies, such as breast cancer, NPC, ovarian cancer, gastric cancer, colorectal carcinoma and prostate cancer.[120–123] In particular, it has been disclosed that BRD7 gene regulates breast cancer cell metabolism,[124] being a negative regulator of aerobic glycolysis essential for tumour progression.[125] In contrast, it has recently been suggested that BRD7 knockdown could be an attractive target for cancer immunotherapy, showing that inactivation of BRD7 sensitizes tumour cells to T cell-mediated killing.[126]

To explore the therapeutic potential of BRD7/9, structure-guided medicinal chemistry campaigns were carried out to identify potent and selective chemical probes. Compounds **I-BRD9**[104], **LP99**[105], ketone "compound **28**"[106], **BI-7273** and **BI-9564**[107], and **GNE-375**[108] (Figure 9) have been used in cells to help clarifying the roles of BRD7/9 in oncology and other disease. For example, pharmacological studies of inhibitors **BI-7273** and **BI-9564** in combination with domain-swap protein engineering revealed BRD9-dependency on sustaining MYC transcription and maintaining the leukemic cellular state in hematopoietic cancer *via* its bromodomain.[107,127] In a separate study, the effect of **LP99** on the expression of pro-inflammatory cytokines suggests BRD7/9 bromodomains as potential targets for anti-inflammatory

treatment.[105] In yet another study, blockade of BRD9 bromodomain with **I-BRD9** identified its role in the regulation of several cancer related genes.[104] These investigations provide a rationale for targeting non-BET protein for treatment of diseases.

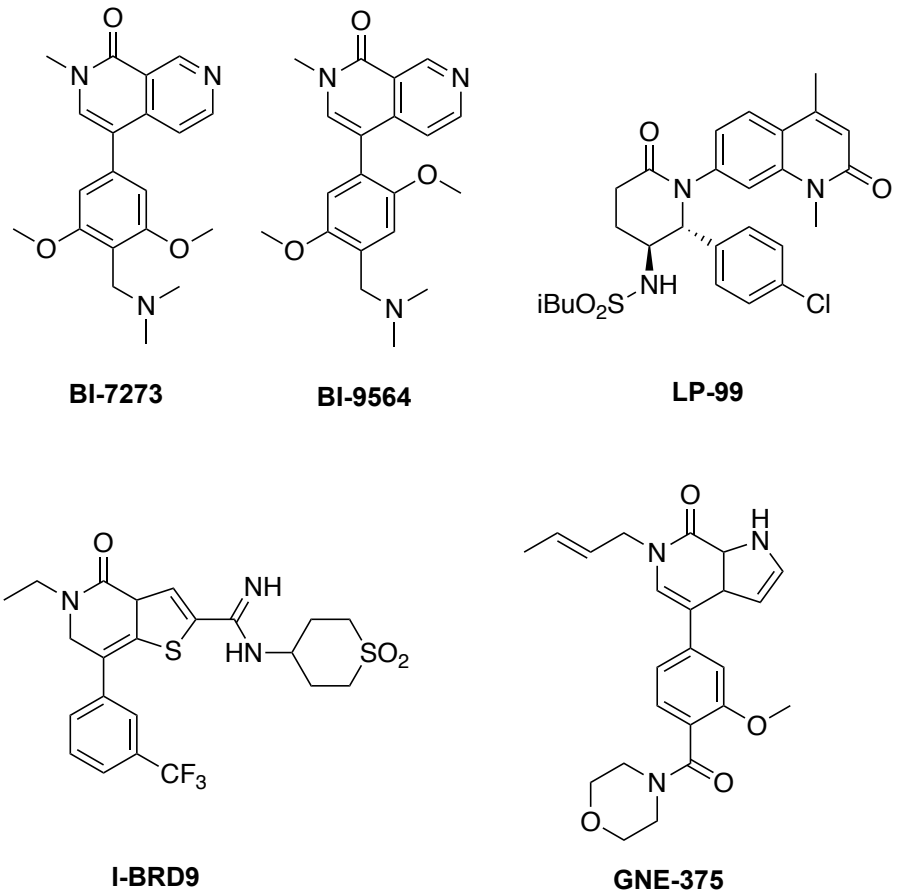

Figure 9. Chemical structures of BRD7 and BRD9 bromodomain inhibitors.

2.1.3 Aims and objective

Although inhibitors are useful tools to explore the therapeutic potential of bromodomain target proteins, significant challenges and limitations of single domain blockade are relevant for multi-domain proteins. In the context of multiprotein complexes, inhibition of a single domain might not be completely essential to target activity which may for example depend on the functions or interactions of other regions or subunits which would remain unaffected. Indeed,

as disclosed by Hohmann *et al.*,[127] BRD9 inhibition determines partial release of the SWI/SNF complex from the chromatin, disrupting only a single interaction with lysine acetylated (KAc) motifs on histone proteins. Moreover, occupancy-driven target inhibition often fails to phenocopy the genetics expected by traditional genetic knock-out/knock-down due to the mechanistically difference between blockade and removal of the protein.[128] These limitations could all be circumvented by inducing pharmacologically protein degradation with a PROTAC. On the basis of these observations, my PhD project was focused on the feasibility of targeting BRD7/9 for degradation and on the identification of a suitable target-ligase pair. In this regards, during the course of this research, Remillard and colleagues[80] described the design and the characterization of **dBRD9**, a selective chemical BRD9 degrader recruiting CRBN E3 ligase. Moreover, in the same work, BRD9-VHL PROTAC combinations were shown to be inactive. Undeterred by these findings and encouraged by our initially results, a structure-activity relationship (SARs) study was carried out to explore the impact of target ligands, linkers composition and conjugation patterners on BRD7/9 degradation.

Therefore, the goal of my PhD project is to design, synthesise and characterize PROTACs targeting BRD7 and BRD9, attractive therapeutic targets in cancer.

2.2 Design, synthesis and biological evaluation of first-generation degraders

In next paragraphs, the design, synthesis and biological evaluation of fist-generation compounds targeting BRD7 and BRD9 proteins will be described.

2.2.1 Design of first-generation compounds

A first set of PROTACs able to induce BRD7/9 degradation by recruiting three different E3 ubiquitin ligases (namely, VHL, CRBN and DCAF15) was designed. The choice of target and E3 ligase ligands was motivated by the availability of high-quality small ligands, allowing us to increase diversity and maximizing the opportunity for complementary surfaces between the bromodomain and the ligase within ternary complexes. By this first series of compounds, the impact of linker length, composition and derivatization vectors on activity was evaluated.

2.2.1.1 BRD7/9 ligand: BI-7273[107]

Derivative **BI-7273**[107] (Figure 9) was selected as BRD7/9 bromodomain ligand because of its high binding affinity and its demonstrated superiority as BRD9 chemical probes over other ligands. The key feature of this compound is the 2-methyl-2,7-naphthyridin-1-one scaffold that improved selectivity for BRD9 over the BET protein family by inducing a change in the torsion angle between the anchor binder and the ZA channel linker rings and by improving π-stacking interaction with Tyr106 in BRD9 anchor region (Figure 10). Moreover, the electron-donating groups on the phenyl group enhanced potency by improving T-stacking interaction with Phe44 side chain (Figure 10).

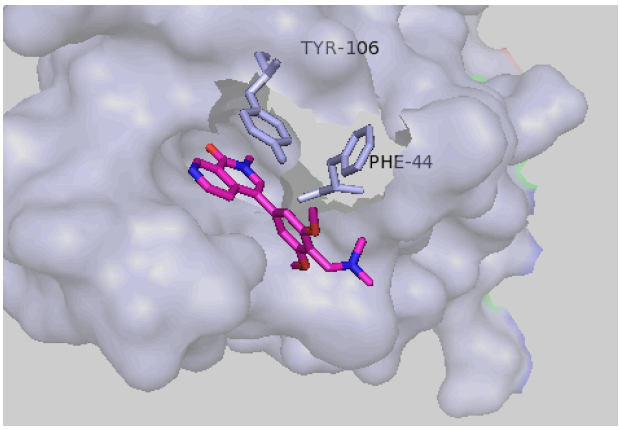

Figure 10. Crystal structure of BI-7273 (magenta) bound to BRD9 (PDB: 5EU1) [Ref.107]. Residues Tyr106 and Phe44 are shown as sticks.

To design the first-generation of degraders, we inspected the crystal structure of **BI-7273** bound to BRD9 (PDB code: 5EU1)[107] to identify solvent exposed attachment points and vectors for linker conjugation, which are known to greatly influence PROTAC degradation profiles.[71,74] The dimethylamine terminal group of the molecule was identified as a suitable group not being involved in any key interactions with the protein (Figure 10). For derivatization purposes, the dimethylamine group of compound **BI-7273** was replaced by a piperazine group (BrdL1), providing a synthetically convenient and isosteric handle (Figure 11).

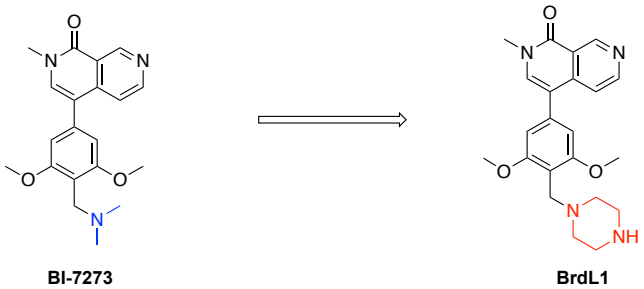

Figure 11. Chemical structures of parent (BI-7273) and modified (BrdL1) BRD7/9 ligand. Functional groups selected for conjugation are shown in blue on parent ligand and in red on modified ligand.

2.2.1.2 Degraders recruiting CRL2^{VHL}

The high-affinity VHL binders VH032 (K_d = 185 nM), VH298 (K_d = 90 nM) and VH101 (K_d = 44 nM)[43,48,129] were selected as VHL E3 ligase recruiting moieties (Figure 12). The SAR studies on VH032 led to compounds VH298 and VH101 with increased binding affinity and cell permeability. The terminal acetyl group of VH032 was replaced with either a cyanocyclopropyl group (VH298, PDB 5LLI) or with fluorocyclopropyl group (VH101, PDB 5NVX). In order to maintain the strong binding affinity of these compounds, the already available co-crystal structures[43,48,129] were analysed to identify the portion suitable for the derivatization of the ligands without perturbing their binding modes. From previous studies, it was reported that the hydroxyproline (Hyp) scaffold forms hydrogen bonds with His115 and Ser111 side chains of VHL.[36,130] Moreover, the methylthiazole ring binds to right-hand side (RHS) pocket of VHL in an energetically stable conformation.[48] It was also known that the *tert*-butyl group points upward resulting in hydrophobic contacts with Phe91 and Trp88 side chains.[48] Therefore, it was assumed that the Hyp, the thiazole ring and the *tert*-butyl group were not available for modification. However, the methyl group of VH032 terminal acetyl group was found eligible for linker conjugation and was modified to afford compound VHL1 without perturbing the key interaction within the VHL binding site, as previously demonstrated (Figure 12).[65,66,77,79] Furthermore, we explored a conjugation vector *via* phenolic position 2 on the phenyl ring of VH032 (VHL2, Figure 12), already reported as suitable linker-conjugation region.[71,72] Concerning VH298 and VH101, they were only derivatized at the position 2 of the phenyl ring (VHL3 and VHL4, respectively; Figure 12), in order to leave undisturbed the key cyano- and fluoro-cyclopropyl groups of the VHL ligands.[43,129]

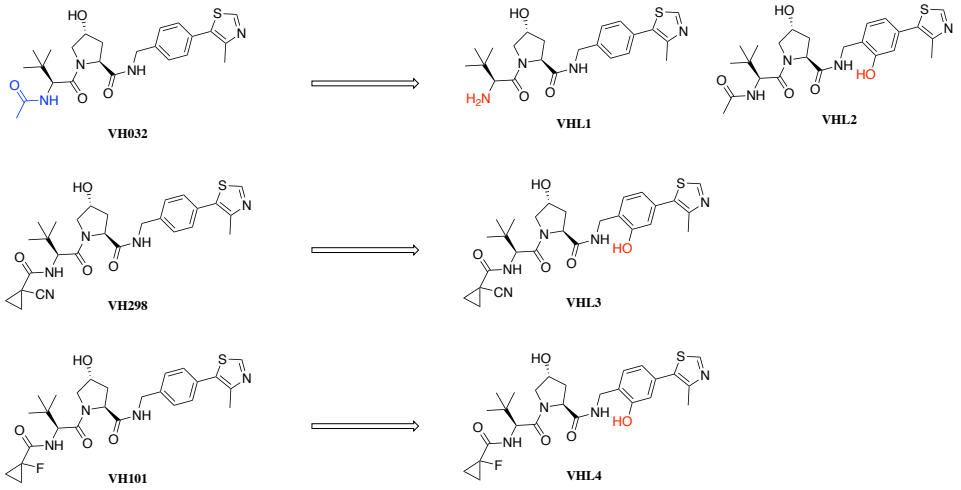

Figure 12. Chemical structures of parent (VH032, VH298 and VH101) and modified (VHL1-4) VHL ligands. Functional groups selected for conjugation are shown in blue on parent ligand and in red on modified ligand.

In addition to the site of attachment, the chemical and physical properties of linkers (e.g. length and composition) are known to impact on compound activity in a target- and context-dependent fashion.[70,71,74,88,89] Widely used linkers are polyethylene glycol (PEG) chains. Their flexibility facilitates the formation of the ternary complex bringing the E3 ligase productively in close proximity to the target protein for ubiquitination and subsequent degradation.

We designed PROTACs recruiting $CRL2^{VHL}$ using PEG linkers composed of two, three, four and five ethylene glycol units and a more lipophilic 11-atoms chain was inserted (Table 1). Moreover, a different attachment to BrdL1 moiety via amide conjugation instead of amine was explored (Table 1).

Table 1. Structural features of first-generation of VHL-based BRD7/9 PROTACs

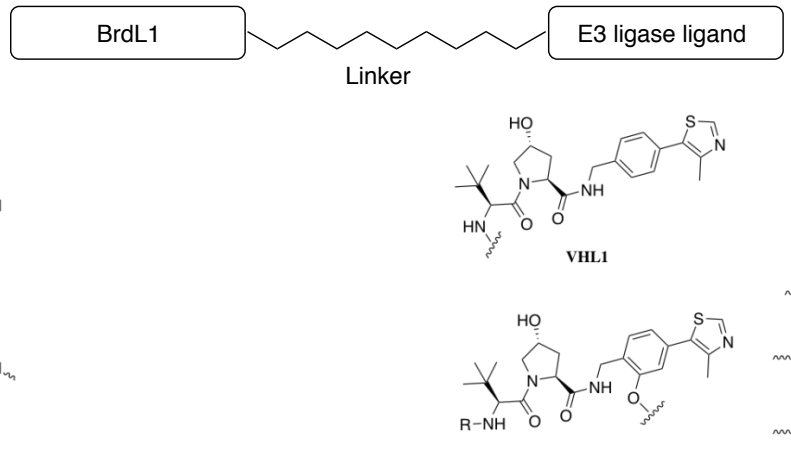

Structural features of first-generation of VHL-based BRD7/9 PROTACs					
Code	**BrdL**	**Linker**	**E3 ligase ligand**	**Linker length (atoms)**	**# of O atoms**
VZ48	BrdL1	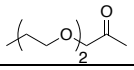	VHL1	8	2
VZ52		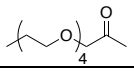		14	4
VZ49		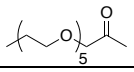		17	5
VZ55		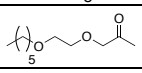		11	2
DAT152[a]		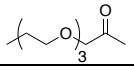		11	3
DAT157[a]		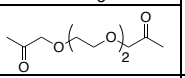		11	3
VZ117		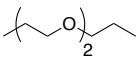	VHL2	8	2
VZ96			VHL3	8	2
VZ95			VHL4	8	2
VZ118		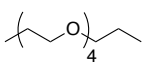	VHL2	14	4
VZ97			VHL3	14	4
VZ98			VHL4	14	4

[a]Provided by Dr Andrea Testa, University of Dundee.

2.2.1.3 Degraders recruiting CRL4^{CRBN}

To explore the possibility of inducing degradation of BRD7/9 proteins with the formation of different ternary complex, a small set of PROTACs recruiting CRL4^{CRBN} was designed (Table 2). Derivatives **VZ109** and **VZ110** were characterized by two or four PEG unit linkers.

In recent years, thalidomide (after being banned for its teratogenic properties) and its derivatives pomalidomide and lenalidomide have gained interest as immunomodulatory drug and antineoplastic (IMIDs). In particular, lenalidomide (marketed as Revlimid® by Celgene) is extensively used as front-line drug for the treatment of multiple myeloma and was the top selling cancer drug in 2016.[50] As reported in the literature, IMIDs act as agonist and antagonist on CRBN.[51] In fact, IMIDs on one hand prevent the binding to CRBN of endogenous substrates such as MEIS2 and, on the other hand, are able to induce the recruitment of the non-physiological substrates Ikaros and Aialos (two transcription factors overexpressed in multiple myeloma) promoting their proteasomal degradation (see section 1.1.4).[51]

Pomalidomide was selected as CRBN ligand because of its great cellular stability. Its crystal structure in complex with CRBN (PDB code: 4CI3)[51] suggested that the amine at position 4 of the phthalimide ring could provide a suitable connecting point for the linkers (Figure 13).

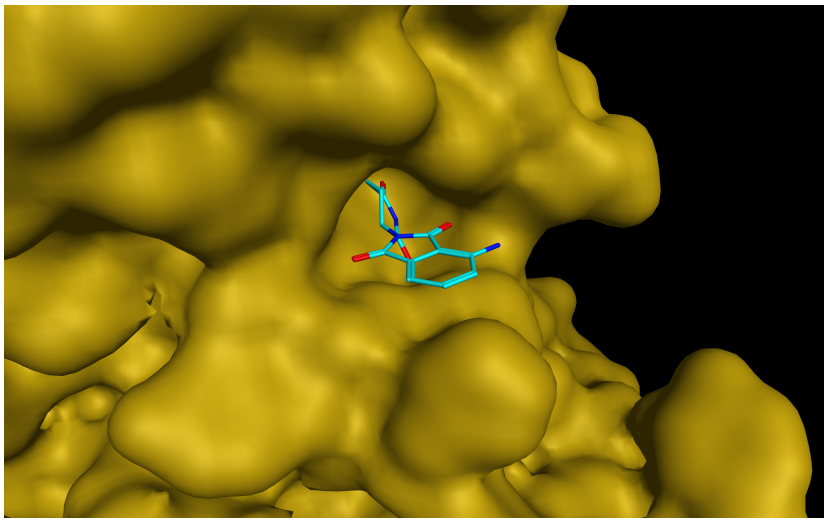

Figure 13. Crystal structure of pomalidomide (cyan) bound to CRBN (PDB code: 4CI3).

Due to the poor reactivity of the aromatic amine group, pomalidomide was converted into POMA compound (Figure 14), characterized by an amine functionality suitable for the conjugation with the linker *via* amide bond.

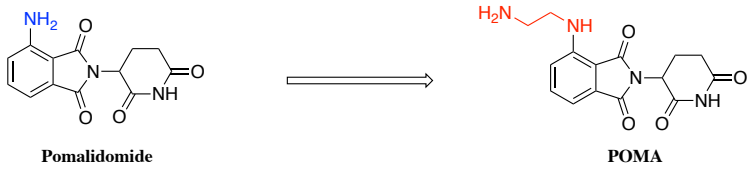

Figure 14. Chemical structures of pomalidomide and its analogue POMA. Functional groups selected for conjugation are shown in blue on parent ligand and in red on modified ligand.

Table 2. Structural features of first-generation of CRBN-based BRD7/9 PROTACs

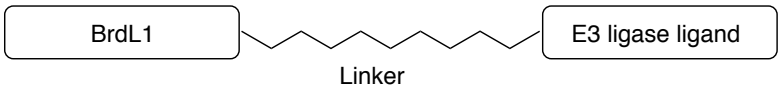

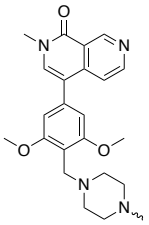

BrdL1

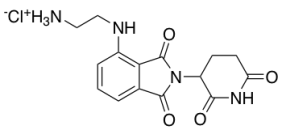

POMA

Structural features of first-generation of CRBN-based BRD7/9 PROTACs					
Code	**BrdL**	**Linker**	**E3 ligase ligand**	**Linker length (atoms)**	**# of O atoms**
VZ109	BrdL1	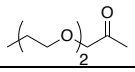	POMA	8	2
VZ110		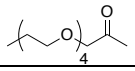		14	4

2.2.1.4 PROTACs recruiting CRL4^{DCAF15}

To further extend the study, we designed BRD7/9 degraders recruiting the E3 ligase CRL4^{DCAF15} (compounds **VZ89** and **VZ90**, Table 3). Indisulam[55,56] was selected as the ligand for CRL4^{DCAF15}. This aryl sulphonamide seems to redirect the activity of the CRL4^{DCAF15} complex towards the neo-substrate CAPERα (also known as RBM39, section 1.1.4).[55,56] As the binding mode of Indisulam is not known, we leveraged information on the activity of a biotinylated photoactive analogue probe to guide our conjugation strategy.[55] Accordingly, a *para*-benzylamine derivative of Indisulam was designed as conjugatable ligase ligand (Figure 15).

PEG linkers composed of two or four ethylene glycol units were used to connect the two warheads, BrdL1 and Indisulam derivative (Table 3).

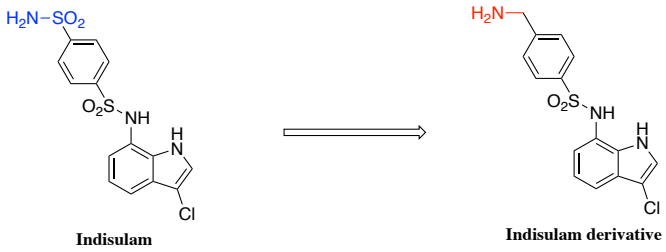

Figure 15. Chemical structures of DCAF15 ligand Indisulam its benzylamine analogue. Functional groups selected for conjugation are shown in blue on parent ligand and in red on modified ligand.

Table 3. Structural features of first-generation of DCAF15-based BRD7/9 PROTACs

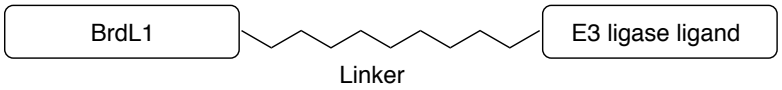

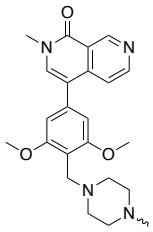

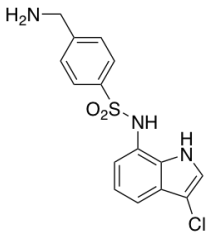

Structural features of first-generation of DCAF15-based BRD7/9 PROTACs					
Code	**BrdL**	**Linker**	**E3 ligase ligand**	**Linker length (atoms)**	**# of O atoms**
VZ89	BrdL1	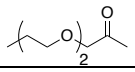	Indisulam Derivative	8	2
VZ90		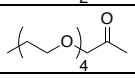		14	4

2.2.2 Synthetic routes of first-generation compounds

In this chapter, the synthetic routes to obtain BRD7/9-targeting degraders of the first generation are described. First, it is reported the synthetic procedures applied to obtain the BRD7/9 and the E3 ligase ligands. Then, the synthesis of the linkers and the assembly of the final compounds are described.

2.2.2.1 Synthesis of BRD7/9 ligand: BrdL1

BrdL1 synthesis has been carried out by a convergent approach as detailed in Scheme 1. Thus, the reaction of 4-methyl-3-cyanopyridine **1** (commercially available) with DMF acetal in refluxing DMF followed by treatment with glacial AcOH/H_2SO_4 led to the formation of 2,7-naphthyridin-1-one (**2**) in 74% yield. Iodination of **2** with I_2/NaOH afforded **3** which was then methylated to yield the key building block **4**. The higher electronegativity of the 1-oxopyridine ring over the unsubstituted pyridine ring determined the high regioselectivity of iodination. Next, Miyaura-Suzuki cross-coupling (one-pot two-step) was conducted between the organic halide **4** and tert-butyl 4-(4-bromo-2,6-dimethoxybenzyl)piperazine-1-carboxylate (**6**), previously obtained by reductive amination between 4-bromo-2,6-dimethoxybenzaldhehyde **5** and boc-piperazine in 97% yield. The Miyaura reaction involved the generation of a mixture of boronate and boronic acid of compounds **6**, while in the second step (Suzuki coupling) **4** and a 2M degassed aqueous solution of K_2CO_3 were added. Microwave heating improved the yield and reduced the reaction time. After cleavage of the tert-butyloxycarbonyl protecting group derivative BrdL1 (**7**) was obtained in quantitative yield.

Scheme 1. Synthesis of BRD7/9 ligand BrdL1

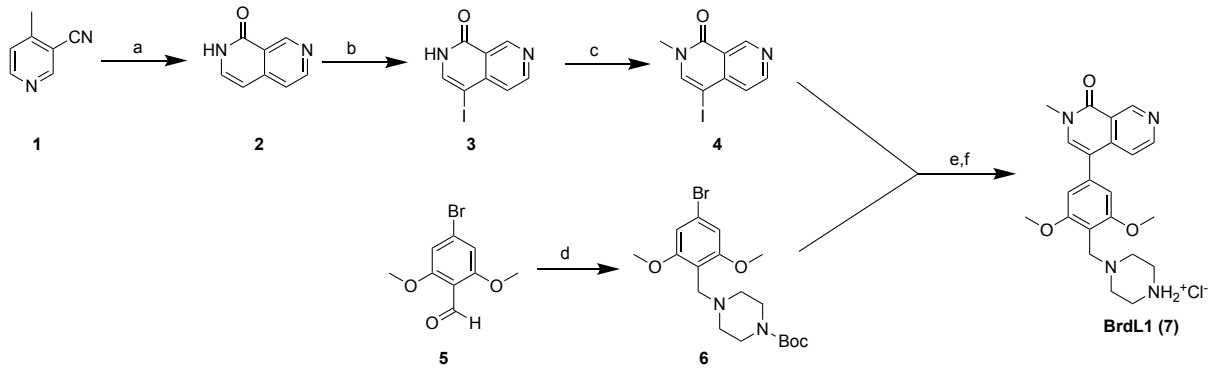

Reagents and conditions: (a) DMF acetal in refluxing DMF, 160 ºC, overnight; then, CH_3COOH, H_2SO_4, 130 ºC, 2 h, yield 74%; (b) I_2, NaOH 0.4N, 80 ºC, 5 h, yield 53%; (c) NaH, CH_3I, DMF, 0 ºC, 5 h, yield 95%; (d) 1-Boc-piperazine, $NaBH(OAc)_3$, THF, rt, overnight, yield 97%; (e) step 1: **6**, B_2pin_2, KOAc, $Pd(dppf)Cl_2$, 1,4 dioxane, µw 140 ºC, 40 min; step 2: **4**, K_2CO_3 (aq) are added to step 1, µw 120 ºC, 30 min, yield 55%; (f) HCl 4M in dioxane, DCM, rt, 1 h, quantitative yield

2.2.2.2 Synthesis of VHL2-4

The synthesis of VHL ligands (VHL2-4)[43,48,71,72,129] characterized by the hydroxyl group at position 2 on the phenyl ring is reported in Scheme 2. The reduction of 2-hydroxy-4-(4-methylthiazol-5-yl)benzonitrile **8** (synthetized as previously reported[48]) led to benzylamine compound **9** that was coupled with Boc-L-hydroxyproline to afford compound **10**. After BOC deprotection, **11** was reacted with Boc-L-*tert*-leucine in the presence of HATU, and the key intermediate **12** was isolated after removal of BOC protecting group. Acetylation of compound **12** using acetyl imidazole led to the formation of VHL2 (**13**) in 51% yields. Alternatively, **12** was coupled with 1-cyano and 1-fluoro-cyclopropanecarboxylic acid in the presence of DIPEA, to afford compounds VHL3 (**14**) and VHL4 (**15**), respectively.

Scheme 2. Synthesis of VHL2-4

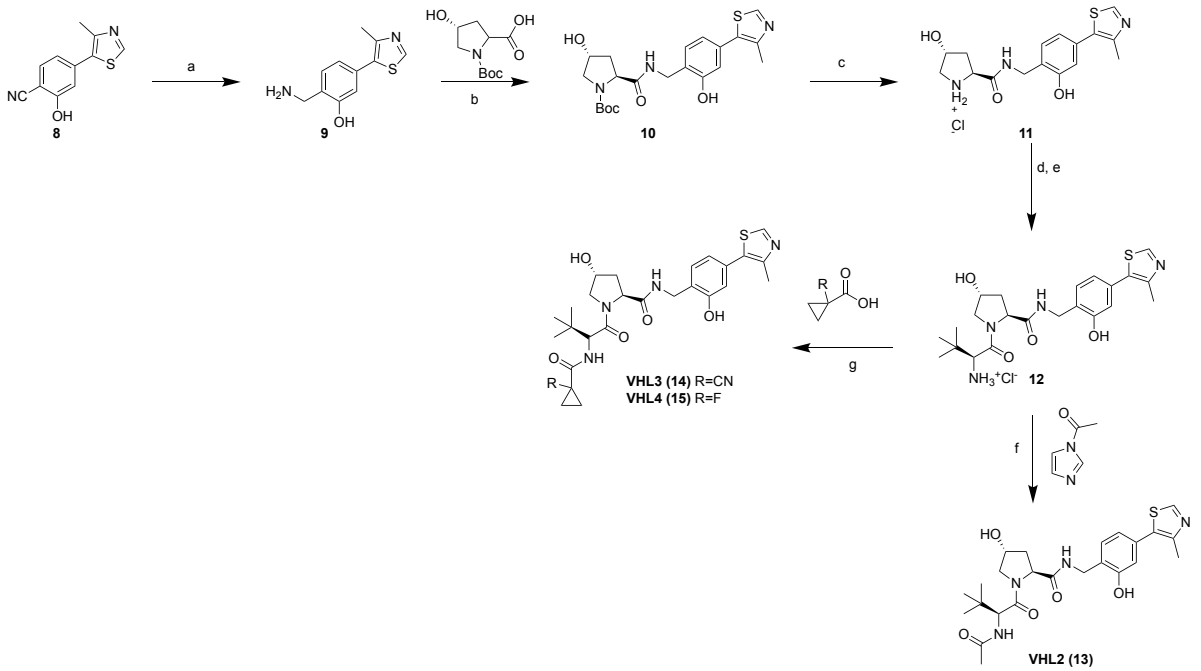

Reagents and conditions: (a) LAH, THF, 55 ºC, overnight, yield 41%; (b) Boc-L-hydroxyproline, HATU, HOAt, DIPEA, DMF, rt, 1 h, yield 78%; (c) 4M HCl in dioxane, quant. yield; (d) Boc-L-*tert*-leucine, HATU, HOAt, DIPEA, DMF, rt, 1 h, yield 94%; (e) 4M HCl in dioxane, quant. yield; (f) 1-acetylimidazole, DIPEA, DMF, rt, 3 h, yield 51%; (g) acid derivatives, HATU, HOAt, DIPEA, DMF, rt, 1 h, yield 50-56%

2.2.2.3 Synthesis of Indisulam derivative

For the synthesis of indisulam analogue **21** we applied minor changes to a procedure already published by Owa *et al*.[131] (Scheme 3). Briefly, the chlorination at position 3 of 7-nitroindole **16** using N-chlorosuccinimide led to 3-chloro-7-nitroindole **17** (94 % yield) which was reduced, in quantitative yields, in a sealed vial with Fe/NH_4Cl. Next, **18** was coupled with 4-formylbenzenesulfonyl chloride **19** in pyridine to afford **20** in good yield. The last reductive amination was a tricky reaction, due to the higher reactivity of the primary amine over the aldehyde. First of all, we tried to generate *in situ* the imine by using NH_4OAc and $NaCNBH_3$ in a EtOH:THF mixture. However, the imine was unstable and it self-condensed giving the undesired compound shown in Figure 16. To overcome this problem, a different approach was applied. The reaction between compound **20** and a mixture of NH_2OH*HCl, HCl 2M, and Zn

in ethanol led to the corresponding oxime that was too stable and it did not reduce to amine, even if more zinc was added and heating was applied. In the final and successful attempt, reductive amination was carried out using an excess of ammonia in order to push the reaction and to avoid self-condensation. Thus, reaction between compound **20**, a saturated solution of NH_4OAc in ethanol, $NaCNBH_3$ and 30% ammonia afforded indisulam derivative (**21**) in 35% yield after HPLC purification using a gradient of 5% to 95% v/v acetonitrile in 0.1% aqueous solution of formic acid.

Scheme 3. Synthesis of Indisulam derivative (21)

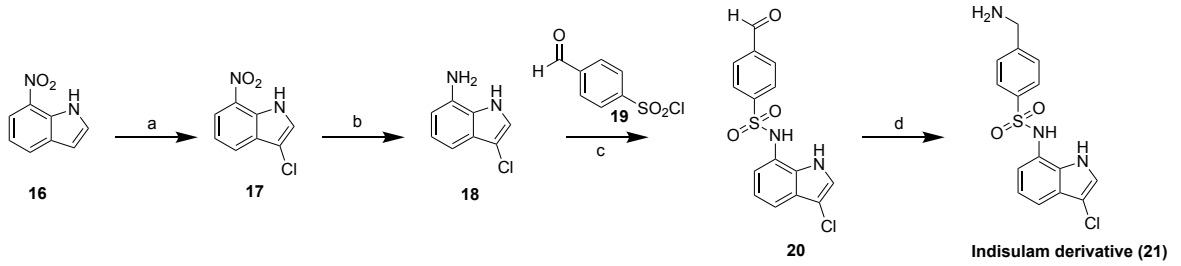

Reagents and conditions: (a) NCS, 0.1N HCl_{aq}, THF, rt, 5 h, yield 94%; (b) Fe, NH_4Cl_{aq}, 2-propanol, 80 ºC, overnight, yield quant.; (c) 4-formylbenzenesulfonyl chloride, Pyr, EtOAc, rt, 3 h, yield 62%; (d) NH_4OAc_{sat} in EtOH, $NaBCNH_3$, 30% NH_3, 100 ºC, 15 min, yield 35%

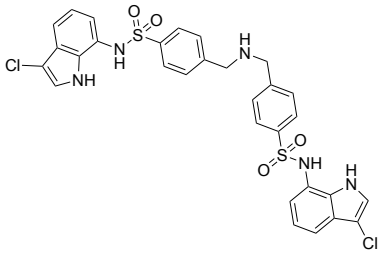

Figure 16. Undesired compound: *N*-(3-chloro-1*H*-indol-7-yl)-4-(((4-(*N*-(3-chloro-1*H*-indol-7-yl)sulfamoyl)benzyl)amino)methyl)benzenesulfonamide

2.2.2.4 Synthesis of PROTACs recruiting $CRL2^{VHL}$

The synthesis of bivalent molecules bearing VHL1 (synthesized as previously reported[48]) and BrdL1, connected by linkers with different lengths is shown in the Scheme 4. First,

polyethylene glycols were mono-protected using benzyl bromide to obtain the corresponding monobenzyl ethers **24** and **25** in good yields. Next, biphasic reaction of compounds **24** and **25** and *tert*-butyl bromoacetic acid in presence of 37% aqueous solution of NaOH, using tetrabutyl ammonium bromide (TBAB) as a phase-transfer catalyst in stoichiometric amount, led to compounds **26** and **27**. The linkers were then deprotected *via* H-cube hydrogenation affording compounds **28** and **29** in excellent yield. Compound **30** was already available in the lab, prepared as described for linkers **28** and **29** starting from PEG5.

The primary alcohol functionality of the linkers **28**-**30** was oxidized to aldehyde group under the Swern reaction conditions and condensed with BrdL1 to afford the desired compounds **31**-**33**. Further deprotection of the tert-butyloxy protecting group in acidic conditions led to intermediates **34**-**36** in quantitative yield. The HATU-mediated coupling of intermediates **34**-**36** with VHL1 led to the final compounds **VZ48**, **VZ49** and **VZ52** which were purified by preparative HPLC.

Scheme 4. Synthesis of compounds VZ48, VZ49 and VZ52

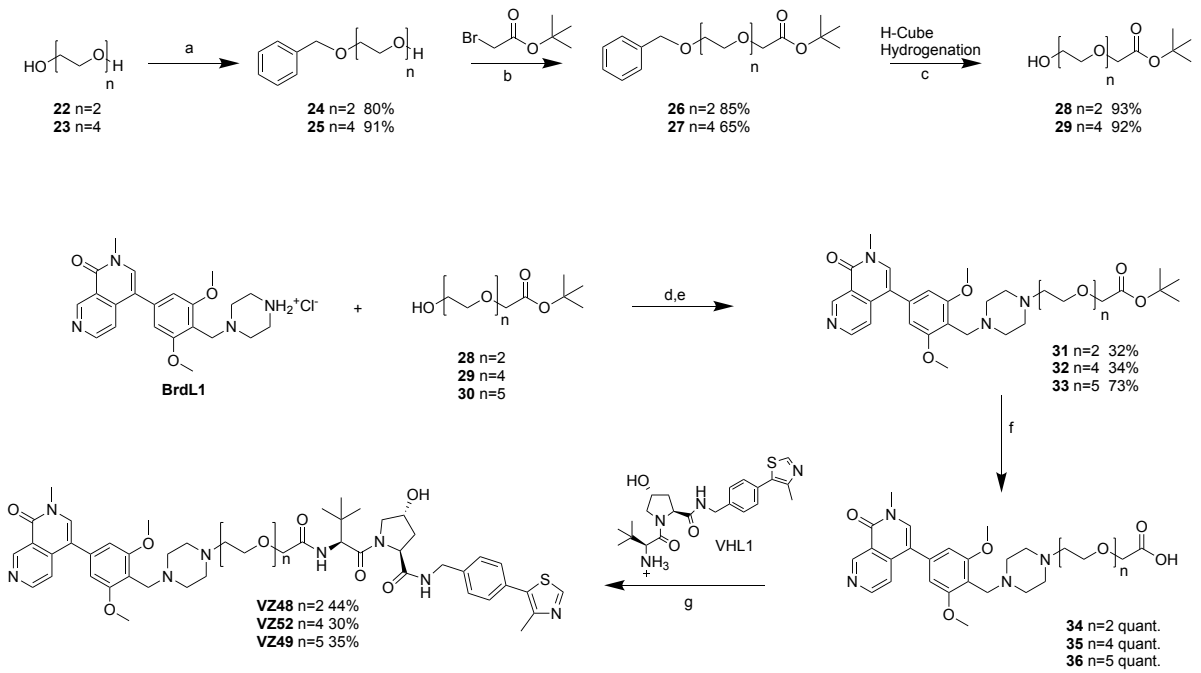

Reagents and conditions: (a) NaH, BnBr, DMF, rt, overnight; (b) *tert*-butyl-bromoacetate, TBAB, 37% NaOH/H_2O, DCM, rt, overnight; (c) EtOH, 65 ºC, 1 atm, 1 mL/min; (d) $(COCl)_2$, TEA, DMSO, DCM, -78 ºC to rt, 2 h; (e) $NaBH(OAc)_3$, TEA, DCE, rt, overnight; (f) TFA, DCM, rt, 2 h; (g) VHL1, HATU, HOAt, DIPEA, DMF, rt, 2 h

The VHL-based PROTAC **VZ55** characterized by a 11-atoms length lipophilic linker containing two oxygen atoms was prepared according to the synthetic route reported in Scheme 5. In details, the nucleophilic attack of diethylene glycol **37**, deprotonated with sodium hydride, to 6-bromo-1-hexene led to compound **38** in good yield. Oxidation of the free hydroxyl group using BAIB and TEMPO afforded the carboxylic acid **39** which was then condensed with VHL1 and compound **40** was isolated. Intermediate **40** was then oxidized under the Lemieux-Johnson conditions to the corresponding aldehyde. This reaction involved the *in situ* formation of the diol using osmium tetroxide and its subsequent cleavage by sodium periodate. The resulting aldehyde derivative was directly used for reductive amination reaction with BrdL1, affording compound **VZ55** that was purified by preparative HPLC.

Scheme 5. Synthesis of compound VZ55

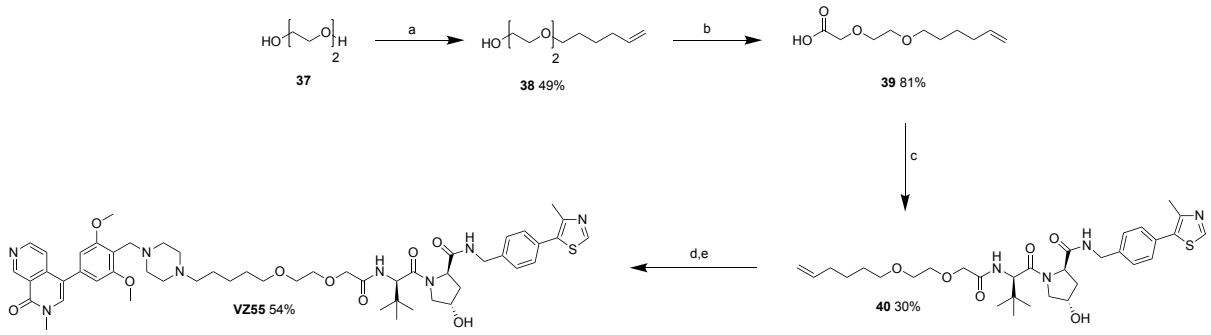

Reagents and conditions: (a) NaH, 6-bromo-1-hexene, DMF/THF, rt, overnight; (b) BAIB, TEMPO, ACN/H_2O, rt, overnight; (c) VHL1, HATU, HOAt, DIPEA, DMF, rt, 2 h; (d) OsO_4 4 wt.% in H_2O, $NaIO_4$, pyridine, dioxane/ H_2O, rt; (e) BrdL1, $NaBH(OAc)_3$, TEA, DMF, rt, overnight

A similar approach was applied for the synthesis of PROTACs **VZ95-98** and **VZ117-118** bearing linkers of 2- and 4-units of ethylene glycols attached at the position 2 of the phenyl

ring of the VHL ligand (Scheme 6). Briefly, the nucleophilic substitution of **41** and **42** with allyl bromide led to compounds **43** and **44** that were activated as mesylates and condensed with VHL2-4 to afford intermediates **45** and **50**. The alkene moieties of **45** and **50** were then oxidized to aldehyde under the Lemieux-Johnson conditions and directly reacted with BrdL1 by reductive amination to obtain the final products **VZ95-98** and **VZ117-118**. All the final compounds were purified by preparative HPLC to obtain compounds of high purity required for biological evaluation.

Scheme 6. Synthesis of compounds VZ95-98 and VZ117-118

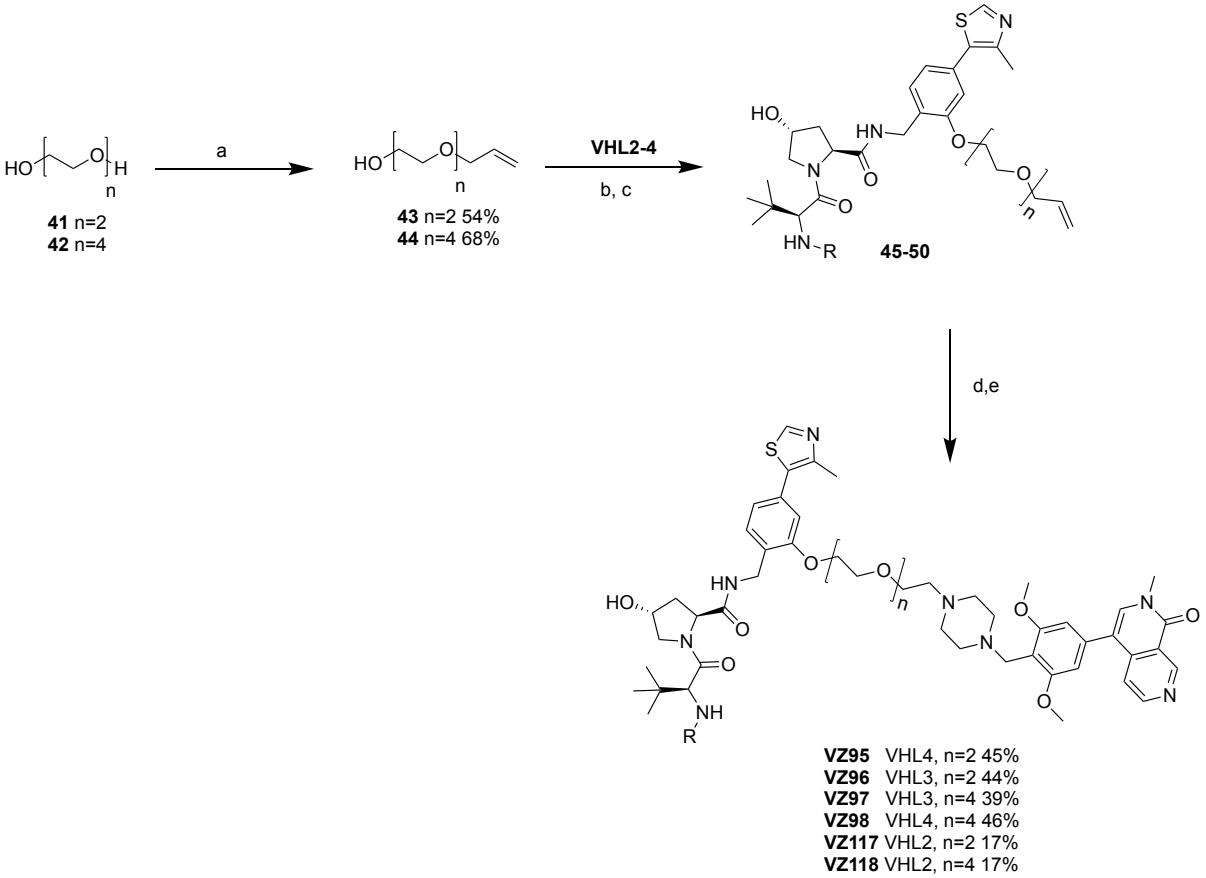

Reagents and conditions: (a) NaOH, allyl bromide, dioxane, rt, overnight; (b) MsCl, TEA, DCM, rt, 3 h; (c) VHL ligands VHL2-4, K_2CO_3, DMF, 70 ºC, overnight; (d) OsO_4, $NaIO_4$, pyridine, dioxane/ H_2O, rt; (e) BrdL1, $NaBH(OAc)_3$, TEA, DMF, rt, overnight

2.2.2.5 Synthesis of PROTACs recruiting CRL4^{CRBN} and CRL4^{DCAF15}

In this paragraph, the synthesis of molecules recruiting CRBN (**VZ109** and **VZ110**, Scheme 7) and DCAF15 (**VZ89** and **VZ90**, Scheme 7) is reported. Compounds **34** and **35** (Scheme 4) were used as key intermediates for a HATU-mediated coupling reaction with the proper E3 ligands (i.e. POMA and Indisulam derivative **21**). POMA was provided by Dr Andrea Testa, University of Dundee. Compounds **VZ89**, **VZ90**, **VZ109** and **VZ110** were purified by preparative HPLC and obtained in good yields (Scheme 7).

Scheme 7. Synthesis of compounds VZ89, VZ90, VZ109 and VZ110

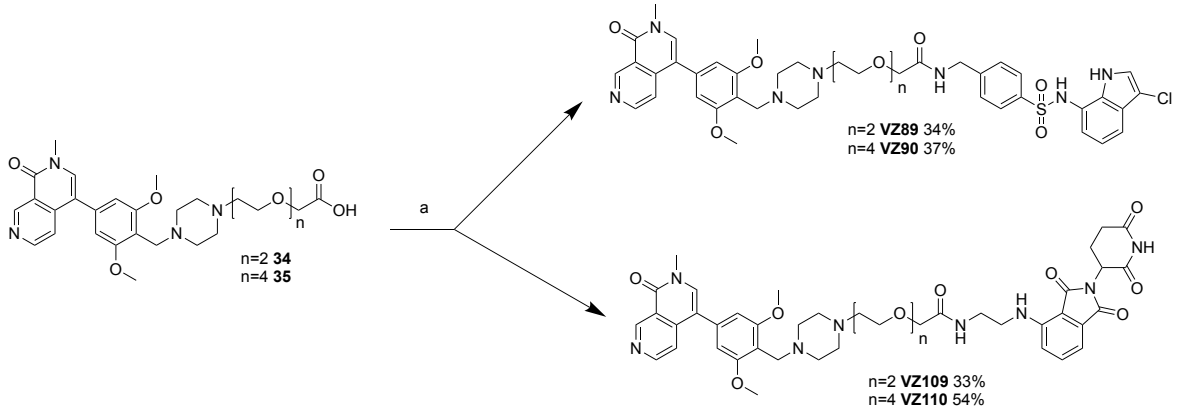

Reagents and conditions: (a) POMA or Indisulam derivative, HATU, HOAt, DIPEA, DMF, rt, 2 h

2.2.3 Biological evaluation of first-generation of PROTACs

The biological evaluation of first-generation compounds in cell-based assays is reported in the following section.

2.2.3.1 Antibodies evaluation

In order to evaluate the quality, the specificity and the ability in picking up a good signal for the protein of interest, BRD9 and BRD7 specific antibodies were tested by western blotting using lysates from both HeLa and U2OS cancer cells (Figure 17A).

For this experiment, HeLa and U2OS cells were seeded in 10 cm dishes with $2.2x10^6$ cells per dish in 10 mL media in order to achieve 85-90% confluence before lysing. In preparing samples for loading into gels, the proteins of interest needed to be released through chemical and/or mechanical methods and protease inhibitors should be added to prevent proteolysis and denaturation. Due to the nature of our target proteins, two cell lysis methods were evaluated: Ripa buffer (RB) and nuclear extraction (NE).

Radio-immunoprecipitation assay (Ripa) buffer (RB) derives its name from the original application for which it was developed, and it is a mixture of three non-ionic and ionic detergents to break membranes. NE is a chemical and physical method useful for studying molecules that interact with the nucleus such as transcription factors which bind to DNA. The solution used in NE is made of Ripa buffer supplemented with $MgCl_2$, EDTA and benzonase. NE involves also the use of ultrasonic processer (sonicator) which produces microbubbles of samples before removal of the insoluble fraction by centrifugation. Cells were lysed using both methods. Then, different concentrations of the soluble fractions (20, 30 and 40 μg) were run by SDS-PAGE on polyacrylamide gels followed by western blot using specific antibodies to probe for BRD9 and BRD7 proteins (Figure 17A). The results showed quite specific antibodies for the target proteins, as no unspecific bands were detected (Figure 17A). A better band

intensity was detected in correspondence of the HeLa cell lysates compared to U2OS, probably due to the difference in protein abundance between the two cell lines, as reported in the Human Protein Atlas (HPA) database. No particular difference in quality was noticed between the samples obtained using RB or NE lysis methods. A good signal was already detectable in the presence of 20 μg of total cell lysate in HeLa cells. For the next experiments, it was decided to use 30 μg of total cell lysate to ensure a good signal and to use RB as lysis method because milder and faster than NE.

Since the different expression levels of E3 ligases might influence PROTAC activities, we explored the protein levels in three cell lines (HeLa, Hek293 and RI-1; Figure 17B). RI-1 cells were included in the study because sensitive to BRD9 inhibition/degradation[80,127] and of clinical relevance. Indeed, RI-1 were assigned to ABC-like lymphoma subtype (activated B-cell) of DLBCL, the most aggressive type of non-Hodgkin lymphoma. Protein levels of CRBN and VHL were evaluated. Unfortunately, no anti-DCAF15 antibody could be found via commercial sources. Different concentrations of the soluble fractions (20, 30 and 40 μg) for each cell line were run by SDS-PAGE on polyacrylamide gels followed by Western Blot using specific antibodies to probe for CRBN and VHL proteins (Figure 17B). The results were analysed and it was observed that CRBN and VHL protein abundance was comparable between the three cell lines (Figure 17B). Of note, slightly less band intensity was detected in correspondence of RI-1 cell lysates compared to the HeLa and Hek293 (Figure 17B). A good signal was already detectable in the presence of 20 μg of total cell lysate.

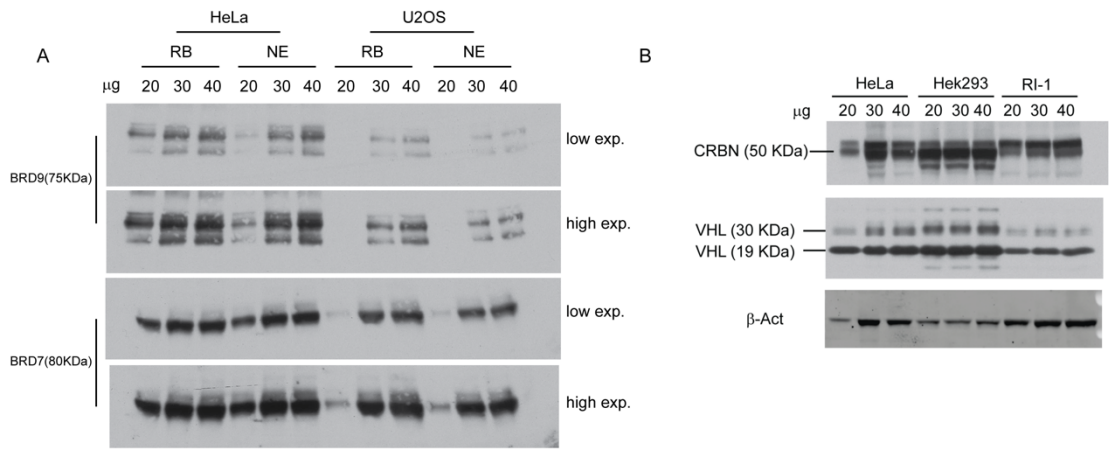

Figure 17. Expression levels of protein evaluation. A) Western-blot analysis of BRD9 and BRD7 expression level in HeLa and U2OS. B) Western-blot analysis of CRBN and VHL expression level in HeLa, Hek293 and RI-1. 20, 30 and 40 µg of soluble protein fractions were loaded for each cell line.

2.2.3.2 BRD7 and BRD9 siRNA experiments

To confirm the reliability of BRD7 and BRD9 antibodies and to be sure that the band decrease belonged to the protein of interest, BRD7 and BRD9 siRNAs were performed in HeLa cells (Figure 18). For this experiment, HeLa cells were seeded in 6 well plates with a density of $0.3x10^6$ cells per plate in 2 mL media in order to achieve 85-90% confluence the day of lysis. Cells were treated with decreasing concentrations of siRNA (from 20 nM to 1.25 nM) and negative control (NC). Knockdown of both proteins was achieved after 48 h of treatment. After cell lysis, the samples were resolved by SDS-PAGE followed by immunoblotting, using the corresponding antibodies to probe for the protein of interest. Since BRD7 blots showed two bands, two types of gels were run to increase separation and to better understand which band was the right one. In 4-12% Bis-Tris gradient pre-casted gels BRD7 correspond to the lower band, instead in 6% Bis-Tris homemade gels it is the upper one. The results confirmed a correct assignment of the bands for BRD7 and BRD9.

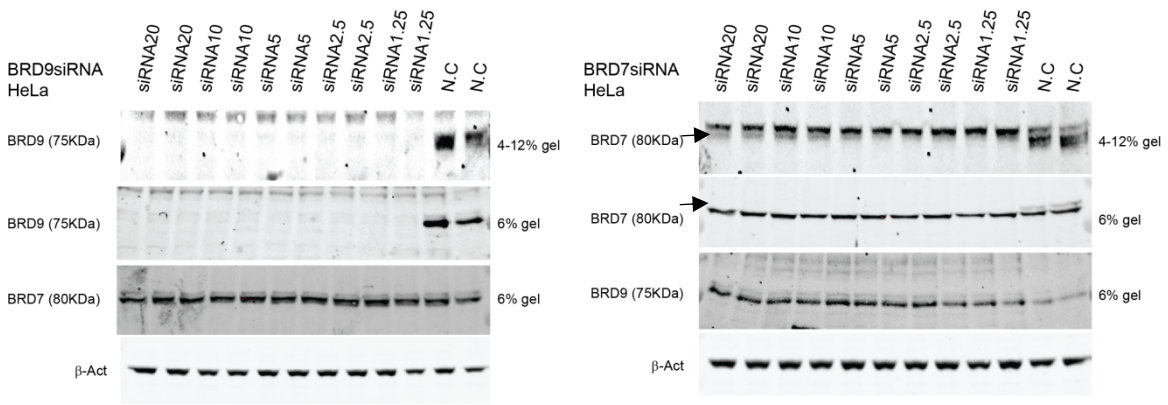

Figure 18. BRD7 and BRD9 siRNA in HeLa cells. Western-blot analysis of BRD9, BRD7 and β-actin after transfection with siRNA targeting BRD7 (blot on the right) and BRD9 (blot on the left) and negative control (N.C.) siRNA for 48 h. siRNA concentration from 1.25 to 20 nM.

The same assay was performed in RI-1 cells. Unfortunately, the silencing of BRD7/9 was not achieved with specific siRNAs in RI-1 cells, despite testing both after 48 h (Figure 19) and 72 h (data not shown). The negative result was probably due to the difficulty to transfect these suspension cells with cation lipid mediated transfection. It could be useful to repeat the experiment using a physical transfection method, like electroporation, that uses an electrical pulse to create temporary pores in cell membranes through which substances like nucleic acids can pass into cells. An alternative approach to knockdown BRD7 and BRD9 proteins should be transduction with short hairpin RNAs (shRNAs), as demonstrated in literature.[127]

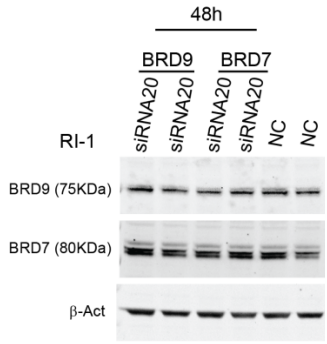

Figure 19. BRD7 and BRD9 siRNA in RI-1 cells. Western-blot analysis of BRD9, BRD7 and β-actin after transfection with 20 nM of siRNA targeting BRD7 and BRD9 and negative control (N.C.) siRNA for 48 h.

2.2.3.3 First-generation compound screening

In a first experiment, we investigated BRD7/9 degradation by recruiting different E3 ubiquitin ligases (i.e. VHL, CRBN, DCAF15), comparing compounds characterized by same BRD7/9 ligand and linkers (Figure 20). **VZ48** and **VZ52** (Table 1, Scheme 4) were chosen to recruit VHL, **VZ109** and **VZ110** (Table 2, Scheme 7) to hijack CRBN, **VZ89** and **VZ90** (Table 3, Scheme 7) for DCAF15. HeLa cells were treated with 1μM of compounds at two time points (4 h and 16 h) before harvesting. CRBN-based degrader **VZ109** and **VZ110** showed strong and preferential degradation of BRD9 already after 4 h of treatment. These data confirmed the strong activity of CRBN-recruiting PROTACs reported by Remillard *et al.*[80] while this research was underway. Conversely, VHL-based compounds as well as indisulam-based PROTACs were poorly active.

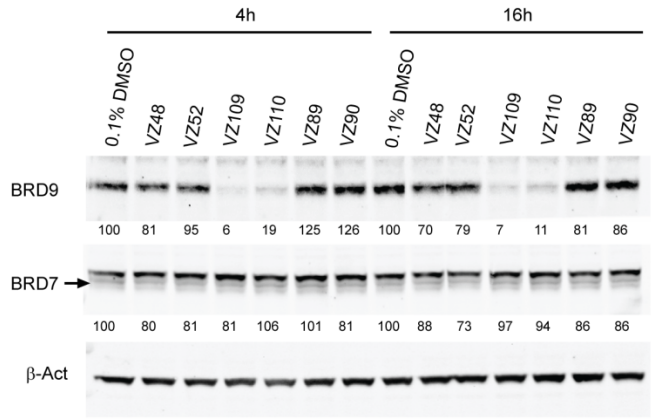

Figure 20. Screening of VZ48, VZ52, VZ109, VZ110, VZ89 and VZ90. Western-blot analysis of BRD9, BRD7 and β-actin after treatment of HeLa cells with 1 μM of compounds for 4 h and 16 h before harvesting. Degradation activity is reported below each lane as % of protein abundance relative to 0.1% DMSO vehicle. Intensity values are quantified as described in the experimental section.

Then, we decided to profile all first-generation compounds for BRD9 and BRD7 to assess their cellular activity. The six PROTACs tested in Figure 20 were included as reference compounds. A first-line screening was performed in HeLa cells treated with compounds at fixed concentration of 1μM in DMSO at two time points (4 h and 16 h) before harvesting (Figure 21). The samples, obtained after treatment and cell lysis, were resolved by SDS-PAGE followed by Western Blot using corresponding antibodies to probe for BRD9 and BRD7. Dimethylsulfoxide (DMSO vehicle, 0.1% v/v) and BI-7273[107] (BRD9 inhibitor) were used as negative controls, as no target degradation was expected under these conditions.

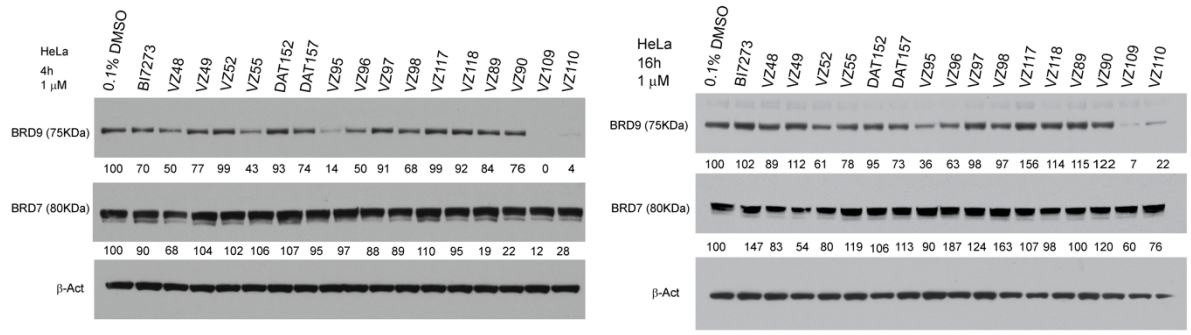

Figure 21. Screening of first generation of compounds in HeLa cells. Western-blot analysis of BRD9, BRD7 and β-actin after treatment of HeLa cells with 1 μM of compounds for 4 h (blot on the left) and 16 h (blot on the right) before harvesting. Degradation activity is reported below each lane as % of protein abundance relative to 0.1% DMSO vehicle. Intensity values are quantified as described in the experimental section.

Compound **VZ109** showed almost complete BRD9 degradation after 4-h treatment (Figure 21). Compound **VZ95** demonstrated marked depletion (around 90%) of BRD9 already after 4 h of treatment in HeLa (Figure 21). Furthermore, the replacement of an oxygen with a methylene group strongly effected BRD9 degradation after 4-h treatment (compare **VZ55** with **DAT152)**. Indeed, around 60% of BRD9 degradation was obtained after treatment with **VZ55** (Figure 21). For given matched pairs, compounds with shorter linkers showed higher degradation level (**VZ95** vs **VZ98**; **VZ96** vs **VZ97**; **VZ48** vs **DAT152**, **VZ52** and **VZ49**). Moreover, amongst conjugates derivatized at the phenolic position of the VHL ligand, the functional groups on the LHS of VHL ligand played a key role for the activity. Compounds bearing the fluoro-cyclopropyl moiety (VHL4) were more potent than those with cyano-cyclopropyl (VHL3) and acetyl group (VHL2). All compounds demonstrated preferential degradation on BRD9 over BRD7.

The first-generation compounds were also screened in Hek293 and RI-1 cells to assess consistency of the cellular effect in different cell lines which could exhibit different expression levels of BRD7 and BRD9 proteins (Figure 22 and 23). The BRD9 degradation profile of first-generation compounds was similar (even if less pronounced) in Hek293 compared to HeLa

(Figure 21 and 22). **VZ109** was the most active compound showing more than 80% of BRD9 depletion, while **VZ95** demonstrated around 50% of BRD9 degradation after 16 h (Figure 22). Quantification of BRD7 proved to be difficult due to the broad bands.

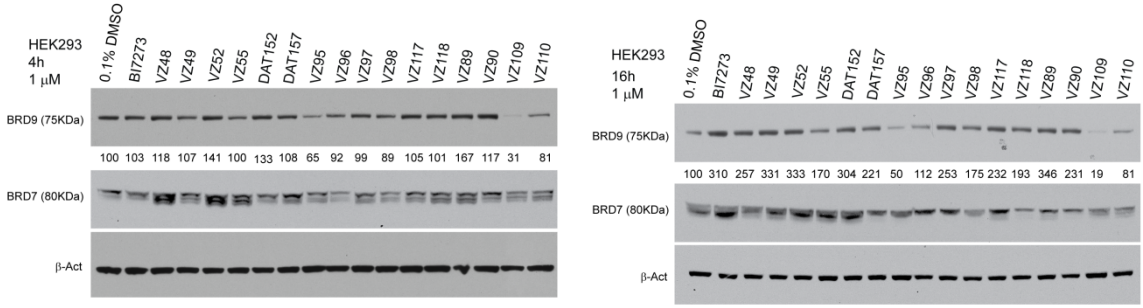

Figure 22. Screening of first generation of compounds in Hek293 cells. Western-blot analysis of BRD9, BRD7 and β-actin after treatment of Hek293 cells with 1 μM of compounds for 4 h (blot on the left) and 16 h (blot on the right) before harvesting. Degradation activity is reported below each lane as % of protein abundance relative to 0.1% DMSO vehicle. Intensity values are quantified as described in the experimental section.

RI-1 cells were treated with 1 μM of compounds for 2 and 8 h before lysis (Figure 23). Shorter time points were chosen compared HeLa and Hek293 cells due to the sensitivity of BRD9 depletion in lymphoma cells. The results confirmed the superior activity of CRBN-based compounds (**VZ109** and **VZ110**) followed by the VHL-based degrader **VZ95** (Figure 23). **VZ109** and **VZ110** induce complete degradation of BRD9 already after 2-h treatment, while **VZ95** reaches 35% of BRD9 depletion (Figure 23).

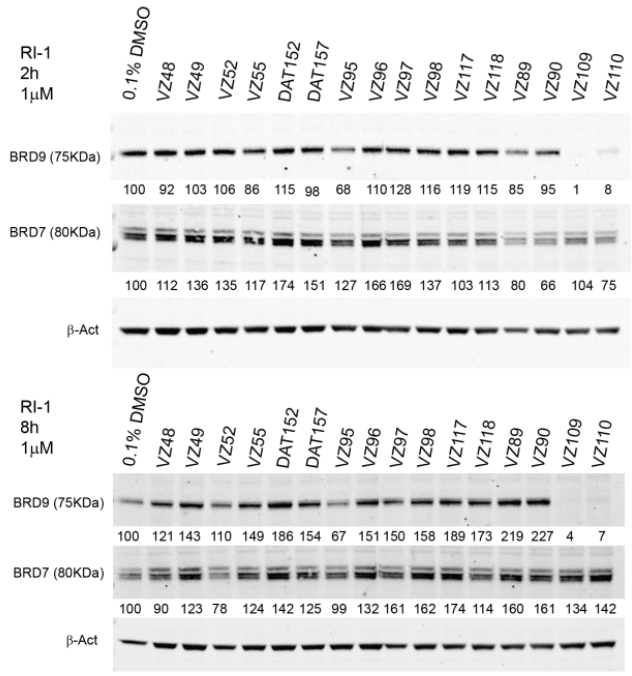

Figure 23. Screening of first generation of compounds in RI-1 cells. Western-blot analysis of BRD9, BRD7 and β-actin after treatment of RI-1 cells with 1 μM of compounds for 2 h (blot on the top) and 8 h (blot on the bottom) before harvesting. Degradation activity is reported below each lane as % of protein abundance relative to 0.1% DMSO vehicle. Intensity values are quantified as described in the experimental section.

2.2.3.4 Time-dependency evaluation VZ55, VZ95 and VZ109

The best compounds identified from the first line screen were profiled for their cellular activities over time. HeLa and Hek293 cells were treated with **VZ55**, **VZ95** and **VZ109** (1 μM concentration) at the desired time points using dimethylsulfoxide (DMSO, 0.1% v/v) as negative vehicle (Figure 24).

The results obtained were consistent with those observed in the previous experiments. Degradation in HeLa cells was more pronounced than in Hek293. A possible explanation could be different permeability of these compounds through the cellular membrane and the different protein expression levels in the two cell lines. Compound **VZ109** was confirmed to be the most active compound in HeLa, decreasing BRD9 level by nearly 90% already after 30 min and almost complete depletion was reached after 4 h treatment. Conversely, **VZ95** induced 70% of degradation after 2 h treatment, resulting in an apparent half-life of 3.5 h (Figure 25). Some

degradation of BRD9 was also observed for **VZ55**, albeit only around 40% after 24 h; based on these results, we decided to drop **VZ55** for further investigation moving forward. Moreover, the results of the degradation assay showed consistent selectivity on BRD9 over BRD7.

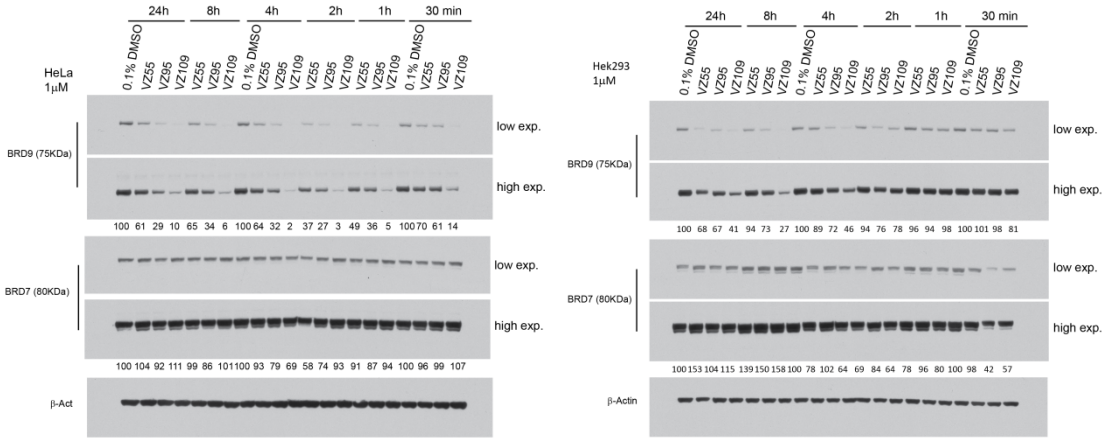

Figure 24. Time dependency evaluation of compounds VZ55, VZ95 and VZ109. Western-blot analysis of BRD9, BRD7 and β-actin after treatment of HeLa (blot on the left) and Hek293 (blot on the right) with 1 μM of compounds at the desired time points before harvesting. Degradation activity is reported below each lane as % of protein abundance relative to 0.1% DMSO vehicle. Intensity values are quantified as described in the experimental section.

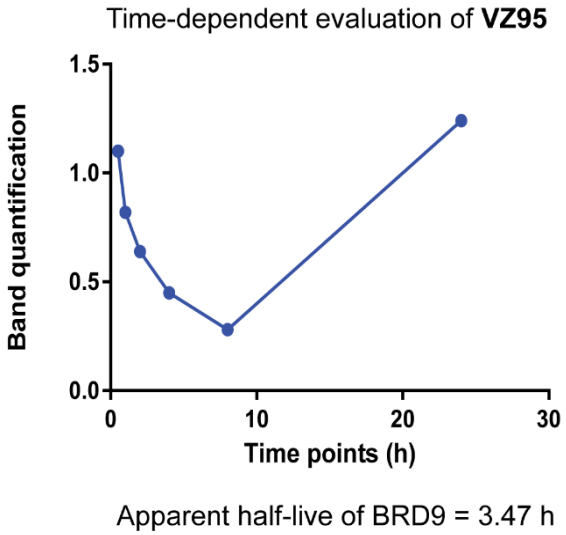

Figure 25. Compound VZ95 induces rapid degradation of BRD9 in HeLa cells. Quantification of BRD9 protein levels after treatment of HeLa with 1 μM of **VZ95** through 24 h. Intensity values and half-live were quantified as described in the experimental section.

2.2.3.5 Concentration-dependency experiment of VZ95 and VZ109

Compounds **VZ95** and **VZ109** were further characterized by profiling their concentration-dependent activity in HeLa and Hek293 cells at early time points, 30 min and 4 h before lysis (Figure 26). Both compounds induced preferential degradation of BRD9 over BRD7 in a concentration-dependent manner, with higher activity at higher concentration. PROTAC **VZ95** induced more than 60% of degradation of BRD9 at 1 μM after 4 h, while maximal degradation (D_{max} around 80%) was reached at 10 μM (Figure 26). The calculated half-degrading concentration (DC_{50}) was 560 nM against BRD9 after 4 h (Figure 27). At high concentrations **VZ95** preferentially acted as inhibitor over degrader. This known effect is described as "hook effect":[90] at high PROTAC concentrations binary complexes (Target protein:PROTAC and E3Ligase:PROTAC) are preferentially formed and compete and ultimately overcome formation of the ternary complex.

VZ109 confirmed to be the most active compound inducing more than 70% of BRD9 degradation at 100 nM after 4 h and reaching maximal degradation (D_{max}) at 10 μM (Figure 26). **VZ95** emerged to be approximately 10-fold less activity than **VZ109** as it needed more time to reach a comparable decrease of intensity of the BRD9 band. Indeed, at 1 μM of **VZ95** more than 60% of depletion of BRD9 was reached after 4 h treatment, while the same degradation rate was obtained after 30 min when cells were treated with **VZ109**.

Consistent with previous observations, the degradation activity of BRD9 was less pronounced in Hek293 cells (Figure 26). **VZ95** induced maximal BRD9 degradation (around 40%) at 10 μM, while more than 90% of depletion of BRD9 level was obtained with 10μM of **VZ109** after 4 h treatment (Figure 26).

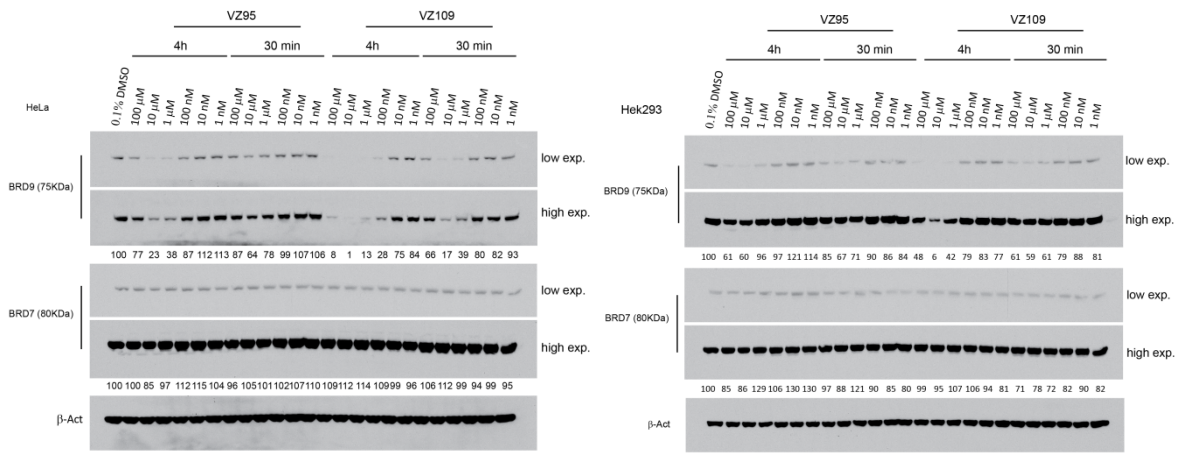

Figure 26. Concentration dependency evaluation of compounds VZ95 and VZ109. Western-blot analysis of BRD9, BRD7 and β-actin after treatment of HeLa (blot on the left) and Hek293 (blot on the right) with six different concentration at 30 min and 4 h before harvesting. Degradation activity is reported below each lane as % of protein abundance relative to 0.1% DMSO vehicle. Intensity values are quantified as described in the experimental section.

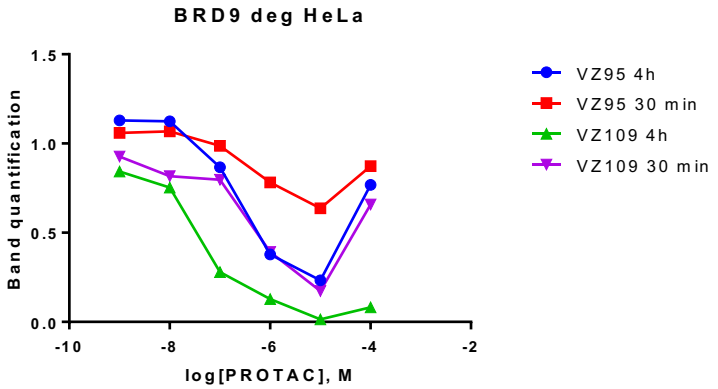

DC_{50} **VZ95** (4h) = 560 nM
DC_{50} **VZ109** (4h) = 45 nM

Figure 27. **Quantification of BRD9 protein level.** HeLa cells were treated with six different concentrations of **VZ95** and **VZ109** at 30 min and 4 h before harvesting. Intensity values and DC_{50} were quantified as described in the experimental section.

2.3 Summary first-generation of compounds

The first generation of compounds allowed the identification of **VZ95** as a novel VHL-based PROTACs targeting BRD9 protein. Following a first-line screening in different cancer cell lines, compound **VZ95** was further characterized by profiling its cellular activity in a concentration-dependent evaluation and over time. CRBN-recruiting PROTAC **VZ109** demonstrated the strongest degradation activity confirming the results disclosed by Remillard *et al*.[80] Nevertheless, we focused our attention to VHL-recruiting PROTACs which could provide advantages compared to PROTACs recruiting CRBN, known to exhibit off-target degradation of IKZF1/3 and GSPT1.[80,132]

2.4 Design, synthesis and biological evaluation of second-generation degraders

The discovery of **VZ95** as VHL-based degrader of BRD9 prompted the design of a second generation of PROTACs with the goal to further improve degradation activity. In the next paragraphs, the design, synthesis and biological evaluation of second-generation compounds targeting BRD7 and BRD9 proteins will be described.

2.4.1 Design of second generation of compounds

The design of the second generation of BRD7/9-targeting PROTACs was guided by the early structure-activity relationship emerged from the first-generation molecules. The new generation compounds comprised three sets of molecules. Two of those were based on **VZ95** by keeping constant the VHL ligand (namely, VHL4) whereas the linker length and composition, as well as the substitution and conjugation chemistry at the BRD7/9 portion were changed. In the third set of derivatives, a different derivatization point on BRD7/9 moiety was identified and VHL1 was selected as VHL ligand.

2.4.1.1 Type of linkers

Linkers characterized by different ratios between hydrophilic and lipophilic portions were explored. Varying the balance between hydrophilicity and lipophilicity might not only affect cell permeability but also influence the conformational equilibria and intrinsic folding propensity of the linker, with direct impact on the process of ternary complex formation. Therefore, linkers with different lengths (i.e. 5, 8, 11 and 14 atoms) and number of oxygen atoms were employed.

2.4.1.2 Design of BrdL1/2- Linker-VHL4 PROTACs (first set)

As previously reported, the design strategy was to keep fixed the VHL4 moiety (VHL ligand) and to hijack BRD7/9 protein with BrdL1 (as first generation) along with its analogue BrdL2 (Table 4). Based on the SARs of BRD7/9 bromodomain inhibitors developed by Martin *et al.*,[107] we reasoned to arrange the methoxy groups on the phenyl ring in either meta (BrdL1 - as first generation) or para (BrdL2) relative to each other (Table 4). Linkers with various length (5-, 8- and 11-atoms) and composition (0-, 1-, 2- and 3- oxygen atoms) were used to connect the two warheads *via* tertiary amine bond (Table 4).

Table 4. First set BrdL1/2- Linker-VHL4

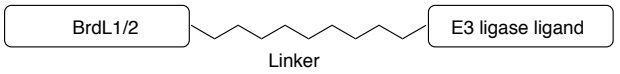

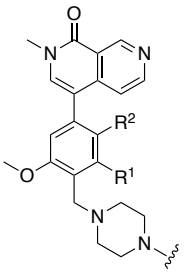

BrdL1 R^1=OCH_3, R^2=H
BrdL2 R^1=H, R^2=OCH_3

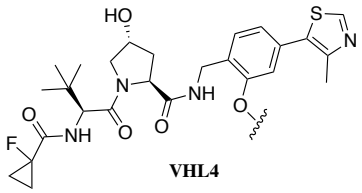

VHL4

Structural features of first-set PROTACs				
Code	**BrdL**	**Linker**	**Linker length (atoms)**	**# of O**
VZ185	BrdL1		5	0
VZ186	BrdL2		5	0
VZ166	BrdL1	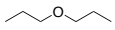	5	1
VZ167	BrdL2		5	1
VZ221	BrdL1	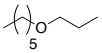	8	1
VZ222	BrdL2		8	1
VZ169	BrdL2	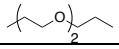	8	2
VZ182	BrdL1	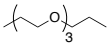	11	3
VZ183	BrdL2		11	3

2.4.1.3 Design of BrdL3/4- Linker-VHL4 PROTACs (second set)

In the second set of compounds we replaced the piperazine moiety of BrdL1/2 with an azetidine group (BrdL3 and BrdL4; Table 5). The azetidine substituent was disclosed by Martin *et al.*[107] as the best vector to boost potency by addressing the backbone carbonyl of His42. BrdL3/4 moieties were connected to the linkers *via* amide bond (Table 5).

Table 5. Second set BrdL3/4- Linker-VHL4

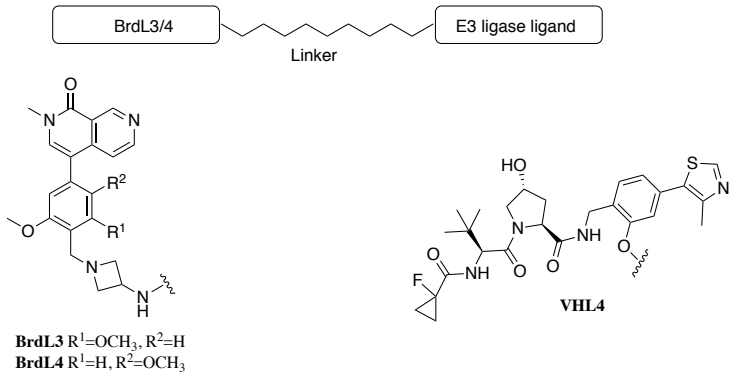

BrdL3 R^1=OCH_3, R^2=H
BrdL4 R^1=H, R^2=OCH_3

Structural features of second-set PROTACs				
Code	**BrdL**	**Linker**	**Linker length (atoms)**	**# of O**
VZ215	BrdL3	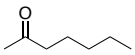	5	0
VZ216	BrdL4		5	0
VZ200	BrdL3	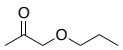	5	1
VZ201	BrdL4		5	1
VZ223	BrdL3	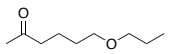	8	1
VZ224	BrdL4		8	1
VZ207	BrdL3	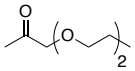	8	2
VZ208	BrdL4		8	2
VZ209	BrdL3	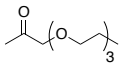	11	3
VZ210	BrdL4		11	3

2.4.1.4 Design of BrdL5/6- Linker-VHL4 PROTACs (third set)

To address the question if the egress point of the linkers on the target ligands would affect the activity of degraders, a third set of molecules was designed characterized by different derivatization vectors of BRD7/9 and VHL ligand.

Guided by the SAR of BRD7/9 ligand published by Crawford *et al.*,[108] we replaced the pyrimido-pyridinone core of BrdL1-4 with a pyrrolo-pyridinone scaffold (Table 6). Pyrrole moiety provided a solvent-exposed vector at position 2 for the attachment of the linkers.[108] We explored both meta- (BrdL5) and para-substituted (BrdL6) dimethoxy group on the phenyl ring (Table 6). As VHL ligand, we replaced VHL4 moiety present in compound **VZ95** with VHL1 (as first generation of degraders). To link the two warheads PEG linkers with 11 and 14 atoms were studied (Table 6).

Table 6. Third set of BrdL5/6- Linker-VHL1

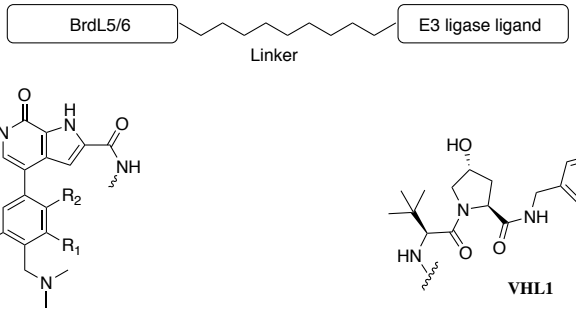

BrdL5 R_1=OCH_3, R_2=H
BrdL6 R_1=H, R_2=OCH_3

Structural features of second-set PROTACs					
Code	**BrdL**	**Linker**	**E3 ligand**	**Linker length (atoms)**	**# of O**
VZ192	BrdL5	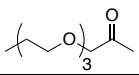	VHL1	11	3
DAT477[a]	BrdL6			11	3
VZ193	BrdL5	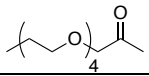		14	4
VZ194	BrdL6			14	4

[a] Provided by Dr Andrea Testa, University of Dundee

2.4.2 Synthetic routes of second-generation compounds

In this chapter, the synthetic procedures to prepare the compounds of the second generation are described. It is reported the synthetic routes of BrdL1 analogues, the synthesis of the linkers and assembly of the final compounds.

2.4.2.1 Synthesis of BRD7/9 ligands BrdL2-6

BrdL2 is a BrdL1 analogue with a different dimethoxy substitution pattern on the phenyl ring. Its synthesis is similar to that reported for BrdL1 (Scheme 1) using 4-bromo-2,5-dimethoxy- instead of 4-bromo-2,6-dimethoxy-benzaldhehyde (Scheme 8).

Scheme 8. Synthesis BrdL2

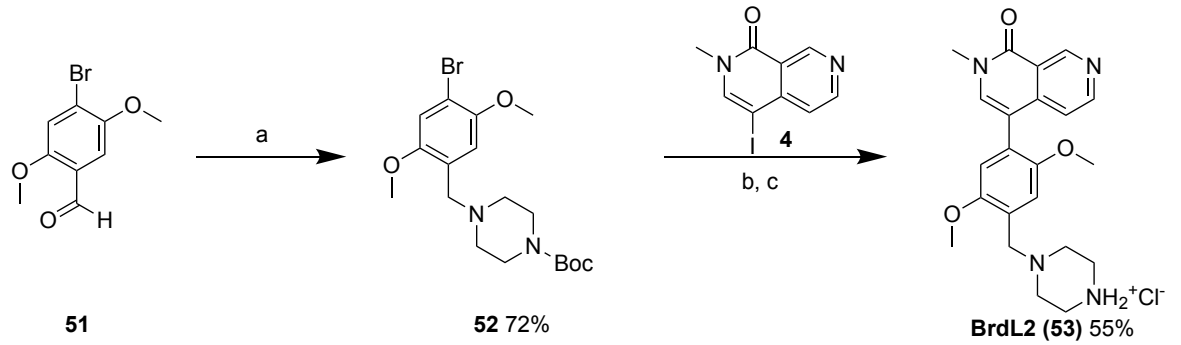

51 **52** 72% **BrdL2 (53)** 55%

Reagents and conditions: (a) Boc-piperazine, $NaBH(OAc)_3$, THF, rt, overnight; (b) step 1: **52**, B_2pin_2, KOAc, $Pd(dppf)Cl_2$, 1,4 dioxane, μw 140 ºC, 40 min; step 2: **4**, K_2CO_3 (aq) are added to step 1, μw 120 ºC, 30 min; (c) HCl 4M in dioxane, DCM, rt, 1 h

A similar approach was applied to obtain BrdL3 (**57**) and BrdL4 (**58**) warheads (Scheme 9). Briefly, compounds **55** and **56** were obtained by reductive amination between 4-bromo-2,6-dimethoxy- (**5**) or 4-bromo-2,5-dimethoxy-benzaldhehyde (**51**) and 3-(Boc-amino)azetidine (**54**) in good yield. Then, Miyaura-Suzuki cross-coupling was conducted between the organic halide **4** and the proper bromophenyl derivative (**55** or **56**). Finally, the cleavage of the tert-

butyloxycarbonyl protecting group in acidic conditions led to the desired compounds **57** and **58** (Scheme 9).

Scheme 9. Synthesis of BrdL3 and BrdL4

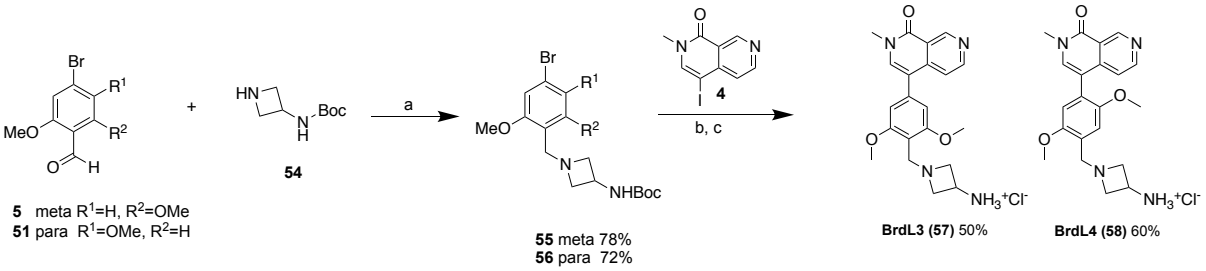

Reagents and conditions: (a) $NaBH(OAc)_3$, THF, rt, overnight; (b) step 1: **55** or **56**, B_2pin_2, KOAc, $Pd(dppf)Cl_2$, 1,4 dioxane, μw 140 ºC, 40 min; step 2: **4**, K_2CO_3 (aq) are added to step 1, μw 120 ºC, 30 min; (c) HCl 4M in dioxane, DCM, rt, 1 h

The synthesis of BrdL5 (**65**) and BrdL6 (**66**) ligands is reported in Scheme 10. In details, Miyaura-Suzuki cross-coupling was conducted between **62** (provided by Dr. Testa, University of Dundee) and **60** or **61**, previously obtained by reductive amination between 4-bromo-2,6-dimethoxy- (**5**) or 4-bromo-2,5-dimethoxy benzaldehyde (**51**) and dimethylamine in quantitative yield. Then, cleavage of tosyl group and hydrolysis of ethyl ester of compounds **63** and **64** was carried out in basic conditions, affording BrdL5 and BrdL6, respectively.

Scheme 10. Synthesis of BrdL5 and BrdL6

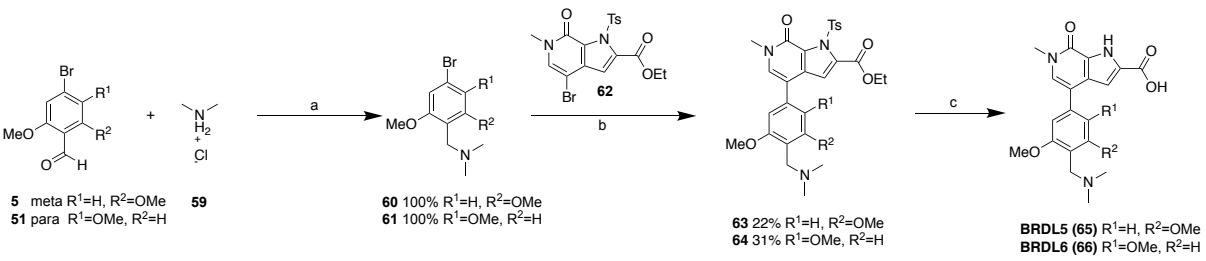

Reagents and conditions: (a) $NaBH(OAc)_3$, NaOAc, AcOH, DCM, rt, overnight; (b) step 1: **60** or **61**, B_2pin_2, KOAc, $Pd(dppf)Cl_2$, 1,4 dioxane, μw 140 ºC, 40 min; step 2: **62**, K_2CO_3 (aq) are added to step 1, μw 120 ºC, 30 min; (c) LiOH/MeOH, rt, 2 h, quant yield

2.4.2.2 Synthesis of BrdL1/2- Linker-VHL4 PROTACs (first set)

The first set of molecules bear VHL4 moiety and BrdL1/2 derivatives, connected by linkers with different lengths (Scheme 11 and 12). For the synthesis of **VZ95** and its analogues, we used osmium tetroxide as reagent for Lemieux-Johnson reaction to oxidize a double bond of the linker to aldehyde. To circumvent the use of this hazardous reagent, the synthetic protocol was modified (Scheme 11 and 12). Briefly, nucleophilic substitution between polyethylene glycols **67**-**69** and bromoacetaldehyde diethyl acetal led to the formation of intermediates **70**-**72** in good yields. In details, PEG was deprotonated using a 1 M solution of NaHMDS in THF at 0 ºC for 1 h, then a DMF solution of bromoacetaldehyde diethyl acetal was added. The reaction mixture was heated at 130 °C in microwave for 2 h in a sealed vial. The use of microwave conditions improved the time (2 days with conventional heating) and the yield of the reactions. Next, compounds **70**-**72** and **83** were activated as mesylates to allow nucleophilic attack by the phenoxy group of VHL4 scaffold. Conversely, the lipophilic chain **74**, obtained from ethyl 5-bromovalerate **73**, was conjugated to VHL4 *via* alkylation. Then, the diacetal functional groups on **75**-**78** and **84** were hydrolyzed under acidic conditions to afford the corresponding aldehydes which were condensed with BrdL1 or BrdL2 *via* reductive amination (Scheme 11 and 12).

The final compounds were purified by preparative HPLC in order to obtain compounds of high purity required for biological evaluation.

Scheme 11. Synthesis of first set of degraders

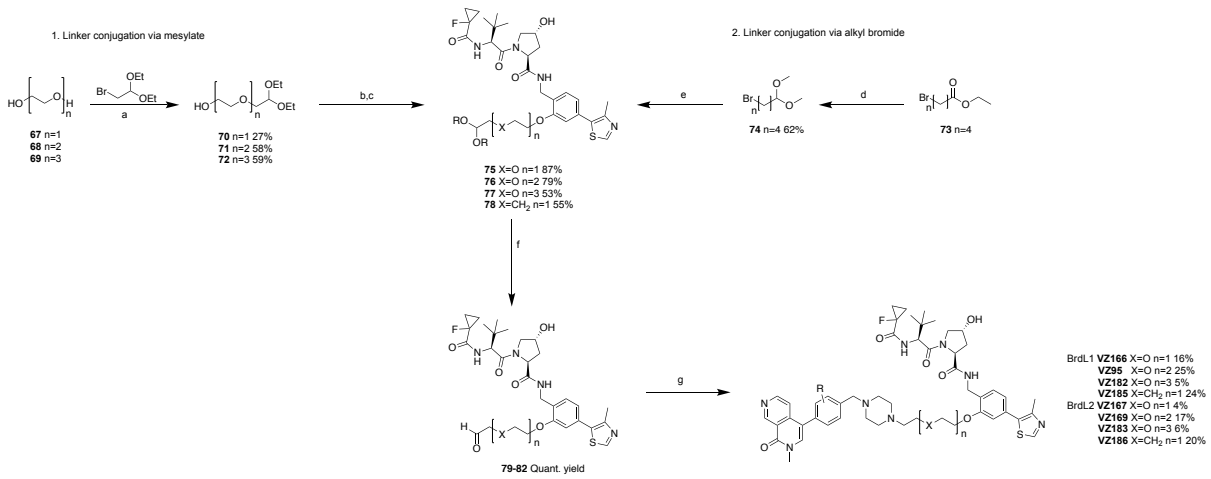

Reagents and conditions: (a) PEG, NaHMDS 1M in THF, 0 ºC, 1 h, then bromoacetaldehyde diethyl acetal, DMF, 130 ºC μw, 2 h; (b) MsCl, TEA, DCM, rt, 3 h; (c) VHL4, K_2CO_3, DMF, 70 ºC, overnight; (d) DIBALH, then MeOH, from -78 ºC to rt, overnight; (e) K_2CO_3, DMF, 70 ºC, overnight; (f) HCl 1N, THF (1:1), 50 ºC, 2 h; (g) BrdL1-2, $NaBH(OAc)_3$, TEA, DMF, rt, overnight.

Scheme 12. Synthesis of first set of degraders VZ221 and VZ222

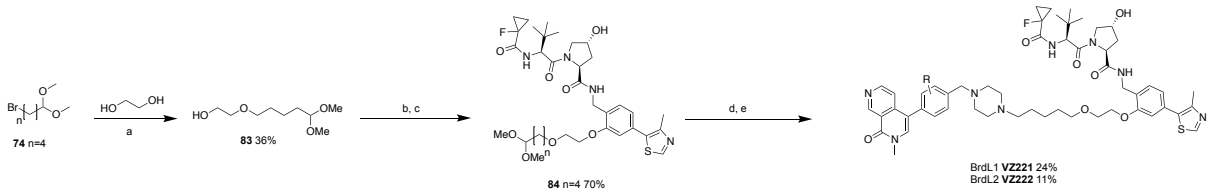

Reagents and conditions: (a) PEG, NaHMDS 1M in THF, 0 ºC, 1 h, then **74**, DMF, 130 ºC μw, 2 h; (b) MsCl, TEA, DCM, rt, 3 h; (c) VHL4, K_2CO_3, DMF, 70 ºC, overnight; (d) HCl 1N, THF (1:1), 50 ºC, 2 h, quant. yield; (e) BrdL1-2, $NaBH(OAc)_3$, TEA, DMF, rt, overnight.

2.4.2.3 Synthesis of BrdL3/4- Linker-VHL4 PROTACs (second set)

In Scheme 13 is reported the synthesis of second set of degraders bearing BrdL3 and BrdL4 moieties as BRD7/9 ligands. VHL-linker aldehyde intermediates **79**-**82** (Scheme 11) and aldehyde obtained from **84** (Scheme 12) were oxidized to acid through Pinnick reaction using sodium chlorite under mild acidic conditions. Then, HATU-mediated couplings with BrdL3 or BrdL4 were applied to obtain the final compounds which were purified by preparative HPLC (Scheme 13).

Scheme 13. Synthesis of second set of degraders

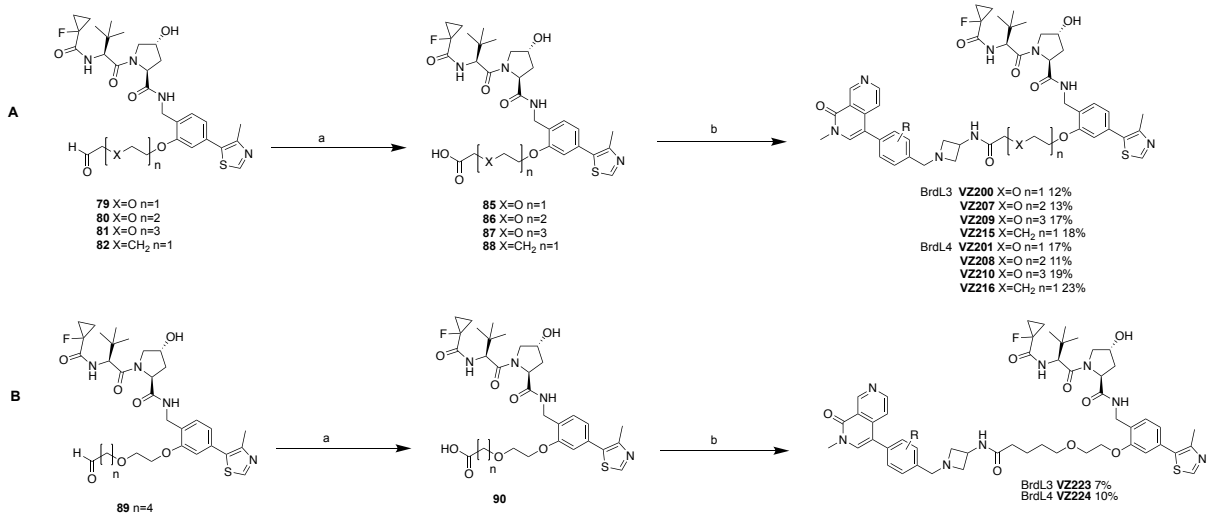

Reagents and conditions: (a) Na_2HPO_4, $NaClO_2$, 2-methyl-2-butene, t-BuOH, H_2O, rt, 4 h, quant. yield; (c) BrdL3-4, HATU, HOAt, DIPEA, DMF, rt, 2 h

2.4.2.4 Synthesis of BrdL5/6- Linker-VHL1 PROTACs (third set)

The synthesis of the third set of compounds included the assembly of final PROTACs starting from some intermediates already published in literature (Scheme 14). First, the linkers bearing a carboxylic acid on one end and an azide on the other end, characterized by 3- (**92**) and 4- (**93**) ethylene glycol units, were connected with the free amine of VHL1 scaffold (synthetized as reported in literature[48]) by amide bond formation using HATU as coupling agent. Then, the desired final compounds were obtained after reduction of the azide groups to amine (**94** and **95**) followed by coupling reactions with the carboxylic acid present on BrdL5 and BrdL6 building blocks. The final molecules **VZ192**, **VZ193**, **DAT477** and **VZ194** were purified by preparative HPLC.

Scheme 14. Synthesis of third set of degraders

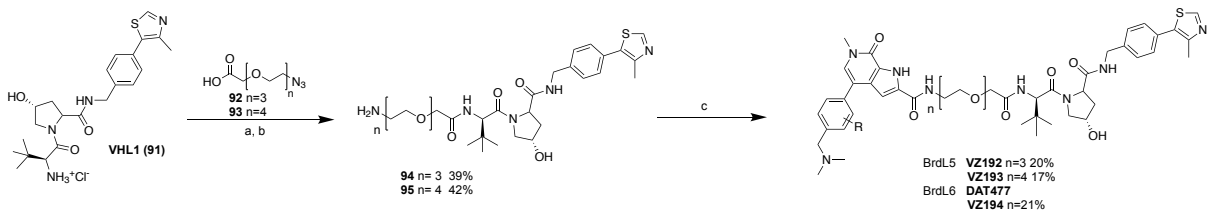

Reagents and conditions: (a) HATU, HOAt, DIPEA, DMF, rt, 2 h; (b) H_2, Pd/C, EtOH, rt, 5 h; (c) BrdL5-6, HATU, HOAt, DIPEA, DMF, rt, 2 h

2.4.2.5 Synthesis of *cis*VZ185

Since the *trans* stereochemistry of the hydroxyl group of the hydroxyproline moiety on VHL ligand is essential for the binding to VHL, the inactive negative control ***cis*VZ185** of our best compound **VZ185** (*vide infra* section 2.4.3.2) has been synthetized (Scheme 15). The synthetic strategy involved the synthesis of *cis*VHL ligand **100** followed its inclusion in the final compound. Briefly, compound **9** (synthesized as reported in Scheme 2) was coupled with N-Boc-*cis*-4-hydroxy-L-proline to obtain derivative **96** that after BOC deprotection was coupled with Boc-L-*tert*-leucine to afford intermediate **98**. Deprotection and HATU-mediated coupling with 1-fluoro-cyclopropanecarboxylic acid led to the desired derivative **100**.

The last steps involved the attachment of the linker and BrdL1 moiety. Thus, the alkylation of derivative **100** with alkyl bromide **74** (Scheme 11) led to the diacetal compound **101** that was hydrolysed to aldehyde **102** and reacted by reductive amination with BrdL1. The final molecules ***cis*VZ185** was purified by preparative HPLC.

Scheme 15. Synthesis of *cis*VZ185

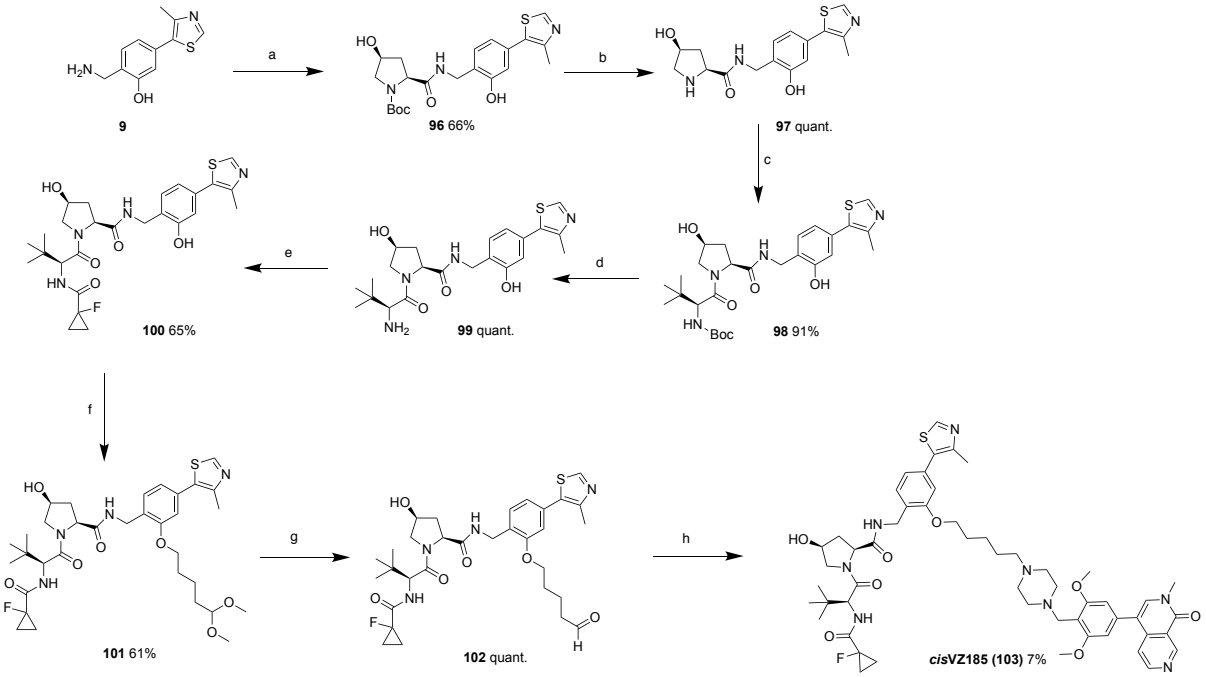

Reagents and conditions: (a) N-Boc-*cis*-4-hydroxy-L-proline, HATU, HOAt, DIPEA, DMF, rt, 1 h; (b) 4M HCl in dioxane, rt, 1.5 h; (d) Boc-L-tert-leucine, HATU, HOAt, DIPEA, DMF, rt, 1 h; (d) 4M HCl in dioxane, rt, 1.5 h; (e) 1-fluoro-cyclopropanecarboxylic acid, HATU, HOAt, DIPEA, DMF, rt, 1 h; (f) **74**, K_2CO_3, DMF, 70 ºC, overnight; (g) HCl 1N, THF (1:1), 50 ºC, 2 h; (h) BrdL1, $NaBH(OAc)_3$, TEA, DMF, rt, overnight.

2.4.3 Biological evaluation of second-generation of PROTACs

In the following section, the biological evaluation of second-generation compounds in cells is reported. The work also includes mechanistic, cytotoxicity evaluation and proteomic experiments of selected compounds.

2.4.3.1 Second-generation compounds screening

In order to assess degradation activity, all compounds of the second generation were screened in different cell lines (Figure 28-31). HeLa cells were treated with 1 μM of compounds in DMSO at two time points (4 and 16 h) (Figure 28). The lysates were evaluated by immunoblotting and the protein levels were monitored by incubation with corresponding antibodies to probe for BRD9 and BRD7. Dimethylsulfoxide (DMSO vehicle, 0.1% v/v) was used as a negative control. **VZ95**, the most active VHL-recruiting degrader of the first generation, was included as a positive control to allow direct comparison. Several compounds (Figure 28) demonstrated efficient degradation (more than 90%) of both BRD7 and BRD9 already after 4 h of treatment. All compounds demonstrated selective degradation of BRD7/9 over BRD4, screened to evaluate potential off-target effects (Figure 29).

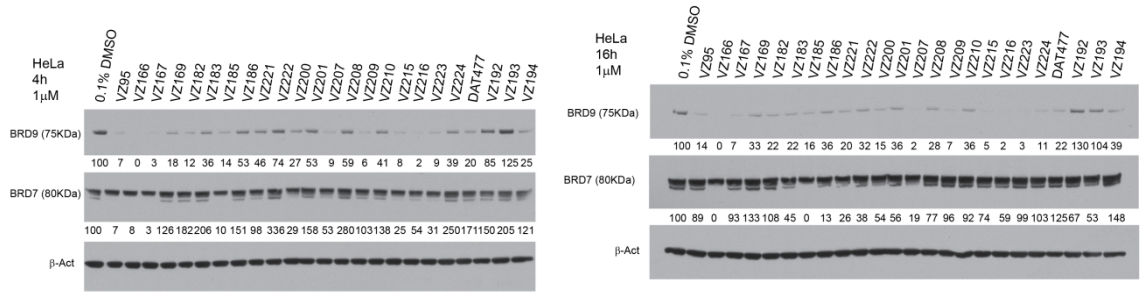

Figure 28. Screening of second generation of degraders in HeLa cells. Western-blot analysis of BRD9, BRD7 and β-actin after treatment of HeLa cells with 1 μM of compounds for 4 h (blot on the left) and 16 h (blot on the right) before harvesting. Degradation activity is reported below each lane as % of protein abundance relative to 0.1% DMSO vehicle. Intensity values quantified as described in the experimental section.

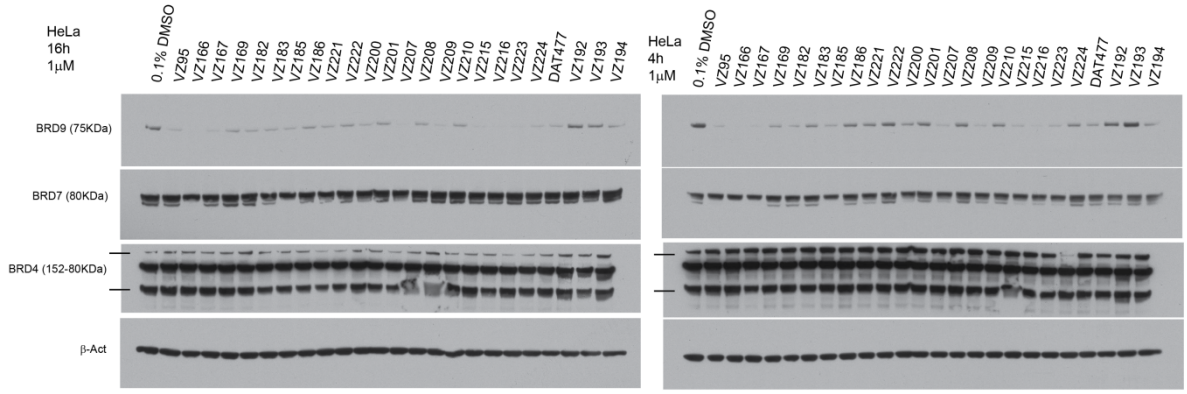

Figure 29. Selectivity evaluation of second generation of degraders for BRD4, BRD7 and BRD9. Western-blot analysis of BRD9, BRD7, BRD4 and β-actin after treatment of HeLa cells with 1 μM of compounds for 4 h (blot on the right) and 16 h (blot on the left) before harvesting.

The same experiments were also performed on Hek293 and RI-1 cell lines, to assess consistency of the degradation effect in different cell lines (Figure 30-31). Comparable degradation profile between HeLa and Hek293 was observed in decreasing both protein levels. Quantification of BRD7 and BRD9 protein levels in Figure 30 has proved to be difficult due to the broad bands. Constantly all compounds showed selectivity for BRD7 and BRD9 over the analogue BET protein BRD4 (Figure 30).

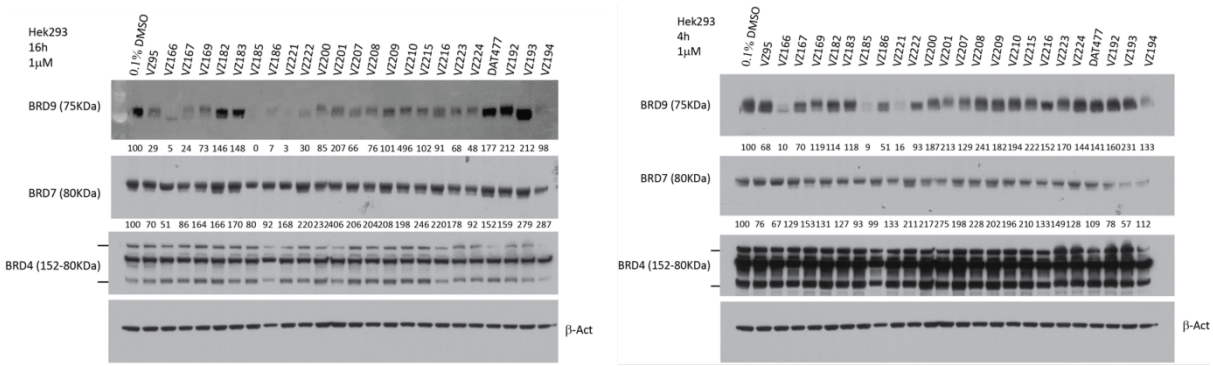

Figure 30. Screening of second generation of degraders in Hek293 cells. Western-blot analysis of BRD9, BRD7, BRD4 and β-actin after treatment of Hek293 cells with 1 μM of compounds for 4 h (blot on the right) and 16 h (blot on the left) before harvesting. Degradation activity is reported below each lane as % of protein abundance relative to 0.1% DMSO vehicle. Intensity values quantified as described in the experimental section.

The screening in RI-1 cells is showed in Figure 31. In detail, RI-1 cells were treated with 1μM of compounds for 2 and 8 h before lysis (Figure 31). After 2 h treatment, compounds **VZ166** and **VZ186** demonstrated great activity on BRD9, while **VZ185** on BRD7. Instead, after 8 h of treatment the most active compounds that induced greatest depletion of BRD7/9 were **VZ166** and **VZ185**. In detail, **VZ166** induced around 85% of degradation of both proteins, while **VZ185** showed higher selectivity for BRD7 (95% of degradation) over BRD9 (50% of degradation). Compounds **VZ166**, **VZ185** and **VZ186** were structure related; in fact, **VZ186** is the analogue of **VZ185** with BrdL2 instead of BrdL1, and both differ from **VZ166** by the absence of one oxygen atom in the linker.

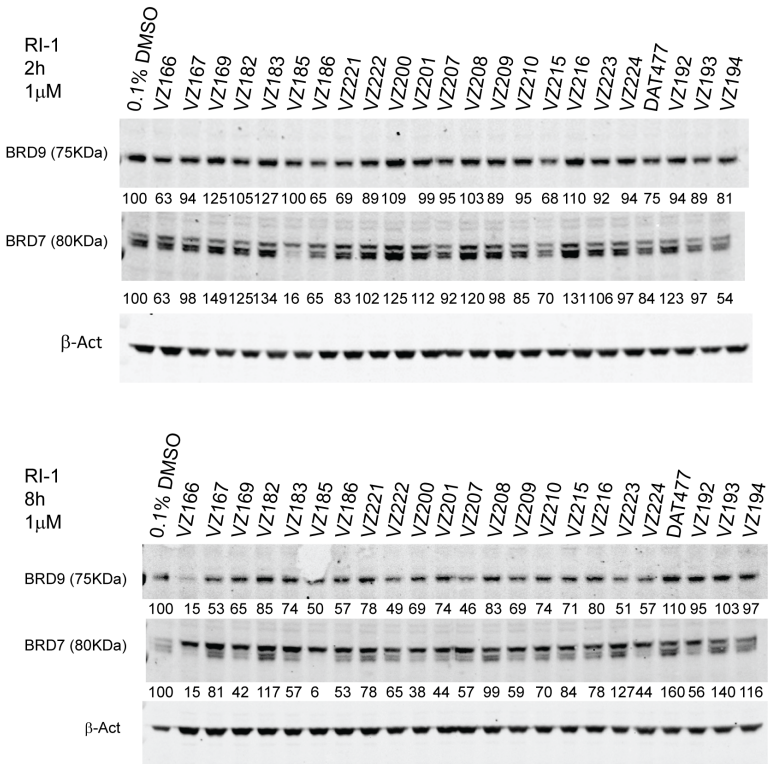

Figure 31. Screening of second generation of degraders in RI-1 cells. Western-blot analysis of BRD9, BRD7 and β-actin after treatment of RI-1 cells with 1 μM of compounds for 2 h (blot on the top) and 8 h (blot on the bottom) before harvesting. Degradation activity is reported below each lane as % of protein abundance relative to 0.1% DMSO vehicle. Intensity values quantified as described in the experimental section.

In HeLa and RI-1 cells, **VZ166** demonstrated the best cellular activity, followed by **VZ185**. Greater degradation activity was observed for compounds containing meta- (BrdL1 and BrdL3) over para- (BrdL2 and BrdL4) substituted dimethoxy groups (Figure 28 and 30). Representative examples were the matched pairs **VZ166** vs **VZ167**, **VZ95** vs **VZ169**, **VZ185** vs **VZ186**.

2.4.3.2 Concentration-dependency experiments of VZ166 and VZ185

Concentration-dependent profile of **VZ166** was studied firstly in HeLa cells treated with six different concentrations at 30 min and 4 h after treatment (Figure 32). **VZ166** showed significant degradation of BRD9 after 4-h treatment at the concentration of 100 nM, achieving maximal degradation with 1 μM already after 30 min (Figure 32). Quantification of the BRD7 and BRD9 protein levels has proved to be difficult due to the blot background.

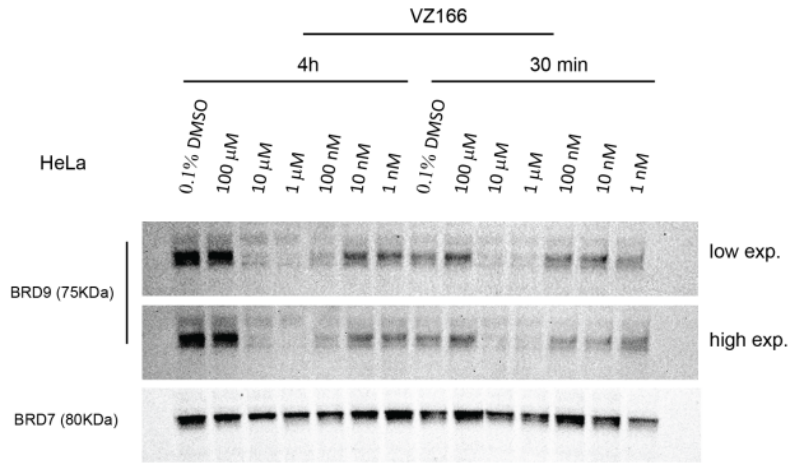

Figure 32. Concentration dependency evaluation of compound VZ166. Western-blot analysis of BRD9 and BRD7 after treatment of HeLa with six different concentration at 30 min and 4 h before harvesting.

Next, we assessed the concentration dependency activity in RI-1 cells of compounds **VZ166** and **VZ185** (Figure 33). RI-1 cells were treated with six different concentrations of compounds at two time points, 2 h and 8 h (Figure 33). Surprisingly, **VZ185** turned out to be the most potent compound. Indeed, the apparent weaker degradation activity of **VZ185** (Figure 31) is explained by the "hook" effect for BRD9 showed at 1 μM, acting preferentially as an inhibitor probably due to the high-binding affinity of BrdL1 and/or VHL4 to their respective targets. **VZ185** demonstrated maximal degradation activity of BRD9 in a concentration range between 10 and 100 nM, and of BRD7 between 100 nM and 1 μM (Figure 33). Therefore, **VZ185** induced preferential degradation of BRD9 over BRD7, resulting in half-degrading concentrations (DC_{50}) of 1.76 nM and 4.5 nM against BRD9 and BRD7, respectively, at the 8 h time-point (Figure 33). In contrast, **VZ166** was approximately 10-fold less active, requiring 1 μM of compound to induced more than 80% of BRD9 degradation (DC_{50} around 180 nM) and around 60% of BRD7 depletion after 8 h before cell harvesting (Figure 33).

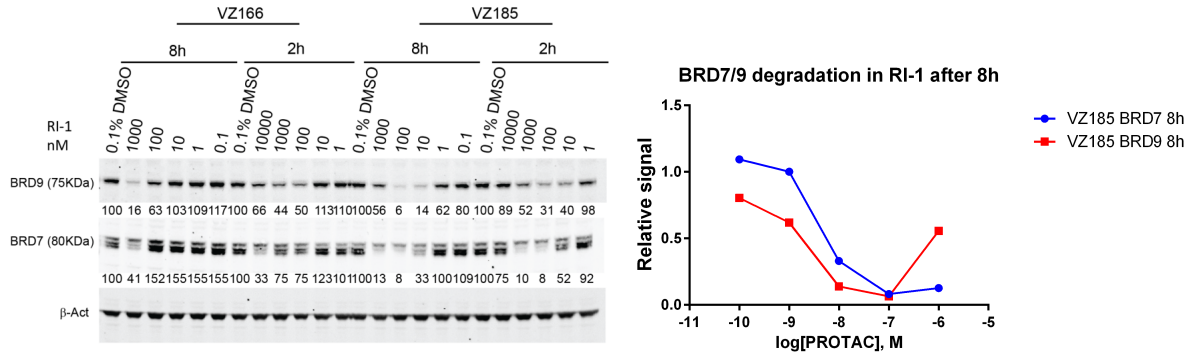

Figure 33. Concentration dependency evaluation of compounds VZ166 and VZ185. Western-blot analysis of BRD9 and BRD7 after treatment of RI-1 with six different concentration at 2 h and 8 h before harvesting. Degradation activity is reported below each lane as % of protein abundance relative to 0.1% DMSO vehicle. Intensity values quantified as described in the experimental section.

2.4.3.3 Time-dependency experiments

Due to the "hook effect" of **VZ185** at 1 μM (section 2.4.3.1), **VZ166** appeared to be the most potent degrader in the first screen. So, we decided to confirm its degradation profile over time in HeLa cells (Figure 34). HeLa cells were treated with 1 μM of compound at different time points. Compound **VZ95** was added as reference and the study was extended to **VZ167** (analogue of **VZ166**) and **VZ216** which demonstrated great activity in HeLa first-line screening (section 2.4.3.1). The results proved fast and potent degradation induced by **VZ166** (Figure 34). The level of BRD7 and BRD9 decreased of about 90% already after 30 min of treatment, reaching maximal degradation after 2 h (Figure 34). No protein recovery was observed up to 24 h of treatment.

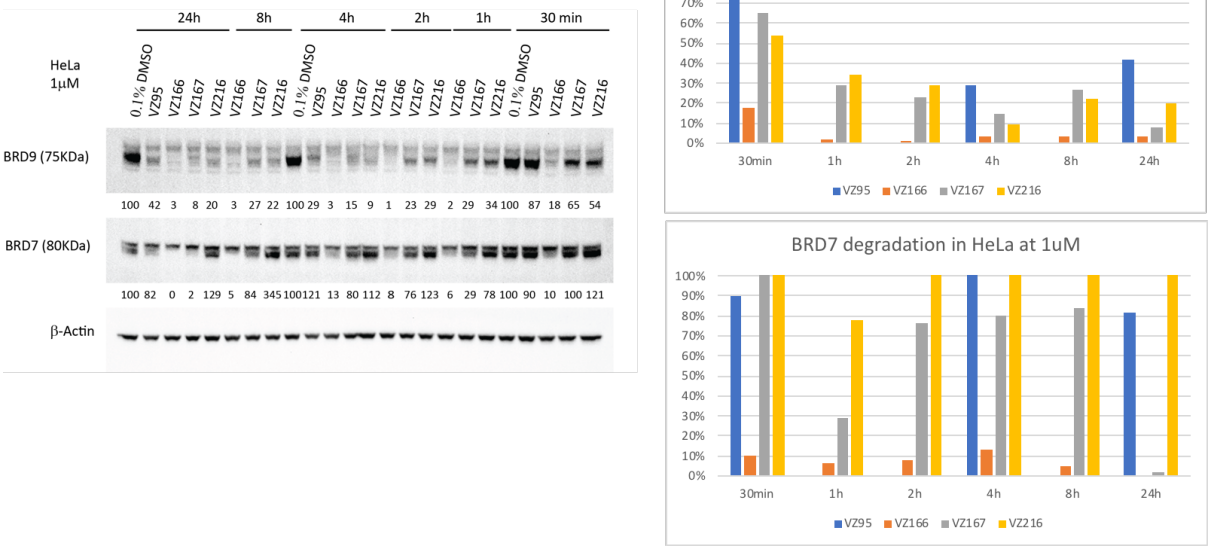

Figure 34. Time dependency evaluation of compounds VZ95, VZ166, VZ167 and VZ216. Western-blot analysis of BRD9, BRD7 and β-actin after treatment of HeLa with 1 μM of compounds at the desired time points before harvesting. Degradation activity is reported below each lane as % of protein abundance relative to 0.1% DMSO vehicle and plotted in the graphs. Intensity values are quantified as described in the experimental section.

To study the time-dependent degradation of **VZ185**, RI-1 were treated with 10 and 100 nM of compound at the desired time points (Figure 35). The results obtained were consistent with those observed in the previous experiments (section 2.4.3.2). Indeed, compound **VZ185** was confirmed to decrease BRD7/9 levels up to 50% already after 30 min of treatment at 100 nM before harvesting, reaching more than 90% of degradation after 4 h of treatment. No recovery of both proteins was observed after 48 h of treatment (Figure 35). Moreover, at 10 nM concentration, our best compound degraded preferentially BRD9 over BRD7 (Figure 35). These data validated the potent and rapid degradation of BRD7/9 protein after treatment with **VZ185**.

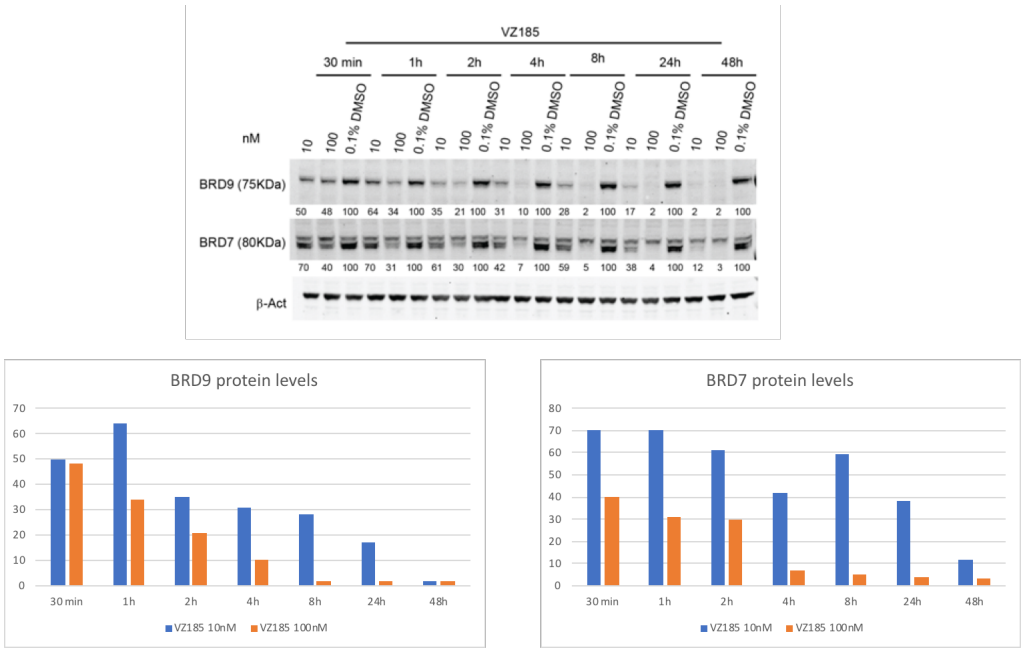

Figure 35. Time dependency evaluation of compounds VZ185. Western-blot analysis of BRD9, BRD7 and β-actin after treatment of RI-1 cells with 10 and 100 nM of compound at the desired time points before harvesting. Degradation activity is reported below each lane as % of protein abundance relative to 0.1% DMSO vehicle and plotted in the graphs. Intensity values are quantified as described in the experimental section.

2.4.3.4 First- and second-generation screening compounds at 4 nM

With the aim to investigate if other compounds suffered of "hook effect" at 1 μM as **VZ185**, we decided to perform a screening of all compounds (first and second generation) at lower concentration. The DC_{50} of **VZ185** guided the design of the experiment. HeLa and RI-1 cells were treated with first- and second-generation compounds at 4 nM for 4 h (Figure 36). The results demonstrated that none of our compounds proved more potent of **VZ185**, confirming the previous data.

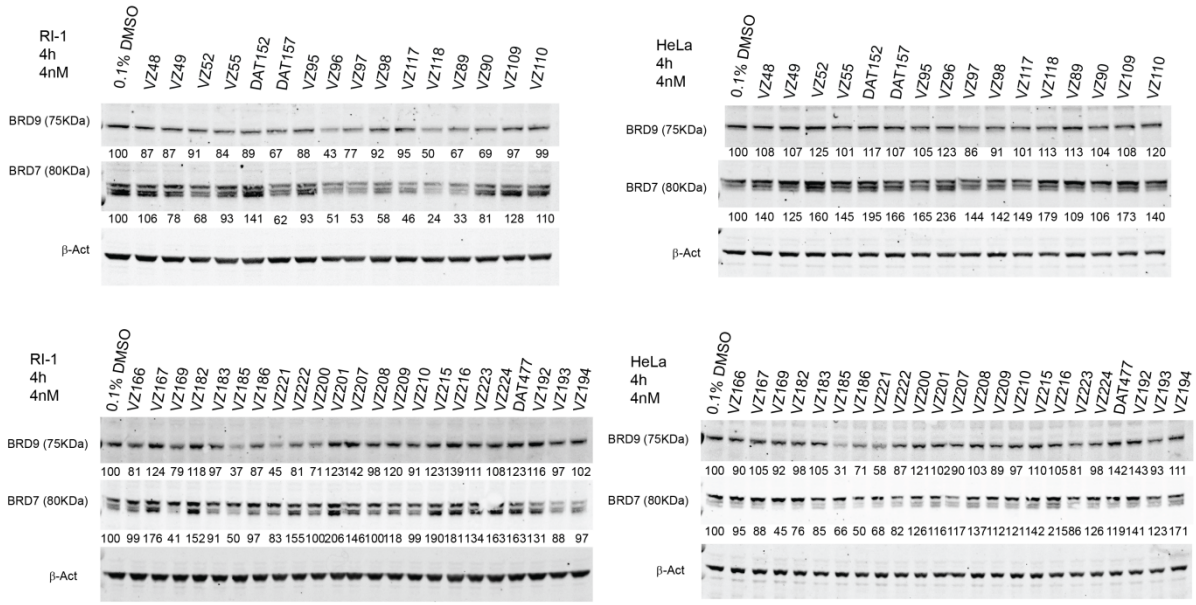

Figure 36. Screening of first and second generation of degraders in RI-1 (blots on the left) and HeLa (blot on the wright) cells. Western-blot analysis of BRD9, BRD7 and β-actin after treatment with 4 nM of compounds for 4 h before harvesting. Degradation activity is reported below each lane as % of protein abundance relative to 0.1% DMSO vehicle. Intensity values quantified as described in the experimental section.

2.4.3.5 Evaluation of mechanism of action of VZ166 and VZ185

To gain insights on the mechanism of action of **VZ166** and **VZ185**, we examined the involvement of the proteasome and $CRL2^{VHL}$ (Figure 37 and 38). The dependency of PROTAC-induced protein degradation on $CRL2^{VHL}$ was assessed by inhibition of Cullin2 neddylation.

Neddylation inhibition was obtained treating cells with 3 μM of MLN4924 (NAE1 inhibitor) 3 h before treatment with **VZ166** or **VZ185**. Instead, the reliance of the degradation on the proteasome was investigated by 30 min pre-treating cells with the proteasome inhibitor MG132 (50 μM) or carfilzomib (400 nM). After adding the desired compound at the proper concentration, the plates were incubated for further 4 h before lysis.

VZ166 mechanistic evaluation was performed in HeLa (Figure 37); for **VZ185** the experiment was carried out in RI-1 cells (Figure 38). Single and combination treatments with DMSO, MLN4924, MG132 and desired compound were performed to consider the individual and the combined effects of compounds. Unsurprisingly, combined treatment of the active degraders with neddylation inhibitor and proteasome inhibitor remarkably suppressed the degradation of both BRD7/9 proteins, clearly proving the dependency on proteasome and $CRL2^{VHL}$ (Figure 37 and 38).

Moreover, to confirm the involvement of VHL in the mechanism of action, a competition assay was performed with VHL inhibitor VH298 (Figure 37 and 38). Cells were pre-treated with VH298 inhibitor (100 μM) 30 min before adding the compound of interest. As expected, VH298 was able to block the degradation activity (Figure 37 and 38).

Furthermore, to confirm the importance of *trans* stereochemistry on the hydroxyl group of the hydroxyproline moiety on **VZ185** for the binding to VHL, treatment with ***cis*VZ185** was performed. As predicted, no BRD7/9 degradation was observed with compound ***cis*VZ185** (Figure 38).

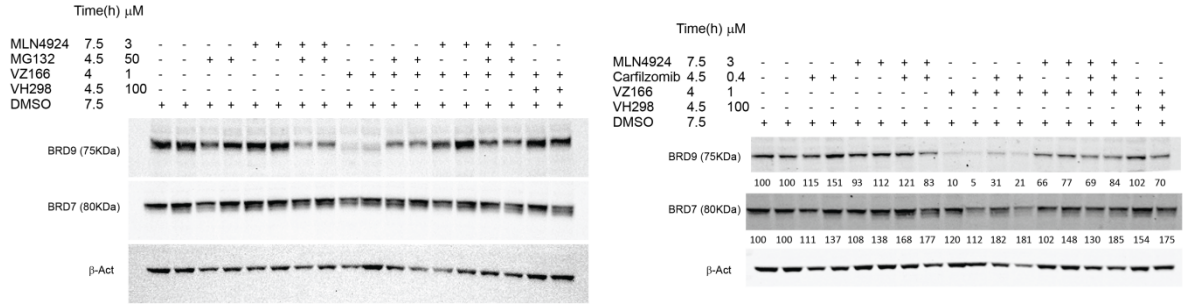

Figure 37. Mechanistic characterization of VZ166 mode of action. VZ166 activity is proteasome and $CRL2^{VHL}$-dependent. HeLa cells were treated in two replicates with MG132 or carfilzomib, MLN4924, VH298 in presence of absence of **VZ166** (1 μM) at desired time points before harvesting. Intensity values quantified as described in the experimental section.

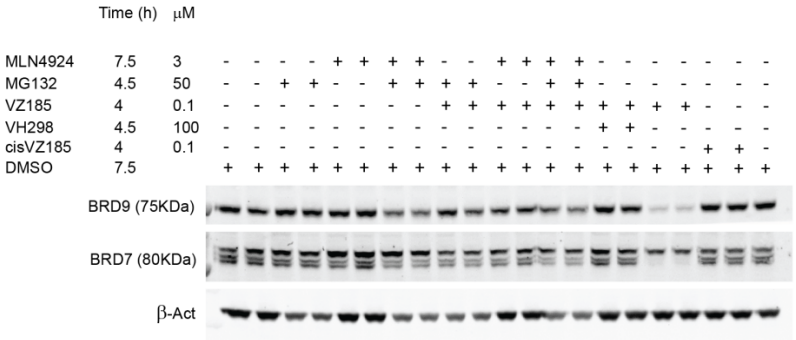

Figure 38. Mechanistic characterization of VZ185 mode of action. VZ185 activity is proteasome and $CRL2^{VHL}$-dependent. RI-1 cells were treated in two replicates with MG132, MLN4924, VH298 in presence of absence of **VZ185** (100 nM) at desired time points before harvesting.

2.4.3.6 Downstream impact and anti-proliferative activity

Hohmann *et al*.[127] reported that BRD9 supports AML cell growth by sustaining *Myc* pathway. Indeed, after BRD9 knockdown, *Myc* was one the most downregulated mRNAs. Therefore, to study the downstream impact on *cMyc* levels in response to protein degradation, we evaluated protein level in the same cellular context over time (Figure 39). RI-1 cells were treated with **VZ185** at 10 and 100 nM at several time points. DMSO vehicle (0.1% v/v) was used as a negative control. The BRD4 degrader MZ1, known to induce *cMyc* depletion, was tested as control at 1 μM for 4 and 20 h (Figure 39).[65,74]

Interestingly, **VZ185** did not show downstream impact on *cMyc* up to 48 h of treatment at the tested concentrations. Instead, the downstream response with the efficient BRD4 degrader MZ1was confirmed in RI-1 cells (Figure 39).[65,74]

Furthermore, we explored the possible activation of apoptosis in RI-1 cells measured as enhancement of PARP cleavage (Figure 39). PARP is one of the apoptotic markers cleaved by cysteine proteases, a group of caspases proteins that play a central role in apoptosis. Compared to the control (i.e. DMSO), increased levels of cleaved PARP were observed only after treatment with 1 μM of MZ1 already at 4 h before lysis. Treatment with 10 or 100 nM of **VZ185** up to 48 h did not determine any increasing of cleaved PARP protein levels, suggesting any apoptotic activity at the tested concentration.

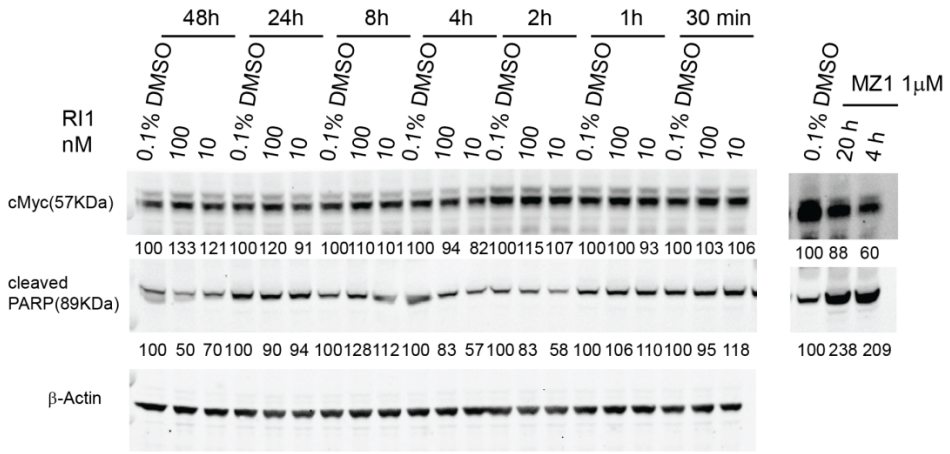

Figure 39. Downstream impact and apoptosis evaluation after treatment with VZ185 and MZ1. Western-blot analysis of *cMyc*, cleaved PARP and β-actin after treatment of RI-1 cells with 10 and 100 nM of **VZ185** and with 1μM of MZ1 at the desired time points before harvesting.

To evaluate possible cytotoxic effects that eventually leads to cell death, we assessed the consequences of BRD7/9 degradation on the viability of sensitive cancer cell lines (RI-1, MOLM-13 and MV4-11 cells) to BRD9 inhibition. Cell viability experiment in presence of **VZ185**, BRD9 inhibitor BI-7273, MZ1 as reference compound and DMSO as vehicle control

was assessed in MOLM13, up to the dosage of 5 μM. The cellular ATP was quantified as signal of metabolically active cells after days of treatment using different numbers of cells (3 x 10^5 and 1.5 x 10^5 cells/mL) (Figure 40A-B). In presence of MZ1, viability of cells was affected confirming the results reported in literature[74] and validating the assay. The antiproliferative effect of **VZ185** was less pronounced in the tested conditions (Figure 40A-C).

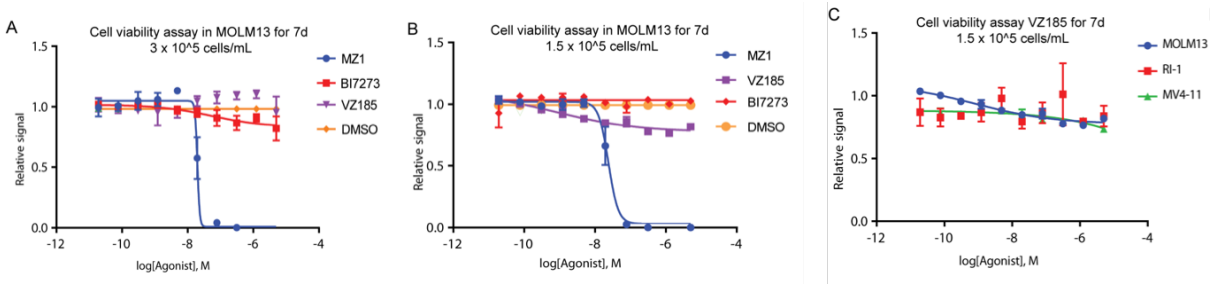

Figure 40. Cell viability assay determined using the CellTiter-Glo luminescent assay kit. A) and B) MOLM13 treated with MZ1, VZ185, BI-7273 and DMSO for 7 days prior to quantification of cell viability; C) MOLM13, RI-1 and MV4-11 treated with VZ185 for 7 days prior to quantification of cell viability.

Collaborators at Boehringer Ingelheim assessed cell viability after treatment with **VZ185** in A-204 (malignant rhabdoid tumor) and EOL-1 (acute myeloid eosinophilic leukemia) cells (Figure 41). EOL-1 and A-204 cells were chosen because of their sensitivity to BRD9 inhibition/degradation[80,127] and their dependency on an active BAF complex[133], respectively. Cell viability decreased after treatment with **VZ185** in both cell lines with EC_{50} comparable to compound dBRD9 confirming results already published by Remillard *et al.*[80] (Figure 41).

The poor antiproliferative effect of BI-7273 and **VZ185** against MOLM13 cells (Figure 40) could be due to the different cell culture conditions (number of cells, type of media, nutrients).

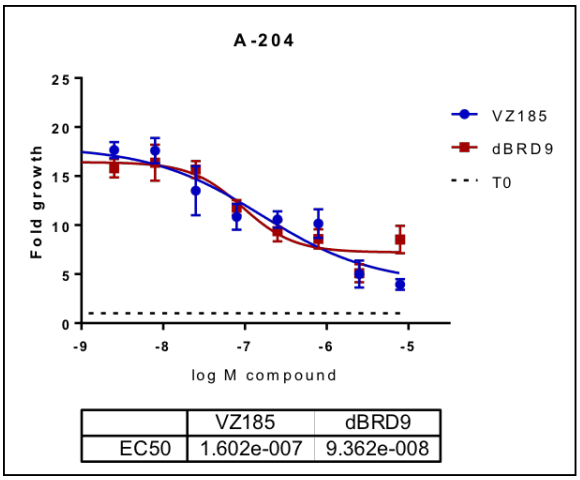

	VZ185	dBRD9
EC50	1.602e-007	9.362e-008

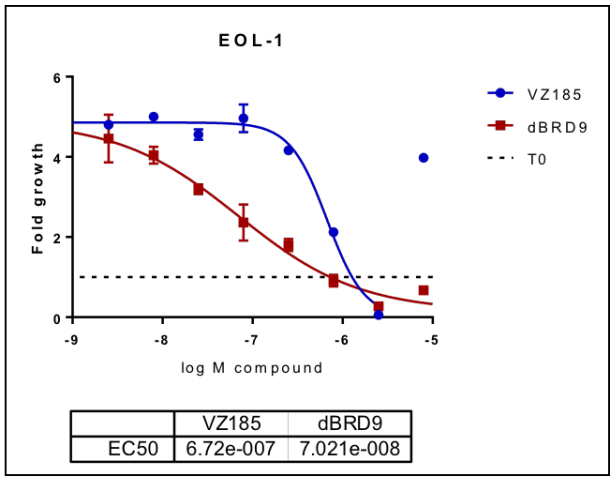

	VZ185	dBRD9
EC50	6.72e-007	7.021e-008

Figure 41. Cell proliferation activity of VZ185 and dBRD9 assessed in A-204 and EOL-1 cells for 8 days by collaborators at Boehringer Ingelheim (data provided by Dr Manfred Koegl, Teresa Gmaschitz and Corinna Wieshofer).

2.4.3.7 Proteomics experiment of VZ185 and *cis*VZ185

Proteomics is a large-scale characterization of the entire protein complement of a cell line, tissue, or organism. It is used to investigate when and where proteins are expressed, protein-protein interactions, post-translational modifications, subcellular locations and involvement of proteins in metabolic pathways.

To investigate the selectivity of **VZ185** against BRD7/9 proteins and to evaluate possible off-target effects, proteomics analysis was conducted in a quantitative and an unbiased manner. 10-Plex tandem mass tags (TMTs-) labelling method enabled simultaneous identification and quantification of protein level from up to 10 different samples.

Proteomic experiments of **VZ185**, ***cis*VZ185** and DMSO, as vehicle control, were performed in triplicate. After labelling each sample with one of TMT isobaric reagents, all samples were pooled together to identify proteins by use of mass spectrometry-based method.

The protocol includes sample preparation, data acquisition and data analysis (Figure 42). In details:

- RI-1 cells were treated with DMSO (0.1% v/v), **VZ185** (100 nM) and ***cis*VZ185** (100 nM) for 4 h of treatment;

- Cells were lysates with 4% SDS- Tris 100 nM (strong conditions) on ice;
- Amount of proteins was quantified with BCA assay (Bradford interferes with SDS);
- FASP- Filtered Aided Sample Preparation to completely remove SDS residues;
- Proteins were digested in peptides through trypsin digestion;
- Peptide quantification;
- Tandem Mass Tag (TMT) Labelling (TMT are chemical labels referred to as isobaric mass tags);
- Fractionation: the pooled sample was fractionated into fractions using high pH reverse-phase chromatography;
- nLC-MS/MS analysis
- Data analysis with Maxquant software

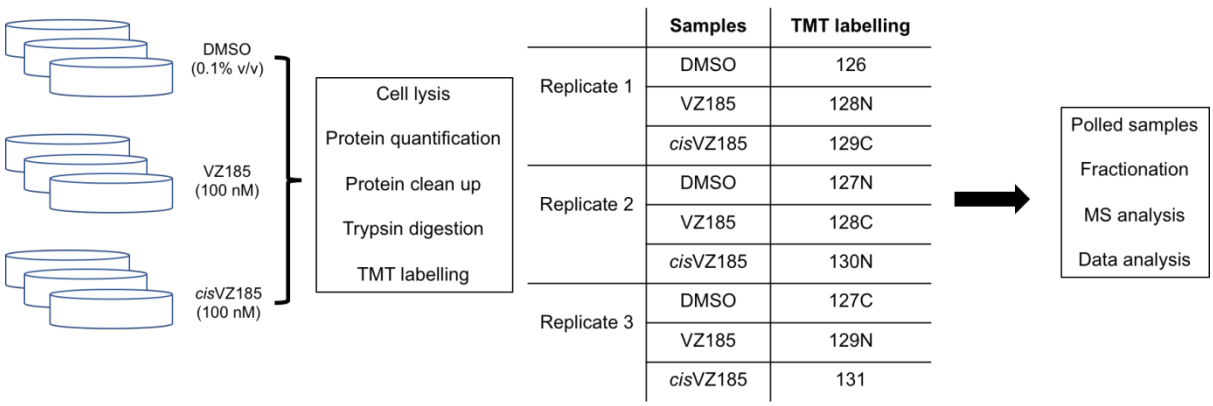

Figure 42. Isobaric tandem mass tag (TMT) proteomics workflow.

6,273 proteins were quantified in this analysis. Amongst the quantified proteins, BRD7 and BRD9 were found to be the only two proteins downregulated after treatment with **VZ185** that satisfy the criteria for a statistically significant change in abundance: p-value y < 0.001 and fold change {x <-20% U x>20%} (Figure 43A and 44). The unaffected levels of other bromodomain proteins confirmed the selectivity of **VZ185** within the bromodomain protein

family. As expected, BRD7/9 proteins were not degraded after treatment with negative control ***cis*VZ185** (Figure 43B and 44).

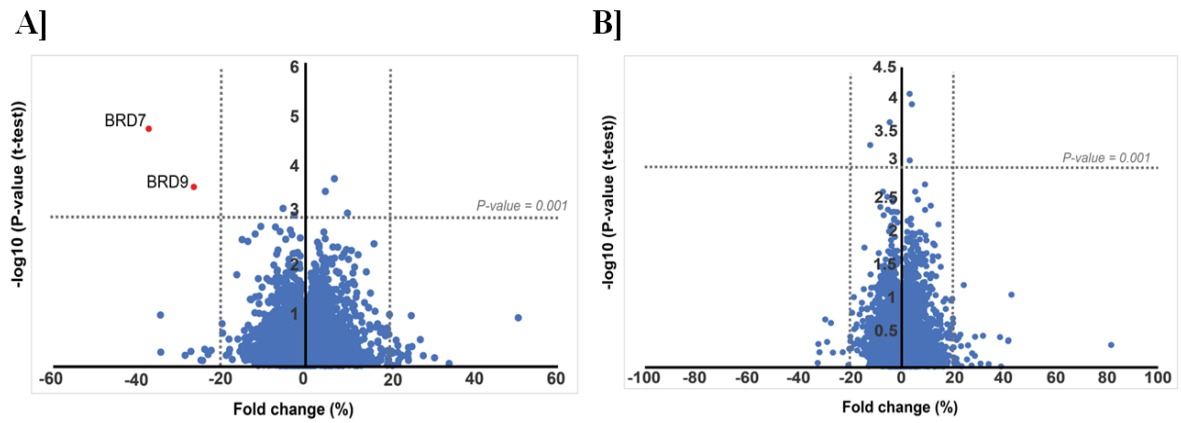

Figure 43. Impact of VZ185 (A) and *cis*VZ185 (B) on the cellular proteome after treatment of RI-1 cells with 100 nM of compound for 4 h before lysis. Data plotted as fold change (%) versus -log10 of p-value (t-test) for a total of 6273 proteins, expressed as mean of the replicates. For quantification see experimental section.

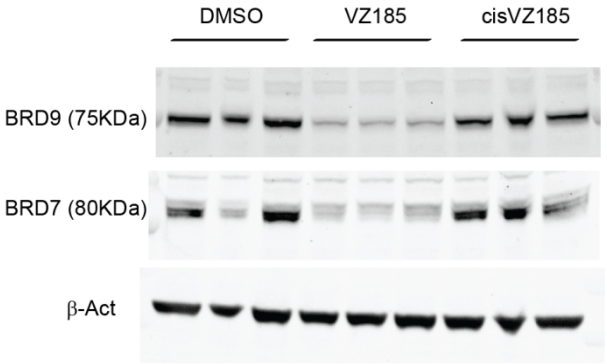

Figure 44. Proteomics sample validation. Western-blot analysis of BRD9, BRD7 and β-actin after treatment of RI-1 cells in three replicates with DMSO, **VZ185** (100 nM) and ***cis*VZ185** (100 nM) for 4 h before harvesting.

2.5 Summary of second-generation of compounds

In this section, the development of an effective and highly selective degrader of BRD7/9 proteins was reported. Starting from a promising compound developed in the first generation, the structure-activity relationship guided the improvements in depletion activity of new compounds. To confirm potent and rapid degradation activity of **VZ185**, concentration-dependent activity and cellular activity over time was assessed. Moreover, we studied the functional mechanism, downstream impact and anti-proliferative activity of **VZ185**. Finally, to assess its cellular selectivity for BRD7/9 depletion and to identify possible off-targets, multiplexed isobaric tagging mass spectrometry proteomic experiment was performed on **VZ185** as well as on its inactive isomer ***cis*VZ185**.

2.6 Conclusion

In this chapter, I have described the development of new series of PROTACs against BDR7 and BRD9 proteins by recruitment of VHL E3 ligase, a target-ligase pair previously considered unproductive. To date, despite several successful examples of target proteins degraded by PROTAC, a general methodology for an efficient design remains unclear. The process for the development of active PROTACs can be laborious and unpredictable. Variables that make the design challenging are the choice of E3 ligase and target ligands as well as the linkers and the conjugation patterns. Availability of small-molecule binders for the protein of interest and for the E3 ligase is also strictly necessary. In addition, it remains unclear whether optimal target-ligase combinations exist and typically an extensive testing of chemical series is required before the identification of a cell-permeable, functional degrader. Few examples show that PROTACs with same target ligands but either VHL or CRBN E3 ligase ligands can exhibit different degradation selectivity and efficacy.[74,78–80] In some systems, CRBN-based degraders show more active profile than VHL-based molecules. The flexibility of CRBN E3 ligase which gives rise to increased accessible Lysine residues for ubiquitination on the target protein could be accounted for this behaviour.[89,134] In light of these observations, it is reasonable to assume that design of VHL-based PROTACs requires more exploration than CRBN-based degraders.

For a given target, the switch of the hijacked ligase could be beneficial and aid targeted protein degradation, even if degradation can be readily obtained by recruiting a given ligase. For instance, there might be chemical liabilities on a particular ligase ligand that could be easily circumvent by switching to a different molecule. Additionally, the expression and the activity of the recruited ligase might vary amongst different cells and tissue types.[135] Furthermore, resistance mechanisms could arise, for example, from the loss of E3 ligase as demonstrated by the correlation between level of CRBN and drug response in MM cell line.[136] Finally, CRBN-

based degraders are known to exhibit off-target depletion of PROTAC-independent factors, as IKZF1/3 and GSPT1.[80,132]

In light of these considerations, we described the development of two series of PROTACs for a ligase-target pair previously deemed unsuitable: VHL E3 ligase and BRD9 protein. VHL-based degraders can be optimized by systematically varying the linkers, the conjugation patterns and monitoring cellular degradation activities. The structure-activity relationship guided the optimization of initially unimpressive compounds, leading to a significant improvement of degradation activity. Indeed, initially molecules hijacking three different E3 ligases characterized by different linkers and conjugation patterns were designed. At this stage, compounds **VZ95** and **VZ109** were identified as the best selective BRD9 degraders hijacking VHL and CRBN, respectively. Encouraged by the BRD9 degradation activity of the initial VHL-based PROTACs (so far considered unproductive), a second round of degraders was designed. A wider variety of linkers (including linker from 5 to 11 atoms and different number of oxygen atoms) as well as different connecting points and ligands were evaluated.

The emerged medicinal chemistry study led the discovery of **VZ185** which is characterized by enhanced target degradation compared to **VZ95** and similar to levels achieved with CRBN-based degrader **VZ109**, but enabling depletion of BRD7.

Finally, **VZ185** was characterized as potent, selective and fast VHL-based dual degrader with slight preference for BRD9 over BRD7 (DC_{50} of 1.7 nM against BRD9, and of 4.5 nM against BRD7). More generally, these SAR studies could be applicable to broadly approach to discover effective target-ligase pair previously considered unproductive. The acquired findings qualify a new chemical probe that could find wide use in chemical and cell biology to explore BRD7 and BRD9 biology and their therapeutic potential.

Section II

3. Targeting Kinase Protein Degradation

3.1 Introduction

Protein kinases play an essential role in the majority of signal transduction networks that are crucial in the regulation of several cellular processes, i.e. cell growth, metabolism, and division, transcription and protein cellular localization. Indeed, protein kinases modify the function of proteins through phosphorylation. Phosphorylation of a target protein is a reversible process that involves the balanced action of protein kinases and phosphatases.[137,138] The human genome encoded approximately 538 kinases, one of the largest families of human enzymes and genes. These proteins share common structural features in the catalytic domains, with consist of 250-300 amino acids. Their catalytic mechanism uses ATP (or GTP) to generate phosphate monoester of protein alcohol (serine or threonine) or phenolic (tyrosine) groups. Therefore, two main subfamilies have been classified: the protein-serine/threonine kinases and the protein-tyrosine kinases.[139] Biochemically, the phosphorylation of an alcohol or phenol group is catalysed by protein kinases following the reaction:[140]

$$MgATP^{1-} + protein{-}O : H \rightarrow protein{-}O : PO3^{2-} + MgADP + H^{+}$$

The main catalytic roles of kinase domains are: i) binding and orientation of the ATP (or GTP) phosphate donor as complex with divalent cation (Mg^{2+} or Mn^{2+}); ii) binding and orientating the substrate protein; iii) transfer phosphate from ATP (or GTP) to acceptor hydroxyl residue on protein substrate.[139]

On the basis of catalytic domain sequence similarity, Manning *et al*. have classified eukaryotic protein kinases in nine groups (Table 7).[137] In the next section, a brief description of some protein kinases is reported.

Table 7. Classification of eukaryotic protein kinases.

Group name	# of members	Kinases in the group
AGC	63	PKA, PKG, PKC families, Akt1/2/3, Aurora kinase, PDK1, RSK1/2/3/4
CAMK	74	CaMK1/2/4, PhKγ1/2, MAPKAPK2/3/5, Nek1-11, MLCK
CK1	12	CK1, TTBK1/2, VRK1/2/3
CMGC	61	CDK, MAPK, CDKL
STE	47	MAPK cascade families
TK	90	58 receptors (i.e. EGFR, Flt) and 32 non-receptor tyrosine kinases (i.e. Abl, JAK, Src)
TKL	43	MLK1-4, LISK, IRAK, Raf, RIPK, STRK
RCG	5	Similar to protein-tyrosine kinases
OTHER	83	

3.1.1 Non-receptor tyrosine kinases (NRTKs)

NRTKs belong to the protein tyrosine kinases (TKs, Table 7) which transfer a phosphate from ATP to tyrosine residues on protein substrates. Based on their sequence homology, NRTKs have been subdivided into nine families: Abl, Src, Jak, Fak, Csk, Tec, Syk, Fes and Ack. For the purpose of this thesis, we will analyse Abl, Src and Jak families.

Abl family

Abelson tyrosine (Abl) family, consisting of c-Abl and Arg (Abl-related protein), has implicated in a range of cellular processes, including regulation of cell proliferation, survival, cell adhesion and migration. c-Abl is localized in the nucleus, cytosol, mitochondria, endoplasmic reticulum and cell cortex. Deregulation and aberrant expression of c-Abl gene has been associated with several types of cancer, such as breast cancer, colon cancer, and non-small-cell lung cancer. c-Abl is responsible to phosphorylate oncogenic signalling pathways by activation of ERK5, Rac/Jnk, and Stat 1/3 pathways.[141] Furthermore, c-Abl is also known to

be implicated in the genesis of chronic myelogenous leukemia (CML). The responsible oncogene is Bcr-Abl, also called Philadelphia chromosome (Ph). This gene is formed after translocation and fusion of the Abl proto-oncogene on chromosome 9 to the breakpoint cluster region (Bcr) gene on chromosome 22. Several small-molecules inhibitors have been developed to target c-Abl and Bcr-Abl with the aim to block their kinase activity (section 3.2).[142]

Src family

Src family represents the largest group of NRTKs and is further subdivided into three subfamilies: the Lyn-related family, the Src-related family and the the PTK6/Brk- related family. The Lyn-related family consists of: Lck/Yes-related tyrosine kinase (Lyn), hematopoietic cell kinase (Hck), lymphocyte-specific protein tyrosine kinase (Lck), and B lymphocyte kinase (Blk). The Src-related family includes the PTK with oncogenic potential Fyn, Yes-related kinase (Yrk), and Yamaguchi sarcoma oncogene (Yes). Finally, the PTK6/Brk- related family consists of protein tyrosine kinase 6 (PTK6), also known as breast cancer kinase (Brk) and Fyn-related kinase (Frk), also known as Rak- and Src-related kinase lacking C-terminal regulatory tyrosine and N-terminal myristylation sites (Srms). Src kinases take part to several cellular processes, such as cell growth, differentiation, apoptosis, survival and proliferation. Dysregulation of Src has been found in different type of malignancies, such as melanoma, breast, colon and lung carcinoma.[141]

Jak family

The Janus kinases (Jak) family consists of Jak1, Jak2, Jak3 and tyrosine kinase-2 (Tyk 2). All of them comprise two catalytic domains, one of which is inactive. Jak principal activity is the phosphorylation and activation of the signal transducers and activators of transcription (Stat) factors. Phosphorylated Stat proteins dimerize and translocate into the nucleus. As

consequence, expression of genes linked to cellular stress, proliferation and differentiation are activated. Jak/Stat pathway has been involved in haematopoiesis, inflammation, and immunity response. Moreover, deregulation of Jak activity has been observed in a number of disorders including acute lymphoblastic leukaemia (ALL), acute myeloid leukaemia (AML), rheumatoid arthritis, psoriasis, polycythaemia vera, and myeloproliferative diseases.[141]

3.1.2 Aurora kinases

The aurora kinases are protein-serine/threonine kinases, evolutionarily conserved in eukaryotes and able to coordinate cell division.[143] This family consists of three members: aurora A, B and C. These proteins play essential roles in centrosome maturation, mitotic spindle formation, chromosome segregation and cytokinesis.[144]

Dysregulation of aurora kinase levels have been associates with different types of human cancers and therefore have become targets for inhibition of tumor cell division.[145,146]

3.1.3 c-Kit

c-Kit is a protein-tyrosine kinase also known as Mast/stem cell growth factor receptor (SCFR) or CD117. This proto-oncogene is a receptor tyrosine kinase protein encoded by the KIT gene.[147] c-Kit was first described by the German biochemist Axel Ullrich in 1987 as the cellular homolog of the feline sarcoma viral oncogene *v-kit*.[148] Upon binding to stem cell factor (SCF), c-Kit is activated leading to its autophosphorylation and initiation of signal transduction. Signalling proteins are recruited to activated c-Kit by interaction domains (i.e. SH2 and PTB) that specifically bind to phosphorylated tyrosine residues of c-Kit. Activation of c-Kit signalling has been found to be important in several cellular processes, for example to mediate cell survival, migration, and proliferation. Thereby, signalling from c-Kit is essential for normal haematopoiesis, pigmentation, fertility, gut movement, and some aspects of the nervous

system. However, c-Kit kinase activity has been found to be deregulated in diseases such cancer and allergy. It has been observed that mutations in c-Kit can promote tumor formation and progression, thereby, therapeutics agents targeting this receptor have been developed. Furthermore, also downregulation of c-Kit has been associated to pathologic conditions, namely piebaldism.[149]

3.1.4 Mek1/2 and P44/42 MAPK Kinases

Mek1/2 and P44/42 MAPK are two protein kinases that take part to the same signalling pathway. The MAPK/ERK pathway, also known as the Ras-Raf-MEK-ERK pathway, is a cascade of signals which includes many proteins, including MEK and MAPK, also called ERK (extracellular signal-regulated kinases). MEK1/2 are serine/tyrosine/threonine kinase proteins, while MAPK is a serine-threonine kinase protein. Both proteins are mitogen-activated protein kinases. Upon binding of a signalling molecule to the receptor on the cell surface, proteins communicate the signal to the DNA in the nucleus to produce cellular responses, such as protein expression or cell division. Regulation of MAPK/ERK pathway is crucial for cell cycle entry promoting cell growth and proliferation. Instead, deregulation of this pathway has been associated with the promotion of tumor cell growth of a variety of cancers.[150]

3.2 Protein kinases as targets for pathologic conditions

Mutations and dysregulation of protein kinases has been associated with human diseases, including carcinogenesis, immune, neurological and infectious diseases.[151–154] In light of these observations, these enzymes have become interesting drug targets in the last years. Since the development of the first protein kinase inhibitor, in the early 1980s, 35 kinase inhibitors have received FDA approval, 31 of which for treatment of malignancies such as breast and lung cancer (Figure 45).[155] In addition to small-molecule inhibitors, kinase-targeted antibodies, have

demonstrated efficacy in cancer treatment, for example transtuzumab in breast cancer and cetuximab in colorectal and head/neck cancer.[156,157]

The breakthrough occurred in 2001 when imatinib, a phenyl-amino-pyridine derivative, was approved for the treatment of CML. Later on, several molecules have been approved for treatment of imatinib-resistant tumor and other various malignancies. In addition to the approved kinase inhibitors, there are more than 3000 ongoing Phase I-III clinical studies for hundreds of new molecules.[155]

Despite the encouraging results, many challenges are associated with drug resistance, selectivity, toxicity and efficacy, confusing the clinical efficacy of these molecules.[140]

For the purpose of this thesis, imatinib dasatinib and nilotinib inhibitors will be described in the next section.

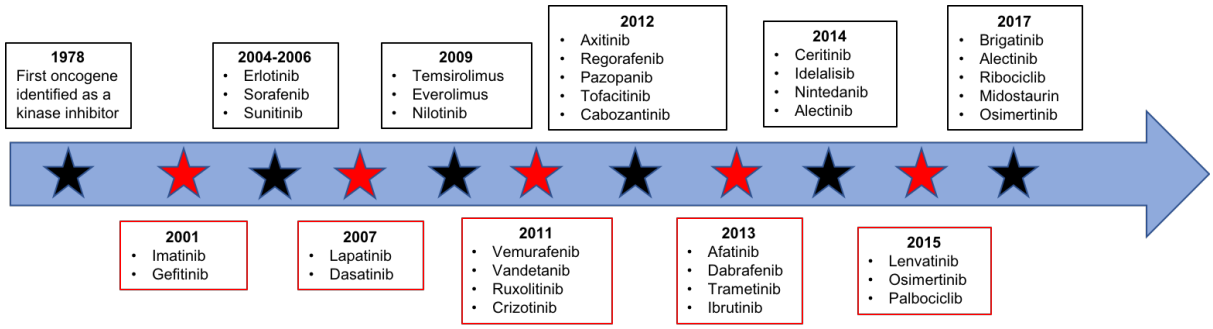

Figure 45. Timeline of key events in the development of protein kinase inhibitors

3.2.1 Tyrosine kinase inhibitors (TKIs): overview of imatinib, dasatinib and nilotinib

In the last years, several TKIs have been developed to block the ATP-binding site and inhibit autophosphorylation of the tyrosine residues of proto-oncogenes. Thereby, intracellular signal-transduction pathways were inhibited in tumor cells, leading to deregulation of key cellular activities.[158,159]

Imatinib mesylate, also known as Gleevec® (STI571), was the first commercially available TKI (Figure 46). It has been approved for the treatment of CML and gastro-intestinal stromal tumors (GISTs).[160] Imatinib is a phenyl amino pyrimidine derivative that blocks, upon binding, the catalytic domain of different oncogenic tyrosine kinases, including Bcr-Abl, c-Kit, PDGFR (platelet-derived growth factor receptor), CSF-1R (colony-stimulating factor receptor-1) and DDR (discoidin domain receptor).[161]

Despite the success of imatinib as human cancer drug, many patients developed polyclonal resistances due to mutations in the Bcr-Abl domain. To overcome these limitations, a second-generation of TKIs was developed, including dasatinib (Sprycel®, BMS-354825) and nilotinib (Tasigna®, AMN107) (Figure 46). Both compounds were more potent than first-generation TKIs and were employed for the treatment of imatinib-resistant tumors. In details, dasatinib is highly active against Bcr-Abl, Src- and Btk-family kinases, PDGFR, c-Kit and ephrin-A2 receptor. Nilotinib is a potent inhibitor of Bcr-Abl, c-Kit, CSF-1R, amongst others.[162,163]

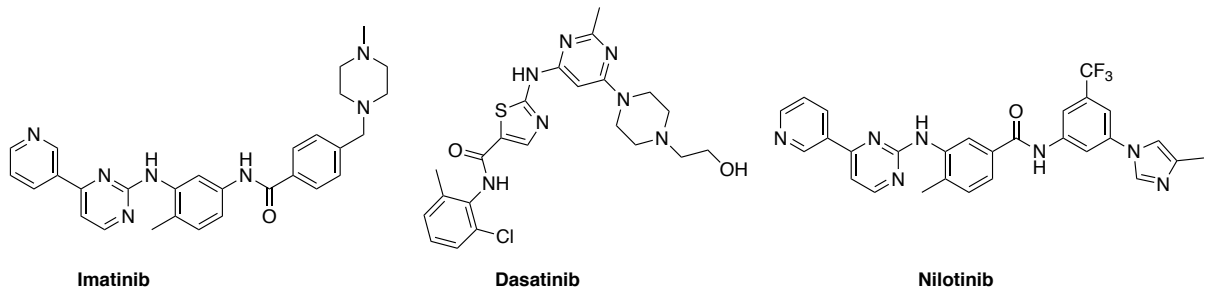

Figure 46. Chemical structure of Imatinib, Dasatinib and Nilotinib.

3.3 Aims and objectives

Multiple mutations of different genes are responsible of oncogenic transformations. Increased tyrosine kinase activity results in a loss of cell cycle control and cell proliferation, leading to human cancer initiation and progression. Moreover, dysregulation of kinases has been associated with others human disorders, such as infectious, neurological and immune diseases. In the last years, several small-molecules inhibitors have been successfully developed to target cancer-specific molecules and signalling pathways. However, despite the peculiarities of small-molecules inhibitors (i.e. ADME properties), the employ of these agents is associated with side-effects and drug resistance. With the aim to overcome limitations of inhibition, we have decided to employ PROTAC strategy to degrade protein kinases of interest.

This one-year project has been carried out at Nerviano Medical Sciences (NMS), under the supervision of Dr Eduard Felder. Starting from a proof of concept already published in literature, we designed, synthesised degraders targeting other protein kinases. The biological characterization was carried out by the Department of Biology of NMS.

3.4 Design of bifunctional small molecules targeting protein kinases

Protein kinases are amongst the key players of the cellular functions by transferring a phosphate group to a protein. Moreover, recent works have elucidated that protein kinase dysregulation occurs in many diseases including cancer and inflammatory disorders. We therefore became interested in the opportunity to degrade these targets using PROTAC approach.

Firstly, we planned to study a literature example to confirm the proof of concept with the prospect of extending the development of PROTACs to other targets. Among the available molecules, compound **DAS-6-2-2-6-CRBN**, developed by Lai *et al*,[79] was chosen. This molecule induces degradation of c-ABL and BCR-ABL oncogenic tyrosine kinase via recruitment of $CRL4^{CRBN}$ (Figure 47). This compound bears CRBN ligand (pomalidomide) and tyrosine kinase inhibitor (dasatinib precursor) connected by a linker. The connecting chain was linked to pomalidomide (amine at C-4) and dasatinib (piperazine nitrogen) in solvent exposed moieties not involved in key interactions with proteins. The linker is characterized by 19-atom length and two ethylene glycol units between two hexamethylene chains.

Based on **DAS-6-2-2-6-CRBN**,[79] we designed **VZ-6-2-2-6-POMA** aiming to induce degradation of serine/threonine kinases (Figure 47). This molecule bears pomalidomide (POMA) to recruit CRBN and an aminopyrazole kinase inhibitor to target the protein of interest. Same linker and attachment points of **DAS-6-2-2-6-CRBN** were chosen to connect the target ligands.

Furthermore, to address the question if the linker length and composition could affect the degradation, we designed **DAS-6-2-2-2-POMA** and **DAS-6am-2-2am-6-POMA**, sharing with **VZ-6-2-2-6-POMA** the derivatization points but characterized by linkers with different hydrophobic and hydrophilic properties (Figure 47). In details, **DAS-6-2-2-2-POMA** bears a shorter linker (14 atoms, 3 oxygen) whereas, **DAS-6am-2-2am-6-POMA** is characterized by

the same linker length of **DAS-6-2-2-6-CRBN** but two oxamethylene units were replaced with two amide bonds.

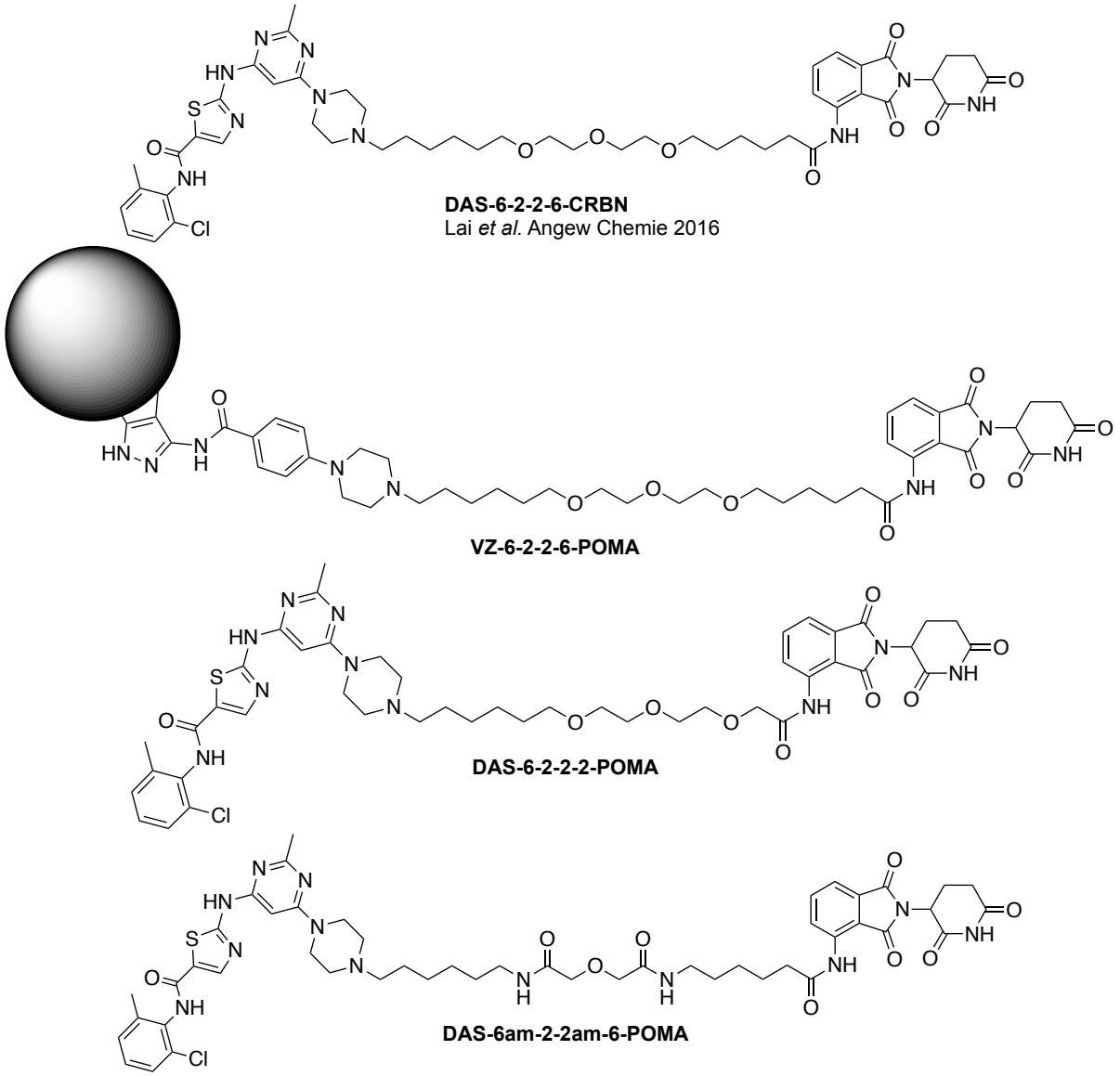

Figure 47. Structures of PROTACs designed to recruit protein kinases at one side and CRL4^{CRBN} at the other end.

3.5 Synthetic routes to protein kinase-targeting compounds

The desired compounds were obtained through a convergent synthetic strategy, which involved the preparation of the target protein ligands (i.e. pomalidomide and dasatinib precursor) and the linker chains, which were then assembled.

3.5.1 Synthesis of Pomalidomide

The synthesis of pomalidomide can be divided into three parts: synthesis of the glutarimide ring, synthesis of the phthalimide ring and the assembly of the two parts (Figure 48).[164] Thalidomide known for its teratogenic and immunosuppressive effects is marketed as a racemic mixture, although it has been suggested that the teratogenic effects are associated with the (S)-isomer and the sedative hypnotic effect is associated with the (R)-isomer. Follow this statement, pomalidomide, thalidomide derivative, has been synthetized and reported as racemic mixture as well, since studies about exact mechanism of action remain elusive and they are beyond the scope of this thesis.

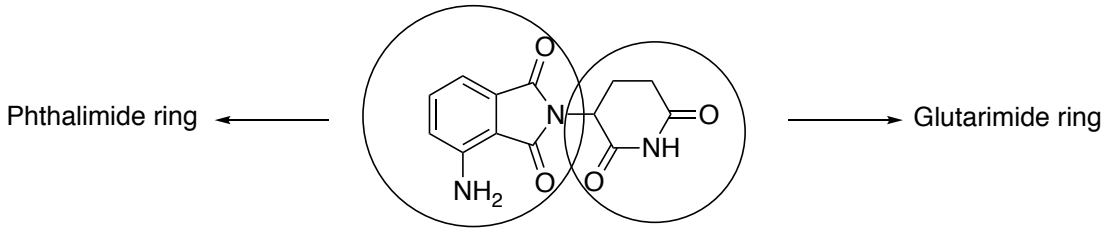

Figure 48. Structure of Pomalidomide.

The glutarimide ring was prepared by a two-step approach, starting from the commercially available Boc-L-glutamine. As shown in Scheme 16, treatment of Boc-L-glutamine (**104**) with 1,1'-carbonyldiimidazole (CDI) and 4-dimethylamino pyridine (4-DMAP) in refluxing THF

led to **105** in 59% yield. The BOC protecting group was subsequently cleaved by TFA at rt to afford the glutarimide derivative **106** as TFA salt in quantitative yield.

Scheme 16. Synthesis of glutarimide ring.

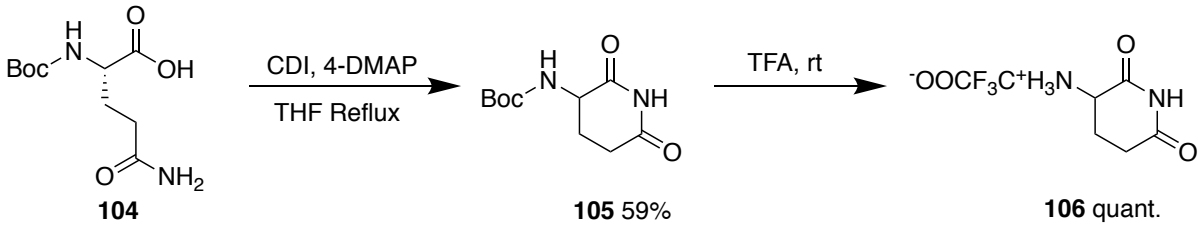

104 **105** 59% **106** quant.

Then, the phthalimide ring was synthetized starting from the commercially available 3-nitrophthalic acid (**107**, Scheme 17). Compound **107** was heated in acetic anhydride for 30 min affording 3-nitrophthalic anhydride (**108**) in 89% yield. The condensation between glutarimide ring **106** and **108** in glacial acetic led to compound **109** in 58% yield. Reduction of the nitro group by transfer hydrogenation was carried out with $NaH_2PO_2*H_2O$ and Pd/C 10% in THF, affording the desired compound **110** in 84% yield.

Scheme 17. Synthesis of phthalimide ring and final compound pomalidomide (110).

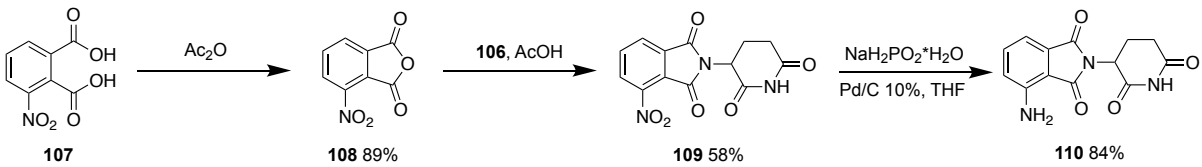

107 **108** 89% **109** 58% **110** 84%

Probably due to the high presence of salt residues accumulated in the reduction step by transfer hydrogenation, compound **110** was characterized by a low NMR purity (32%). So, to increase the purity of **110** (Figure 48), a new route was employed (Scheme 18). As reported in the literature,[165] the reaction between 4-nitrophthalic anhydride **108** and **106** in the presence of TEA, used as base, in THF led to the formation of intermediate **111** (61% yield). The solution of

intermediate **111** in methanol was hydrogenated (50 psi) in the presence of Pd/C 10% at rt for 30 min to yield the reduced intermediate that, without further purification, was refluxed in methanol for 2 h to yield the desired product **110** in 37% yield and with a 96% NMR purity.

Scheme 18. **Alternative synthesis of Pomalidomide (110).**

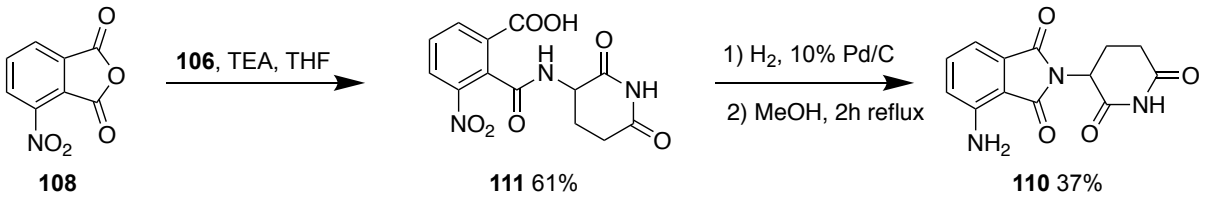

3.5.2 Synthesis of Dasatinib derivative

The synthesis of dasatinib (Figure 49) was carried out according to the procedure already published in literature.[166]

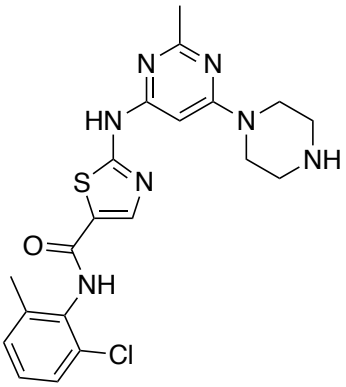

Figure 49. Structure of Dasatinib derivative.

Briefly, the commercially available compound **112** (Scheme 19A) was hydrolysed to the acid derivative **113** (82% yield), converted into the corresponding acyl chloride and coupled with 2-chloro-6-methylaniline to afford the desired intermediate **114** in very low yield (7%). This

disappointing result was presumably due to the difficulty of 2-chloro-6-methylaniline to act as a good nucleophile, because of the steric hindrance of the 2,6-disubstitution.

To overcome this problem, a more efficient approach was followed (Scheme 19B).[167] This route involved a chemoselective α-bromination of β-ethoxyacrylamide followed by a one-pot treatment with thiourea to give the desired compound **119** in good yield. Moreover, another advantage of this approach would be the elimination of the protection and deprotection steps needed in the previous synthesis. In details (Scheme 19B), condensation between ethyl vinyl ether **115** and oxalyl chloride **116** led to the β-ethoxy acryloyl chloride **117** which, as crude material, was condensed with 2-chloro-6-methylaniline to afford **118** in 60% yield. The yield of **118** was marginally affected using a distilled batch of **117**[168] (60% with crude **117** vs 50% with distilled **117**). Compound **118** was treated with NBS and then with thiourea to afford compound **119** in 65% yield. No N-bromination or phenyl ring bromination by-products were isolated under these reaction conditions. Successively, **119** was treated with 4,6-dichloro-2-methylpyrimidine **120** in the presence of *t*-BuONa as base keeping the temperature between 0 °C and rt to limit the formation of side-product 6-chloro-N-(2-chloro-6-methylphenyl)-2-methylpyrimidin-4-amine. The desired product **121** was obtained in 62% yield. Aromatic nucleophilic substitution was achieved treating **121** with piperazine in 1,4-dioxane, under microwave conditions (at 120 °C for 1 h) and using DIPEA as base, which led to the final product **122** in excellent yield.

Scheme 19. Synthesis of Dasatinib derivative.

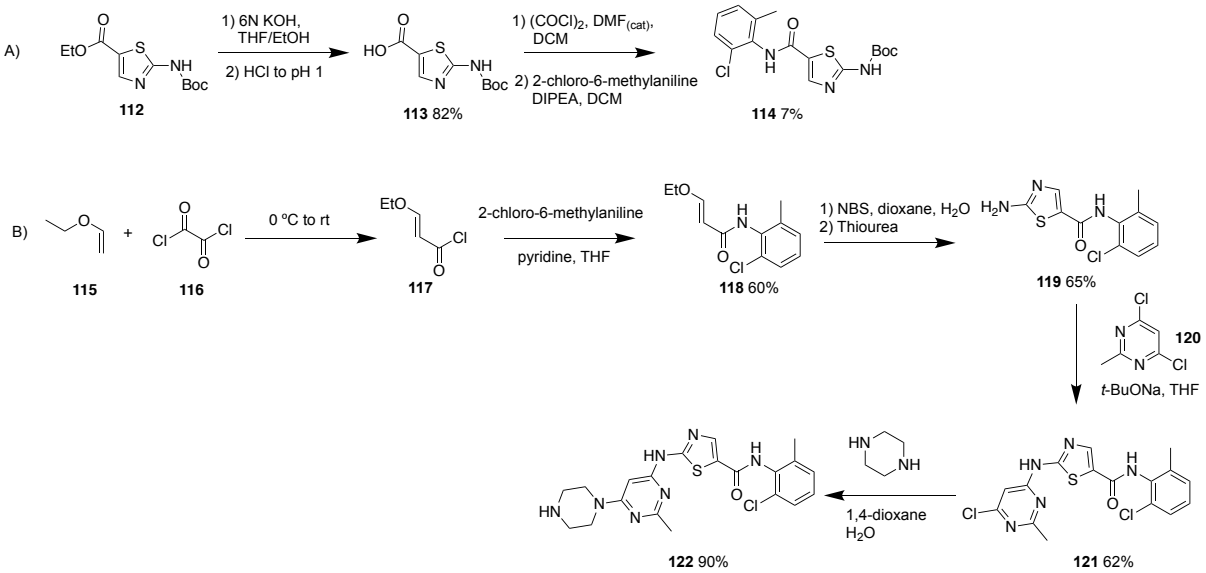

3.5.3 Synthesis of the linkers

3.5.3.1 Linker -6-2-2-6-

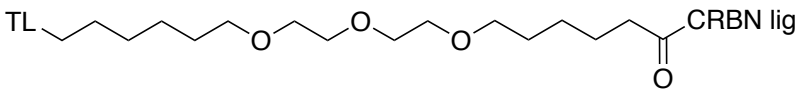

Figure 50. Structure of linker -6-2-2-6- coupled with target ligand (TL) and pomalidomide (CRBN lig)

Initially, we planned to build up **DAS-6-2-2-6-CRBN**[79] by "growing" the linker attached to the pomalidomide end, in order to minimize the difficulties of handling and monitoring PEG analogues derivatives not UV visible. Thus, 6-bromoexanoic acid (**123,** Scheme 20) was activated as acidic chloride (**124**) to allow acylation of **110**, using DIPEA as base. As result a mixture of 6-bromo- and 6-chloro-hexanoyl derivatives (**125**) was obtained in 56% yield. Compounds **125** were then converted into the iodo-derivative **126** applying Finkelstein reaction (yield: 51%).

Intermediates **125** or **126** were used to explore nucleophilic substitution of the halide by diethylene glycol using two different conditions: KOH, DMSO/H_2O or NaOH in H_2O/toluene

and TBAHS as phase-transfer catalyst. Both reactions failed probably due to decomposition of the starting material or the final product.

Scheme 20. Synthesis: growing the linker attached to pomalidomide (110).

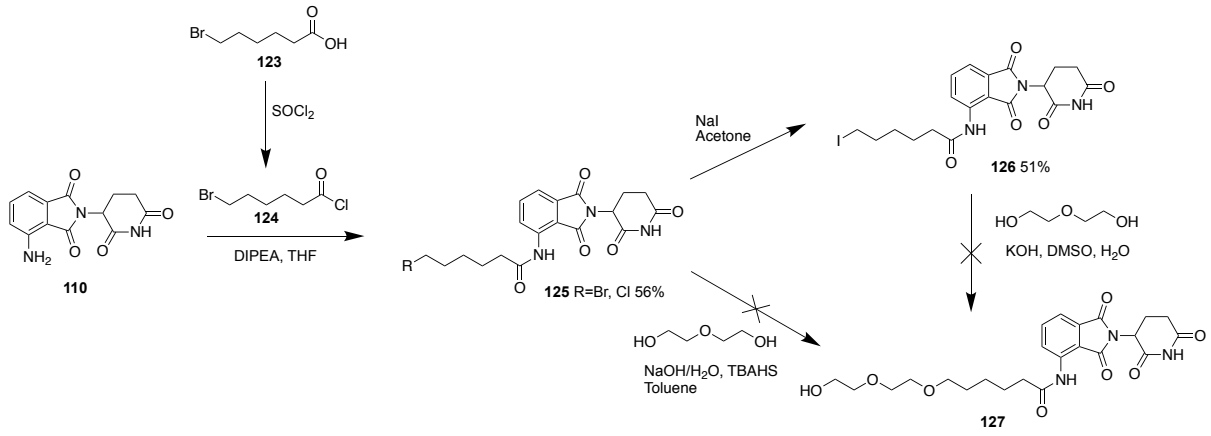

Because of these poor results, we decided first to synthetize the linker and then attach it to CRBN ligand as an alternative synthetic strategy (Scheme 21 and 22). Intermediate **133** was obtained by two strategies, which required or not the mono-protection of diethylene glycol with a trityl group (Scheme 21 and 22).

Multifunctional compounds as synthons present several synthetic challenges. Therefore, mono-protection of water-soluble substrates containing multiple hydroxyl groups is a fundamental requirement for their correct functionalization in multistep reaction sequences.[169] As shown in Scheme 21, a 10-fold excess of diethylene glycol **128** was reacted with trityl chloride in the presence of dry pyridine acting as base and solvent. Microwave irradiation at 80 °C for 30 min led to a mixture of mono- and bis-tritylate (**129**, **130**). The formation of bis-tritylated side product has been avoided by lowering the temperature to 50 °C, affording only **129** in 74% yield (Scheme 21, Table 8).[169]

Scheme 21. Synthesis of compound 133

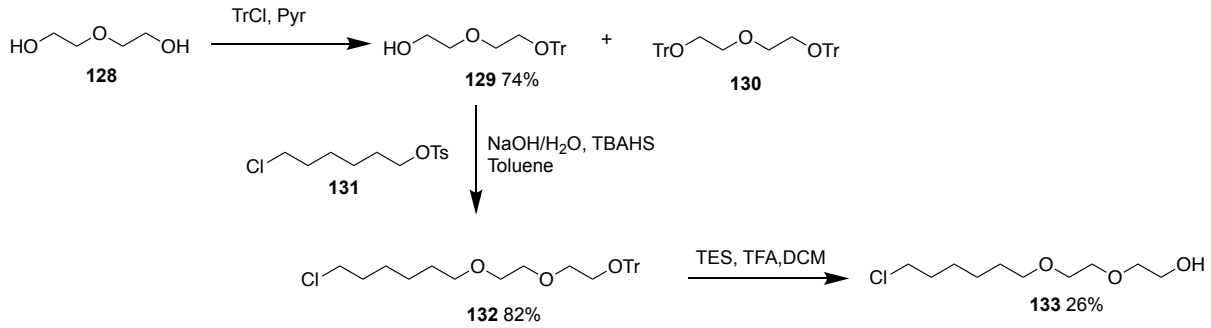

Table 8. Reaction conditions and yields of diethylene glycol

Method	**T** °C	**129**- yield	**130**- yield
A	80	28%	20%
B	50	74%	0%

The reaction between **129** and **131**, previously obtained by tosylation of 6-chloroexanol,[170] was studied evaluating different conditions (Scheme 21, Table 9). The most convenient method involved a biphasic system (water-toluene) in the presence of TBAHS, used as phase-transfer catalyst in stoichiometric amount, and NaOH as a base (method **F**, Table 9). In these conditions **132** was obtained in 82% yield.

The cleavage of the trityl group to obtain **133** (Scheme 21) can be carried out using either TES, TFA in DCM (procedure A, yield: 26%) or 1,4-cyclohexadiene, Pd/C 10% in MeOH, 80-90 °C under conventional and microwave heating (procedure B, yield: 35%). Despite the lower yield, procedure A allowed the isolation of a less contaminated product.

Table 9. Evaluated conditions for the reaction between 129 and 131.

Method	Reagents	T °C	Time	Yield
A	NaOH/H_2O, TBAB, Toluene	rt	7 dd	52%
B	NaOH/H_2O, TBAB, Toluene	MW 60 °C	1 h	21%
C	NaH, THF	rt	15 dd	failed
D	NaOH/H_2O, TBAB	MW 140 °C	30 min	failed
E	NaOH/H_2O, TBAB	MW 100 °C	1 h	76%
F	NaOH/H_2O, TBAHS, Toluene	rt	overnight	82%

To avoid the mono-protection step of diethylene glycol, the synthesis of **133** was also tried by direct reaction between **128** and **131** or **135**, previously obtained by tosylation or mesylation of 6-chloroexanol **134** (Scheme 22).[170] Out of the different evaluated reaction conditions (Table 10), the use of the mesylate **135** and NaH in DMF/THF (1:1) granted the higher yield of the desired compound **133**.

Table 10. Evaluated conditions for the reaction between 128 and 131 or 135.

Method	Reagents	T °C	Time	Yield
A	NaOH, 15-crown-5, THF	0 °C -rt	overnight	failed
B	KOH, H_2O/DMSO	0 °C to rt	overnight	17%
C	NaH, DMF/THF (1:1)	0 °C to rt	overnight	43% (with **135**) 23% (with **131**)

The final step of the synthetic procedure involved the condensation of **133** with *tert*-butyl-6-bromohexanoate (**136**), prepared from 6-bromohexanoic acid **123** and Boc_2O and DMAP in 93% yield. Differently from the literature data,[79] the condensation between **133** and **136** led directly to the unprotected 5-(2-(2-((6-chlorohexyl)oxy)ethoxy)ethoxy) pentanoic acid **137** (37% yield).

Scheme 22. Synthesis of linker 137 (-6-2-2-6-)

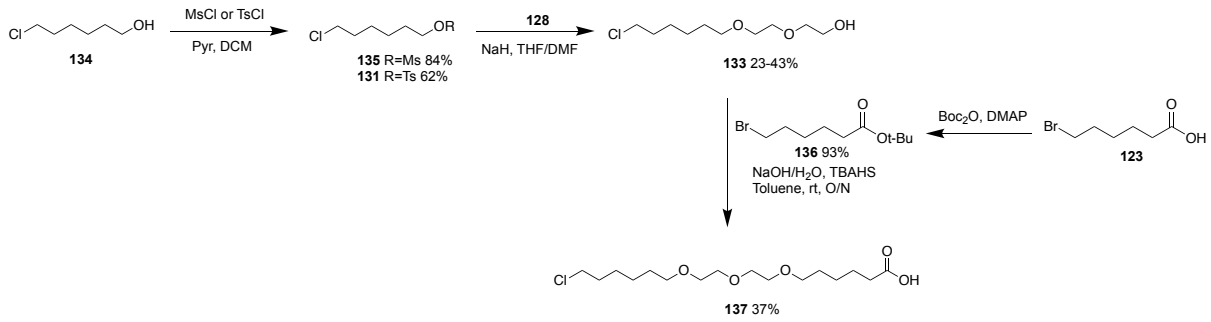

3.5.3.2 Linker -6-2-2-2-

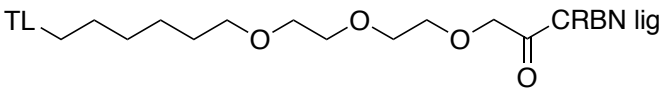

Figure 51. Structure of linker -6-2-2-2- coupled with target ligand (TL) and pomalidomide (CRBN lig)

The linker -6-2-2-2- (Figure 51) was synthesized by reacting intermediate **133** (Scheme 21 and 22) and *tert*-butyl-2-bromoacetate (**138**) in the presence of NaH in a 1:1 mixture of DMF/THF (Scheme 23). The desired compound **139** was obtained in 44% yield.

Scheme 23. Synthesis of linker 139 (-6-2-2-2-)

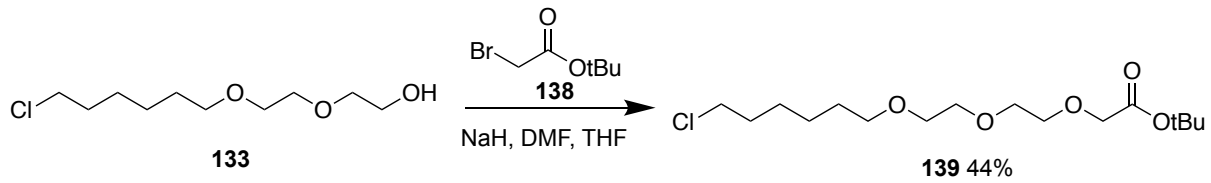

3.5.3.3 Linker -6am-2-2am-6-

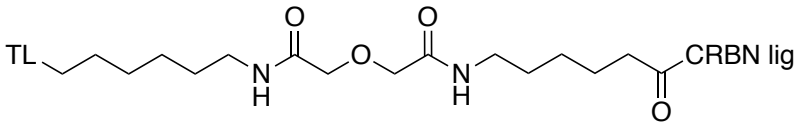

Figure 52. Structure of linker -6am-2-2am-6- coupled with target ligand (TL) and pomalidomide (CRBN lig)

Linker -6am-2-2am-6- (Figure 52) is characterized by 19-atom chain bearing a bis-amide functionality. The synthetic strategy included two different approaches. The first one dealt with the synthesis of the linker, which was then coupled with the appropriate ligands. The second one involved the synthesis of the desired product by "growing" the linker on pomalidomide, as already reported for the synthesis of compound **DAS-6-2-2-6-CRBN** (see section 3.5.3.1).

The first approach involved the coupling between intermediates **142** and **144** (Scheme 24). **142** was synthesized by reaction between diglycolic anhydride **140** and 6-amino-1-hexanol **141** in THF in low yield (9%). This disappointing result was probably due to the low solubility of **141** in THF and also to the high solubility of the final product in water used for work-up. Investigation of the same reaction by using different solvents, such as DMSO, DCM, mesitylene, or t-amyl alcohol was carried out without yield improvement. Therefore, we set up a different approach: reaction between **140** and **141** in DMSO afforded the acid that was converted to the corresponding methyl ester using $TMSCHN_2$, diethyl ether and methanol (62% yield). Finally, the hydrolysis of the ester intermediate using LiOH and a mixture of THF/H_2O/MeOH (2:1:2) led to **142** in quantitative yield.

Esterification of 6-(boc-amino)caproic acid (**143**) was obtained using (trimethylsilyl) diazomethane (TMSD, 2M solution in hexane) in a mixture 1:1 diethyl ether/methanol. TMSD was added dropwise until the solution became persistently pale yellow (Scheme 24). After hydrolysis of the boc-protecting group with TFA in DCM, **144** was obtained in quantitative

yield. The last step involved the coupling between **142** and **144**, using EDC, TEA in DCM. Unfortunately, the reaction failed, and future studies will evaluate other coupling reaction conditions, such as HATU, HOAt or HOBt (Scheme 24).

Scheme 24. Synthesis of linker -6am-2-2am-6 (145)

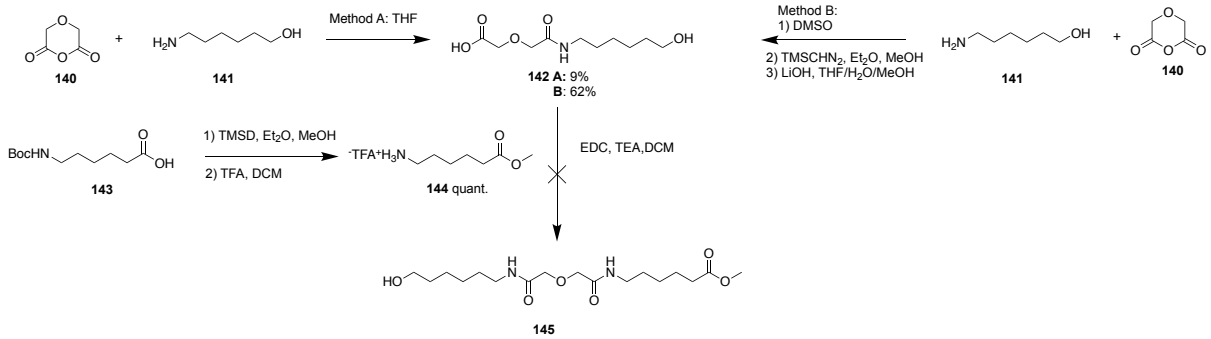

The second approach (Scheme 25), started with amide coupling of **110** with 6-(Boc-amino)caproic acid **143**, performed with phosphorus oxychloride in pyridine at -15 °C for 30 min, that led to **146** in 84% yield. Treatment of **146** with TFA in DCM cleaved the protecting group in quantitative yield (**147**). We also tried using 4M HCl in dioxane, but the reaction was very slow. Derivative **148** was obtained in 23% yield after reaction between **147** and **142** (prepared as reported in Scheme 24), using EDC and HOBt as coupling reagents and DIPEA as base in DMF.

Successively, **148** was activated as mesylate (93% yield) and condensed with the dasatinib precursor **122**, stirring the mixture at rt for 48 h using NMP as solvent and DIPEA as base. The reaction was followed by HPLC-MS where we observed only two peaks, one for compound **122** and the other one with final product +18, due to the presence of water, often seen in this type of compounds. Then the solvent was evaporated with HT12 evaporator and the crude was washed with ether. The crude was purified by HPLC purification. Unfortunately, the ^{1}H-NMR has clarified that the peak isolated was not compound **DAS-6am-2-2am-6-POMA** (**150**), but

the dasatinib mesylate precursor. The molecular weight tricked us because MW of dasatinib mesylate precursor is 522 and in HPLC it is seen as dimer (522 x 2 = 1044; M+1 = 1045). The molecular weight of the dimer (M+1) is the same of **DAS-6-2am-2am-6-POMA** +18. This side reaction was probably due to residues of methansulphonyl chloride, so that the mesylation of the piperazine was favored over the nucleophilic attack between **122** and **149**.

Scheme 25. Synthesis: growing the linker -6am-2-2am-6- attached to pomalidomide

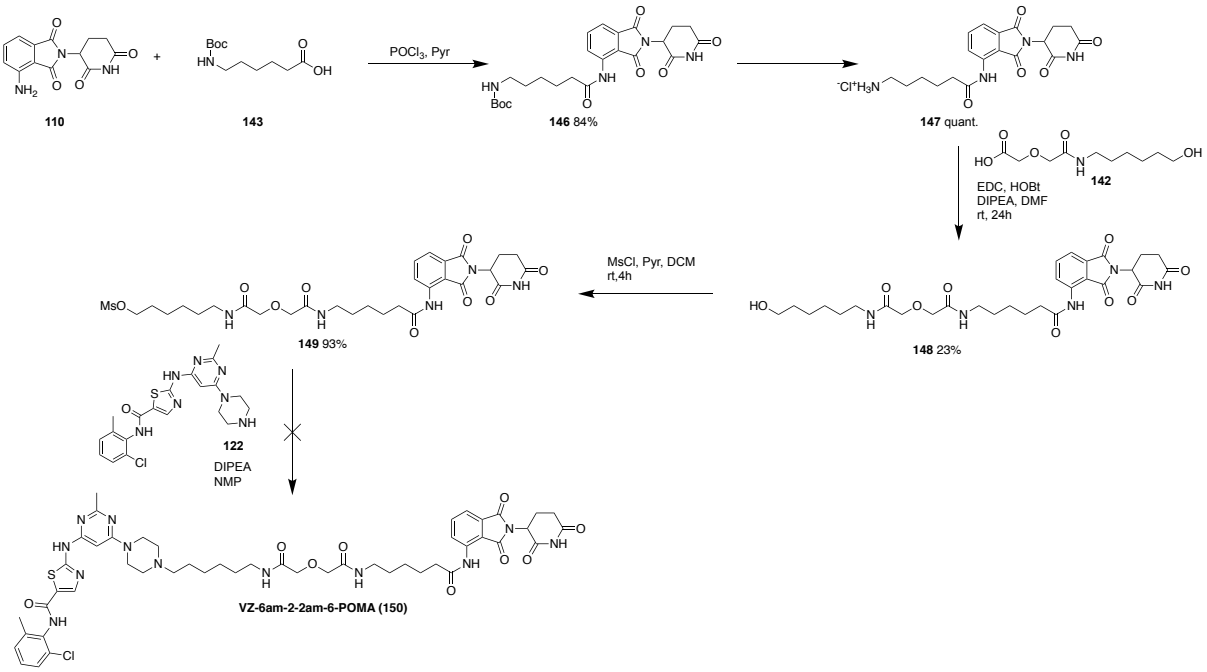

3.5.4 Assembly of final PROTACs bearing linker -6-2-2-6-

In order to obtain **DAS-6-2-2-6-CRBN** we followed the procedure already published with minor changes.[79] The method published employed activation of the carboxylic acid with thionyl chloride in toluene followed by coupling with pomalidomide. This method yielded the desired product **151** in 5% yield after overnight stirring. With the aim to improve the yield and to reduce the reaction time, an alternative reaction condition was then tried (Scheme 26). The acid linker **137** was activated with phosphorus oxychloride in pyridine (essential to catalyse nucleophilic attack) at -15 °C, followed by aminolysis of the mixed anhydride intermediate by

the amino group of pomalidomide. Reaction reached completion within 30 min and the desired product **151** was obtained in higher yield (11%).

Successively, Finkelstein reaction yielded **152** (89%) which was used for nucleophilic substitution of the halide by dasatinib precursor (**122**), heating at 80 °C overnight, using NMP as solvent and DIPEA as base. NMP was used instead of DMF (used in the literature[79]) to avoid the possible reaction of dimethylamine with the alkyl iodide. **DAS-6-2-2-6-CRBN** (**153**) was obtained in 95% yield after purification by preparative HPLC.

Scheme 26. Synthesis of DAS-6-2-2-6-CRBN

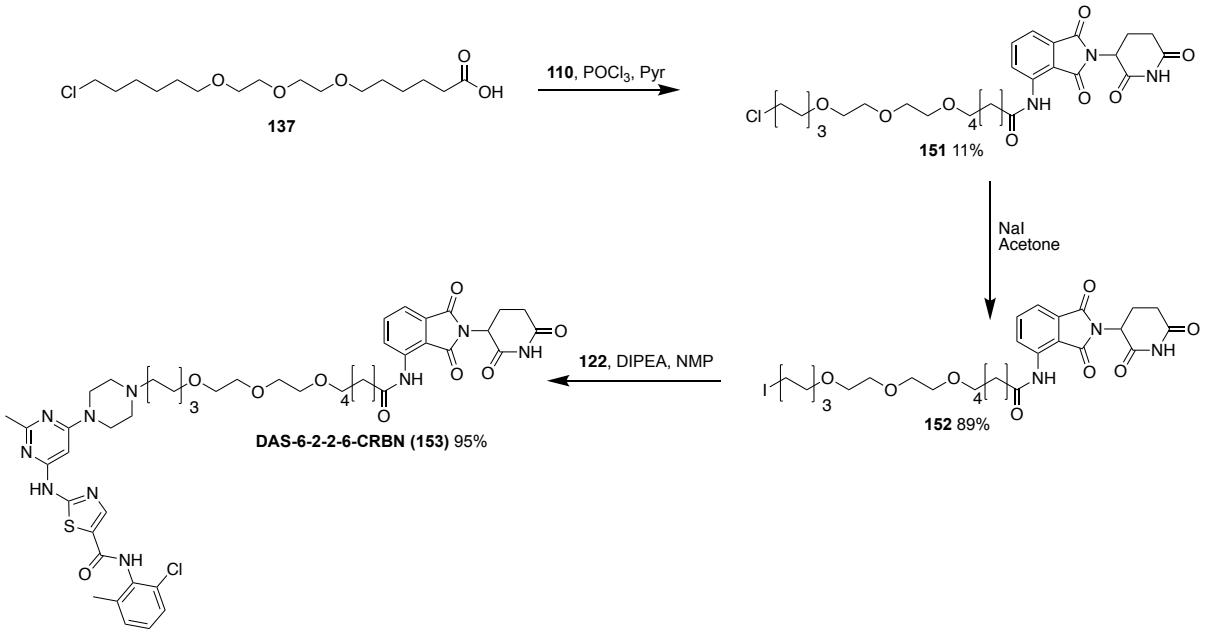

Intermediate **152** was used also for the synthesis of the new PROTACs **VZ-6-2-2-6-POMA** (Scheme 27). The nucleophilic substitution of the halide **152** by aminopyrazole kinase inhibitor (**154**) was carried out at rt stirring overnight, using DIPEA as base and NMP as solvent. NMP was evaporated with HT12 evaporator and the product was suspended with ether. **VZ-6-2-2-6-POMA** (**155**) was purified by preparative HPLC and the final compound was obtained in 28% yield.

Scheme 27. Synthesis of VZ-6-2-2-6-POMA

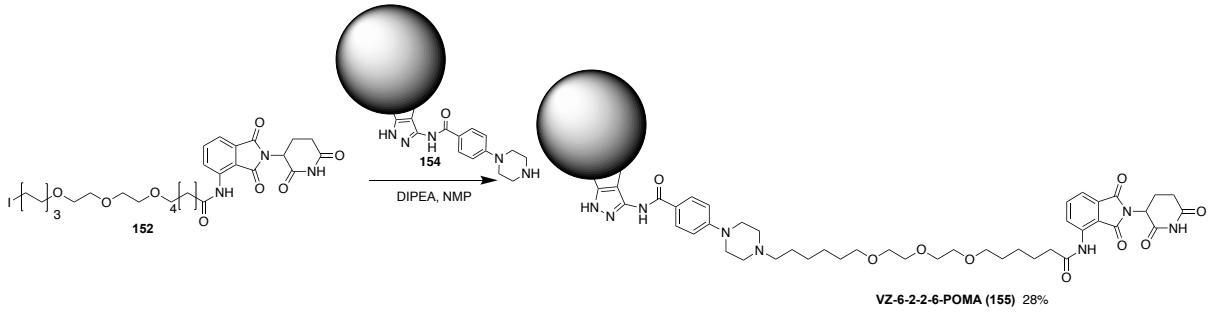

3.5.5 Assembly of final PROTAC bearing linker -6-2-2-2-

To obtain PROTAC **DAS-6-2-2-2-6-POMA**, linker **139** was first coupled with pomalidomide **110** and consequently with dasatinib precursor **122**. As shown in Scheme 28, after hydrolysis of **139** with TFA and DCM, the corresponding acid was activated as acyl chloride refluxing the acid with thionyl chloride in THF. Then, the obtained acyl chloride was coupled with **110** in THF under reflux for 4 h to afford the desired product **156** in 84% yield after column purification. Finkelstein reaction yielded **157** (88% yield) that was then condensed with the **122**, stirring the mixture at room temperature for 24 h, using NMP as solvent and DIPEA as base. The solvent was evaporated with HT12 evaporator and the crude was suspended with ether and the final product was obtained in 89% yield after HPLC purification.

Scheme 28. Synthesis of DAS-6-2-2-2-POMA

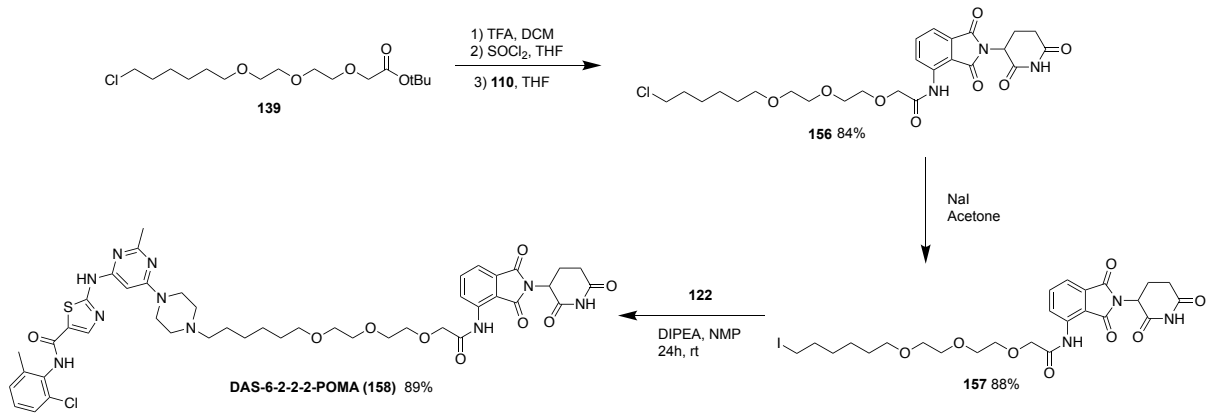

3.6 Biological evaluation of protein kinase-targeting compounds

In the following section, the cellular evaluation of the synthesized protein kinase-targeting compounds is described. The experiments were carried out by the Department of Biology of NMS.

3.6.1 Biological evaluation of DAS-6-2-2-6-CRBN

In order to confirm the data of cellular activity already published,[79] **DAS-6-2-2-6-CRBN** was tested for c-ABL and BCR-ABL degradation in cell culture. K562 cells, human chronic myelogenous leukemia (CML) cell line, were treated with different concentrations of **DAS-6-2-2-6-CRBN** (NMS-P836). Dimethylsulfoxide (DMSO) and dasatinib (1 μM, tyrosine kinase inhibitor) were used as control. After 8 h and 24 h of treatment the samples were resolved by SDS-PAGE and the protein abundance was analysed by Western-Blot using antibodies to probe for c-ABL and BCR-ABL proteins (Figure 53). **DAS-6-2-2-6-CRBN** showed a clear degradation of c-ABL already after 8 h of treatment with 100 nM of compound. It also induced reduction in protein abundance of BCR-ABL already after 8 h of treatment at 250 nM, but maximum effect was registered after 24 h of treatment. The apparent decrease of both protein degradation observed at high concentration was due to the "hook effect", characterized by the formation of binary complexes (protein of interest-compound and CRBN-compound) rather than ternary complex (protein of interest-compound-CRBN).[79] Our data were in line with Lai *et al*.[79] results.

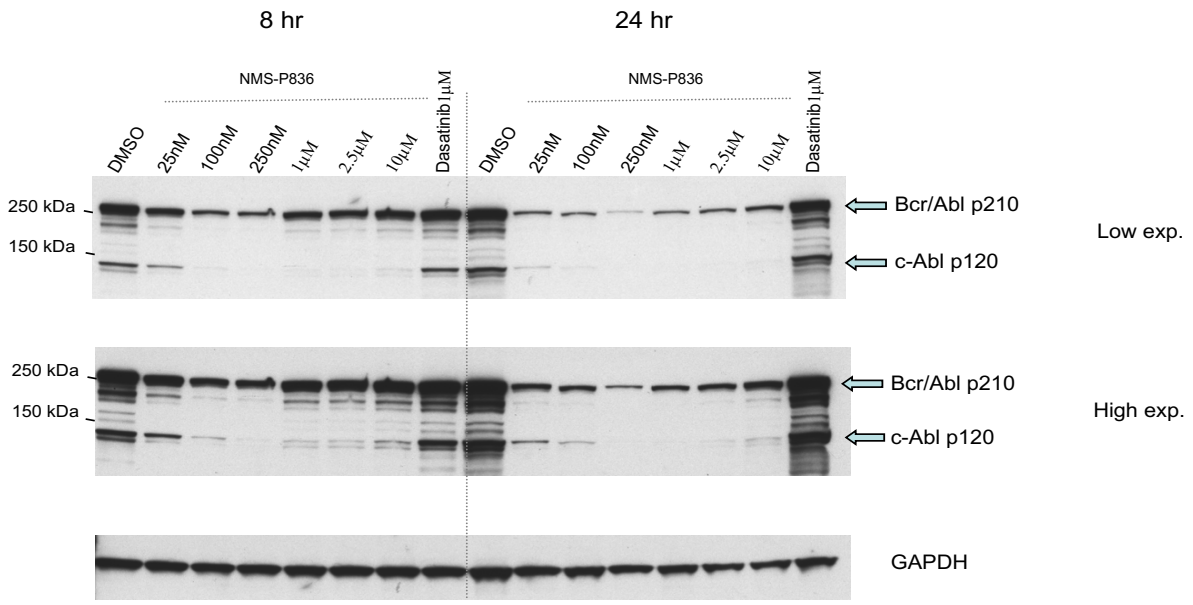

Figure 53. Evaluation of c-ABL and BCR-ABL degradation in K562 cells treated with different concentrations of compound DAS-6-2-2-6-CRBN (NMS-P836) for 8 h and 24 h before harvesting. DMSO and dasatinib were used as control.

To assess degradation activity of compound over others tyrosine protein kinases, **DAS-6-2-2-6-CRBN** was then tested for Src, Yes, Lck, Jak2, Mek1/2 and P44/42 MAPK proteins in K252 cells treated for 24 h (Figure 54). DMSO and dasatinib (1 μM, tyrosine kinase inhibitor) were used as control. **DAS-6-2-2-6-CRBN** demonstrated visible depletion of Src, Yes and Lck proteins already at the concentration of 25 nM, whereas no degradation of Jak2, Mek1/2 and P44/42 MAPK proteins was observed at any concentration tested.

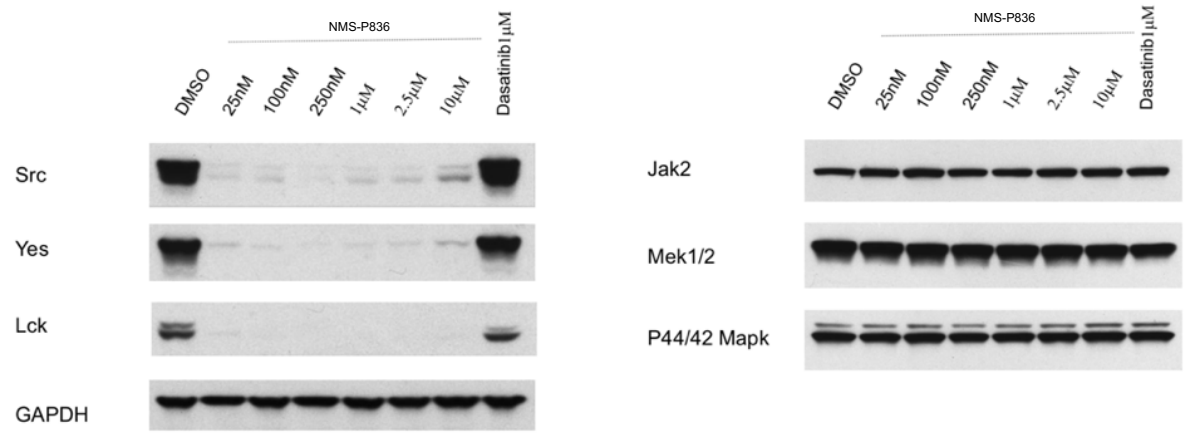

Figure 54. Evaluation of Src, Yes, Lck, Jak2, Mek1/2 and P44/42 MAPK degradation in K562 cells treated with different concentrations of compound DAS-6-2-2-6-CRBN (NMS-P836) for 24 h before harvesting. DMSO and dasatinib were used as control.

DAS-6-2-2-6-CRBN activity was also evaluated in GIST-882 cells, gastrointestinal stromal tumor cell line, bearing an activated form of KIT protein (Figure 55). DMSO and dasatinib (1 μM, tyrosine kinase inhibitor) were used as control. After treatment with different concentration of compound for 24 h, c-KIT and P-p44/42 MAPK were probed using the corresponding specific antibodies. The results showed strong degradation of P-p44/42 MAPK already at 1 μM.

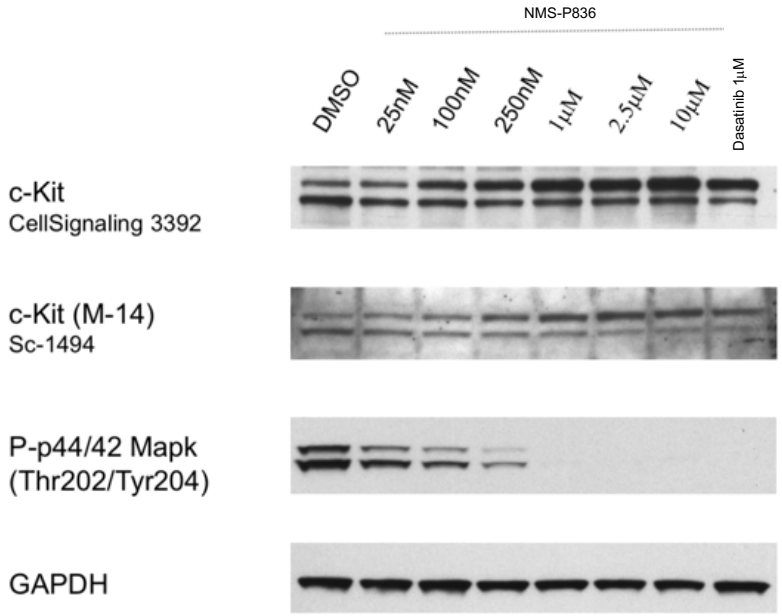

Figure 55. Evaluation of c-KIT and P-p44/42 MAPK degradation in GIST-882 cells treated with different concentrations of compound DAS-6-2-2-6-CRBN (NMS-P836) for 24 h before harvesting. DMSO and dasatinib were used as control.

3.6.2 Biological evaluation of DAS-6-2-2-2-POMA

To evaluate if **DAS-6-2-2-2-POMA** degrader could induce c-ABL, BCR-ABL, Scr and Yes depletion, protein abundance of these proteins was evaluated. K562 cells were treated with different concentrations of **DAS-6-2-2-2-POMA** (NMS-P324) for 24 h before cell lysis (Figure

56). DMSO and dasatinib (1 μM, tyrosine kinase inhibitor) were used as control. **DAS-6-2-2-2-POMA** demonstrated strong degradation of c-ABL, Src and Yes at concentrations as low as 25 nM. Moreover, at high concentration (10 μM) "hook effect" was noticed. However, some degradation of BRC-ABL was also observed.

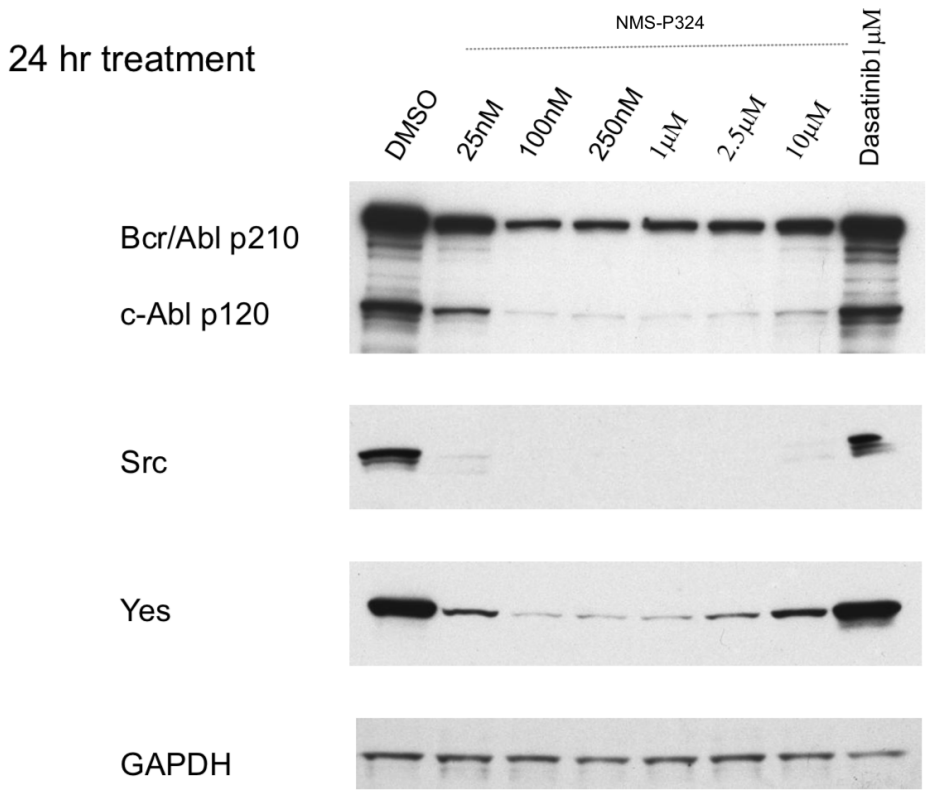

Figure 56. Evaluation of c-ABL, BCR-ABL, Src, Yes degradation in K562 cells treated with different concentrations of compound DAS-6-2-2-2-POMA (NMS-P324) for 24 h before harvesting. DMSO and dasatinib were used as control.

3.6.3 Biological evaluation of VZ-6-2-2-6-POMA

In order to assess cellular activity of **VZ-6-2-2-6-POMA** (NMS-P180), levels of c-ABL, BCR-ABL and Aurora A proteins were evaluated in K562 cells (Figure 57). DMSO and VZ reference (1 μM) were used as control. After 24 h of treatment with different concentration of compound and cell lysis, samples were resolved by electrophoresis followed by Western blot. **VZ-6-2-2-**

6-POMA showed selective degradation of Aurora A protein over c-ABL and BCR-ABL. In details, more than 50 % of Aurora A was visibly depleted already at 250 nM of compound (Figure 57).

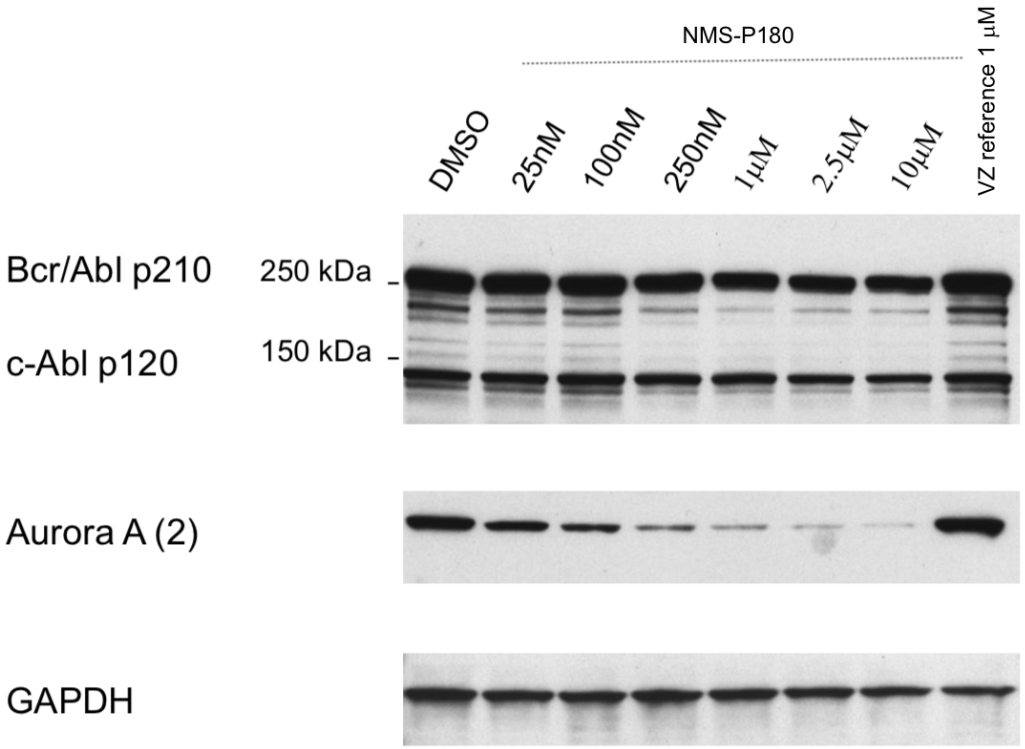

Figure 57. Evaluation of c-ABL, BCR-ABL and Aurora A degradation in K562 cells treated with different concentrations of compound **VZ-6-2-2-6-POMA** (NMS-P180) for 24 h before harvesting. DMSO and VZ reference were used as control.

Furthermore, the selectivity of **VZ-6-2-2-6-POMA** (NMS-P180) to induce Aurora A degradation over Aurora B was studied (Figure 58). In details, the human ovarian carcinoma A2780 cells were treated with different concentration of compound for 24 h. The results showed preferential degradation of Aurora A. Instead, depletion of Aurora B was less pronounced and only appreciated at higher concentration (1-2 μM more than 50%). Moreover, to evaluate if the inhibition and degradation of Aurora proteins could have an impact on phosphorylation of Ser10 on histone H3, levels of this protein were evaluated in A2780 cells

(Figure 58). Indeed, it was observed that treatment with aurora kinase inhibitor (VZ reference) led to inhibition of histone H3 phosphorylation. Similar impact was detected after treatment with 2-10 μM of **VZ-6-2-2-6-POMA** degrader. This effect also confirmed the mechanism of action of Aurora B to induce phosphorylation of Ser10 on histone H3.

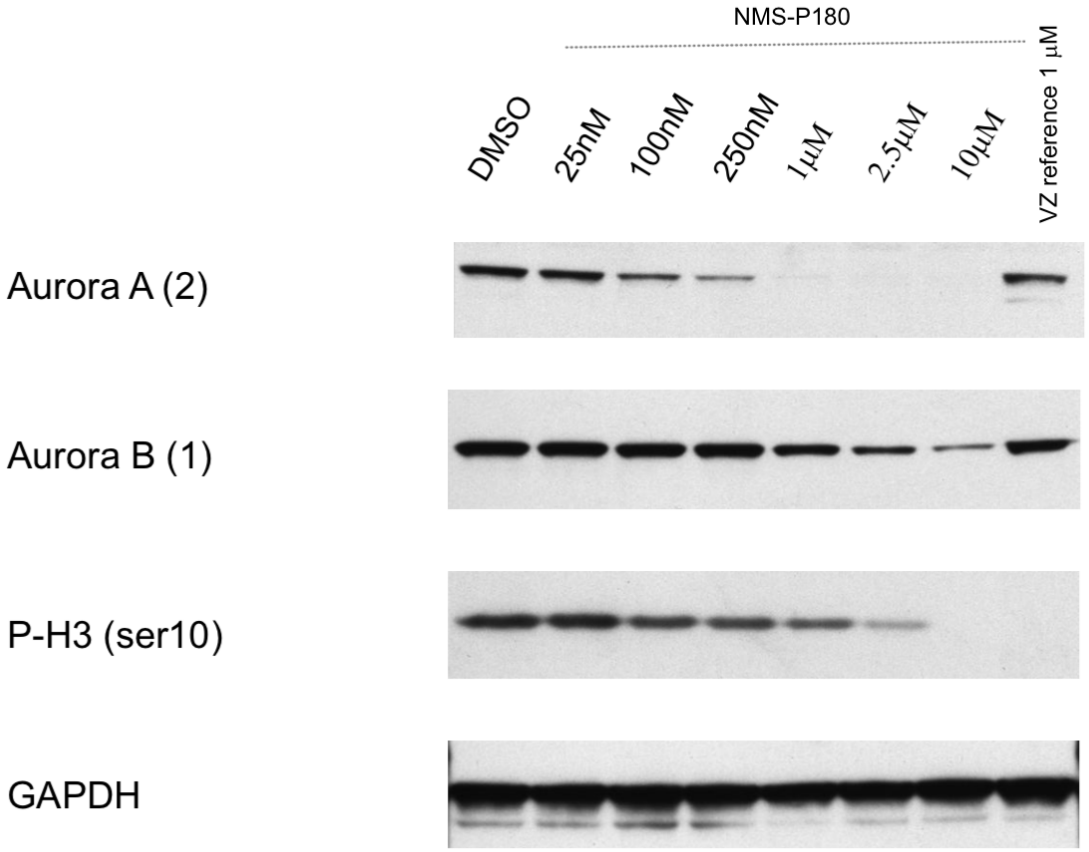

Figure 58. Evaluation of Aurora A and B degradation and levels of P-H3 (Ser10) in A2780 cells treated with different concentrations of compound VZ-6-2-2-6-POMA (NMS-P180) for 24 h before harvesting. DMSO and VZ reference were used as control.

3.7 *In silico* activities

Linker length and composition play a key role in PROTAC efficacy, since these factors are supposed to allow optimal interaction between target protein, E3 ligase and PROTAC, in order to achieve efficient ubiquitination of the target protein and its ultimate degradation. However,

at the moment, linker features for optimal ternary complex formation remain rather empirical. Hence, in order to generate a preliminary model and gain experience with its applicability, an *in silico* study of the ternary complex formation was carried out. **DAS-6-2-2-6-CRBN** was taken as reference compound, trying to find out the best distance for a PROTAC hooking ABL and CRBN.

X-ray crystal structure of dasatinib (BMS-354825) bound to activated ABL Kinase domain (PDB code: 2GQG) and that of pomalidomide bound to DDB1-CRBN (PDB code: 4CI3) were used as model components. The approach started with *ab initio* geometry optimization of **DAS-6-2-2-6-CRBN** structure conformation. Two minimized conformations were chosen, a V-shaped structure and an extended conformation of DAS-6-2-2-6-CRBN (Figure 59). The optimized structures were then transferred to the dedicated software (Discovery Studio Visualizer). Pomalidomide and dasatinib structures were superimposed over their original crystal structure, maintaining linker conformation as in the *ab initio* optimization. Superimposition a V-shaped structure of DAS-6-2-2-6-CRBN in the ternary complex results in negative steric interactions of ABL (blue) and CRBN (light blue) (Figure 60A). In the second case, using an extended optimized conformation of DAS-6-2-2-6-CRBN, the negative interactions were not observed (Figure 60B).

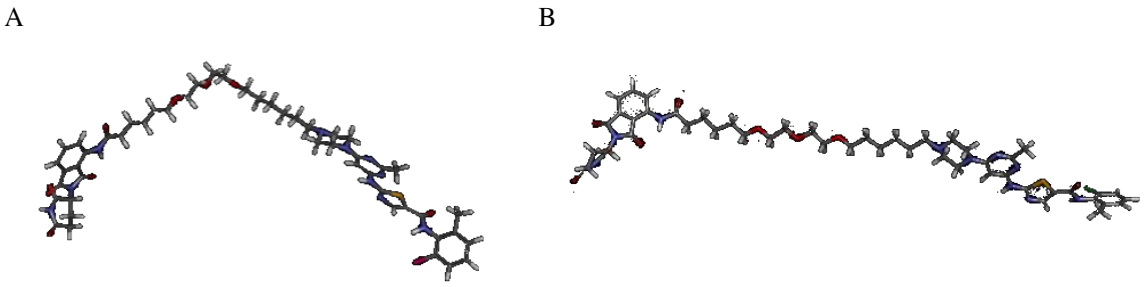

Figure 59. V-shaped (A) and extended (B) optimized ***ab initio*** **conformations of DAS-6-2-2-6-CRBN.**[79]

A)

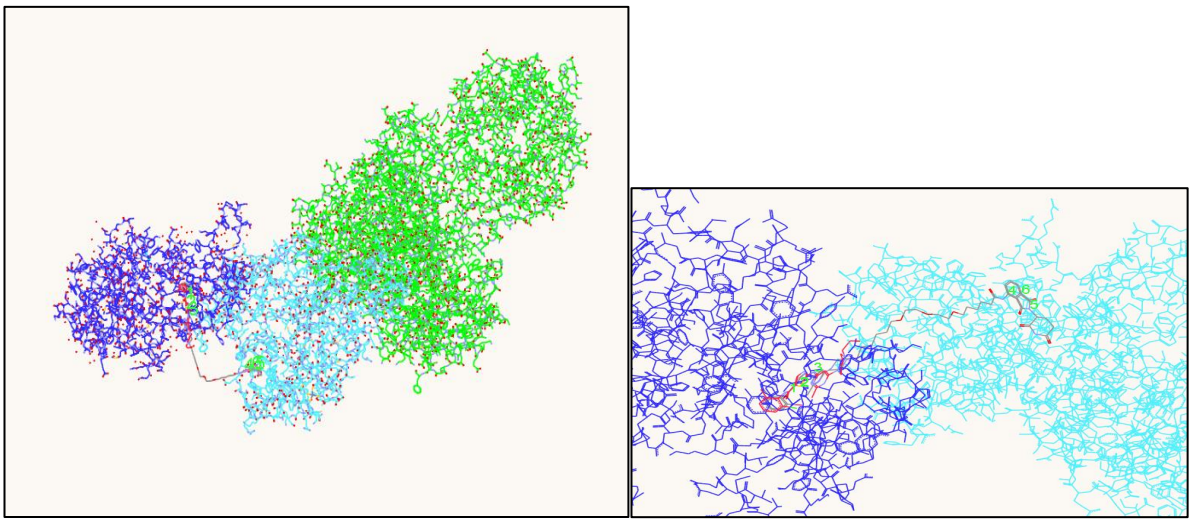

B)

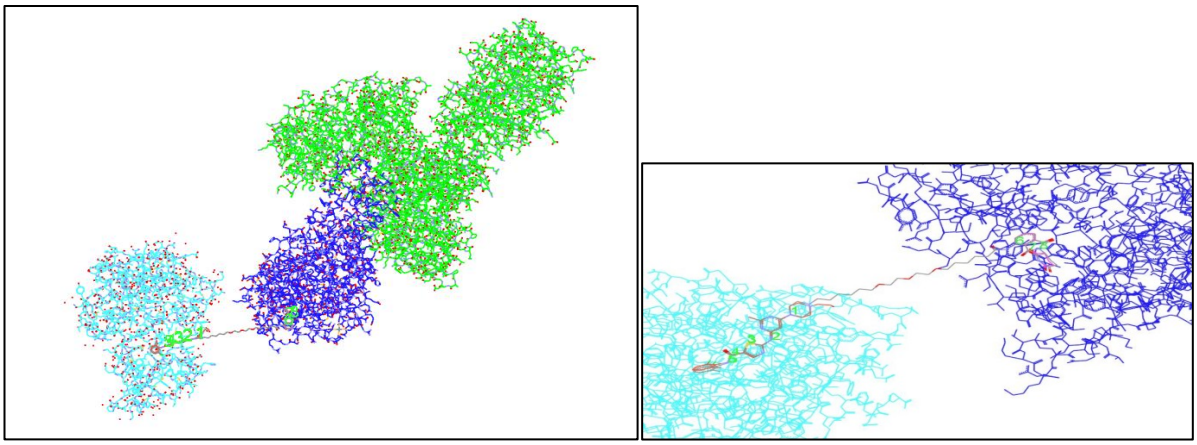

Figure 60. ***In silico*** **ternary complex formation.**

Applying this method, we generated a small library of ternary complexes that could be a starting point to make some consideration about correlation of biological activity and conformation. Additionally to **DAS-6-2-2-6-CRBN**, the studied PROTACs were **DAS-6-5-6-CRBN**, **DAS-6-2-2-CRBN**, **DAS-6-2-2-2-2-2-2-CRBN** published by Lai *et al*.,[79] and the two new PROTACs **DAS-6-2-2-2-POMA** and **DAS-6am-2-2am-6-POMA** (Figure 61).

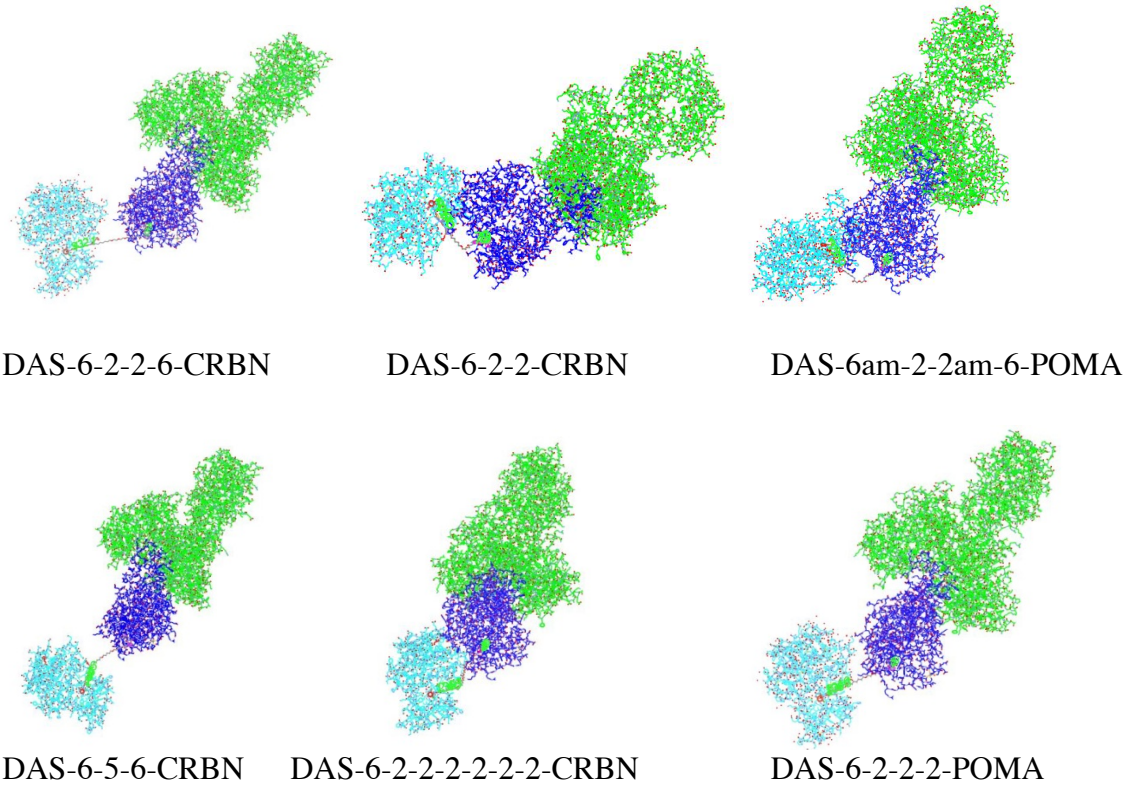

Figure 61. Ternary complexes with *ab initio* geometry optimization of PROTACs.

3.8 Conclusion

In summary, in this section we reported the design, the synthesis and biological characterization of PROTACs targeting protein kinases. The aim of this project was to study a literature example to confirm a proof of concept. Amongst those available, we chose **DAS-6-2-2-6-CRBN**, based on a potent tyrosine kinase inhibitor and CRBN ligand that induce degradation of c-ABL and BCR-ABL. After synthesis of **DAS-6-2-2-6-CRBN**, its cellular activity was assessed in cells. As expected, our results were consistent with those already published. Furthermore, we decided to extend the development of degraders focusing on how target ligand and linker composition affect efficacy and selectivity. Based on the same target ligands of **DAS-6-2-2-6-CRBN**, we designed two compounds with different linkers: **DAS-6-2-2-2-POMA** characterized by a shorter linker and **DAS-6-2am-2am-6-POMA** bearing a di-amide functionality. Only **DAS-6-2-2-2-POMA** was successfully synthesized and biologically characterized. It demonstrated pronounced degradation of c-ABL, Src and Yes proteins.

The last bifunctional molecule was developed to address the question if other protein kinases could be degraded. So, we designed a degrader **VZ-6-2-2-6-POMA** based on an aminopyrazole kinase inhibitor targeting seronine/threonine protein kinases. It showed preferential degradation of Aurora A already at 250 nM after 24 h of treatment. Moreover, it degraded Aurora B at high concentration, leading to inhibition of phosphorylation of histone H3.